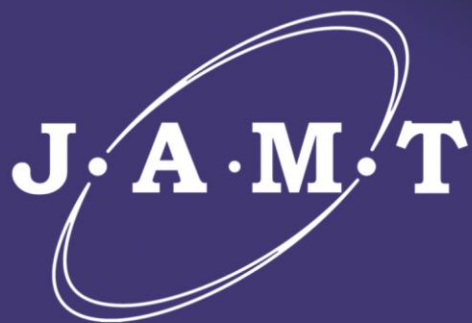


ISSN 2782-2192 (Print)

ISSN 2782-2206 (Online)

Journal of Advanced Materials and Technologies

J·A·M·T



**Vol. 8, No. 2.
2023**



ISSN 2782-2192 (Print)
ISSN 2782-2206 (Online)
DOI: 10.17277/issn.2782-2192



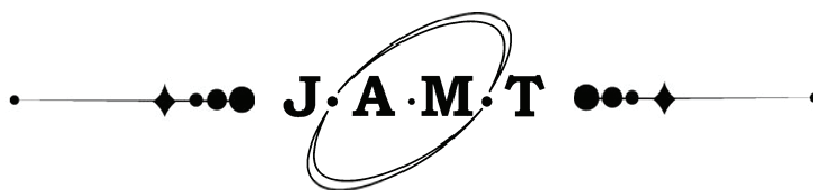
Journal of Advanced Materials and Technologies

**Vol. 8, No. 2.
2023**

**Tom 8, № 2.
2023**

16+

© Tambov State Technical University, Tambov, Russian Federation, 2023
© Merzhanov Institute of Structural Macrokinetics and Materials Sciences of Russian Academy of Sciences,
Chernogolovka, Moscow region, Russian Federation, 2023
© Design by TSTU Publishing, 2023



Journal of Advanced Materials and Technologies

Scientific Journal

“**Journal of Advanced Materials and Technologies**” is a peer-reviewed scientific journal of research in materials science and related issues in materials physics and mechanics.

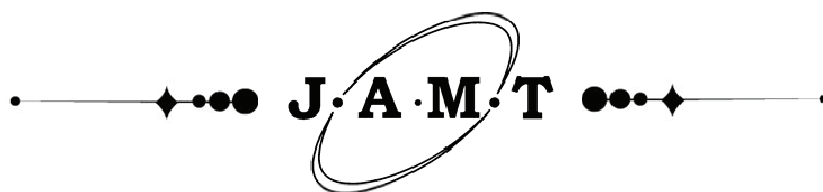
“**Journal of Advanced Materials and Technologies**” publishes original articles, reviews, short reports written by both renowned scientists and young researchers that contribute to the development of modern materials science.

The journal promotes research and exchange of information in the field of theoretical and practical research into materials science, modeling of processes involved in the creation of new materials, including nanomaterials, their properties and application.

The journal papers and metadata are available at Chemical Abstracts, CAS (American Chemical Society), Google Scholar, WorldCat, ROAR (Registry of Open Access Repositories), OpenAIRE (OpenAIRE - Open Access Infrastructure for Research in Europe), BASE (Bielefeld Academic Search Engine), RePEc: Research Papers in Economics, EBSCO.

ISSN 2782-2192 (Print), ISSN 2782-2206 (Online)

<i>Rename information</i>	Advanced materials & technologies (2016-2021) Print ISSN 2414-4606, Online ISSN 2541-8513
<i>The journal was founded</i>	2016
<i>Publication frequency</i>	Quarterly
<i>Founders</i>	Tambov State Technical University (TSTU), Merzhanov Institute of Structural Macrokinetics and Materials Sciences of Russian Academy of Sciences (ISMAN)
<i>Postal address</i>	TSTU: Bld. 2, 106/5, Sovetskaya St., Tambov, 392000 ISMAN: 8, Academician Osipyan St., Moscow region, Chernogolovka, 142432
<i>Editorial office address</i>	Bld. 2, 106/5, Sovetskaya St., Tambov, 392000
<i>Contacts</i>	Phone + 7 4752 63 03 91; amt.journal@yandex.ru
<i>Printing House</i>	TSTU Publishing, 112A, Michurinskaya St., Tambov, 392032 Phone + 7 4752 63 03 91; + 7 4752 63 07 46
<i>Website</i>	http://amt.tstu.ru/
<i>E-mail</i>	amt.journal@yandex.ru
<i>Phone</i>	+7 4752 63 92 93
<i>Subscription</i>	The electronic version of the Journal is freely available on the journal’s website, as well as in open access databases. The subscription index for the Journal printed version in the unified catalog “Press of Russia” is 80453
<i>Editor-in-Chief</i>	Mikhail I. Alymov, D. Sc. (Engineering), Professor, Corresponding Member of the Russian Academy of Sciences



Journal of Advanced Materials and Technologies

Научный журнал

«Journal of Advanced Materials and Technologies» – научный рецензируемый журнал, посвященный исследованиям в области материаловедения и примыкающих вопросов физики и механики материалов.

Журнал «Journal of Advanced Materials and Technologies» публикует оригинальные статьи, обзоры, краткие сообщения, содействующие развитию современной науки о материалах, подготовленные как известными учеными, так и молодыми специалистами.

Миссия журнала – обмен актуальной научной информацией в области теоретических и практических исследований и моделирования процессов, связанных с получением, определением свойств новых материалов, в том числе наноразмерных, и их применения.

Средство массовой информации периодическое печатное издание, журнал «Journal of Advanced Materials and Technologies» зарегистрировано Федеральной службой по надзору в сфере связи, информационных технологий и массовых коммуникаций. Регистрационный номер СМИ ПИ № ФС 77-74804 от 25.01.2019.

Журнал входит в перечень рецензируемых научных изданий (перечень ВАК Минобрнауки РФ) от 16 декабря 2021 г. по научным специальностям: 1.4.15 – Химия твердого тела; 2.6.6 – Нанотехнологии и наноматериалы; 2.6.13 – Процессы и аппараты химических технологий; 2.6.17 – Материаловедение.

Материалы журнала размещены в РИНЦ, Chemical Abstracts, CAS (American Chemical Society), Академия Google (Google Scholar), WorldCat, СОЦИОНЕТ, ROAR (Registry of Open Access Repositories), OpenAIRE (OpenAIRE - Open Access Infrastructure for Research in Europe), BASE (Bielefeld Academic Search Engine), RePEc: Research Papers in Economics, EBSCO.

ISSN 2782-2192 (Print), ISSN 2782-2206 (Online)

Сведения о переименовании	«Advanced materials & technologies» (2016–2021) Print ISSN 2414-4606, Online ISSN 2541-8513
Журнал основан	2016 г.
Периодичность	4 раза в год
Учредители	Федеральное государственное бюджетное образовательное учреждение высшего образования «Тамбовский государственный технический университет» (ФГБОУ ВО «ТГТУ»), Федеральное государственное бюджетное учреждение науки Институт структурной макрокинетики и проблем материаловедения им. А. Г. Мерджанова Российской академии наук (ИСМАН)
Адреса учредителей	ФГБОУ ВО «ТГТУ»: 392000, Тамбовская область, г.о. город Тамбов, г. Тамбов, ул. Советская, д. 106/5, помещ. 2, ИСМАН: 142432, Московская область, г. Черноголовка, ул. Академика Осипьяна, д. 8
Адрес издателя	ФГБОУ ВО «ТГТУ»: 392000, Тамбовская область, г.о. город Тамбов, г. Тамбов, ул. Советская, д. 106/5, помещ. 2
Адрес редакции	392000, Тамбовская область, г.о. город Тамбов, г. Тамбов, ул. Советская, д. 106/5, помещ. 2
Контакты	Тел.: + 7 4752 63 03 91; amt.journal@yandex.ru
Адрес типографии	392032, Тамбовская обл., г. Тамбов, ул. Мичуринская, д. 112А Тел.: + 7 4752 63 03 91; + 7 4752 63 07 46
Сайт	http://amt.tstu.ru/
E-mail	amt.journal@yandex.ru
Телефон	+7 4752 63 92 93
Подписка	Подписку на печатную версию журнала можно оформить по объединенному каталогу «Пресса России». Подписной индекс – 80453
Главный редактор	Алымов Михаил Иванович, д. т. н., профессор, член-корреспондент РАН

EDITORS

- Mikhail I. Alymov**, D. Sc. (Eng.), Professor, Corresponding Member of the Russian Academy of Sciences (RAS), Director of Merzhanov Institute of Structural Macrokinetics and Materials Sciences RAS (ISMAN), Chernogolovka, Moscow Region, Russian Federation
- Mikhail N. Krasnyansky**, D. Sc. (Eng.), Professor, Rector of Tambov State Technical University (TSTU), Tambov, Russian Federation
- Alexey G. Tkachev**, D. Sc. (Eng.), Professor, Head of Department of Technologies and Methods of Nanoproducts Manufacturing, TSTU, Tambov, Russian Federation
- Irina V. Burakova**, Ph.D., Associate Professor of Department of Technologies and Methods of Nanoproducts Manufacturing, TSTU, Tambov, Russian Federation
- Imran Ali**, Ph.D., FRSC, Professor, Department of Chemistry, Jamia Millia Islamia (Central University), New Delhi, India
- Vyacheslav M. Buznik**, D. Sc. (Chem.), Professor, RAS Academician, All-Russian Scientific Research Institute of Aviation Materials, Moscow, Russian Federation
- Stepan N. Kalmykov**, D. Sc. (Chem.), Professor, RAS Academician, Dean of the Faculty of Chemistry at the Lomonosov Moscow State University, Moscow, Russian Federation
- Valeriy P. Meshalkin**, D. Sc. (Eng.), Professor, RAS Academician, Head of Department of Logistics and Economic Informatics, Mendeleev University of Chemical Technology of Russia, Moscow, Russian Federation
- Alexander G. Divin**, D. Sc. (Eng.), Associate Professor, Head of Department of Mechatronics and Technological Measurements, TSTU, Tambov, Russian Federation
- Tatyana P. Dyachkova**, D. Sc. (Chem.), Professor, Director of Center for Collective Use of Scientific Equipment “Production and Application of Multifunctional Nanomaterials”, TSTU, Tambov, Russian Federation
- Yury I. Golovin**, D. Sc. (Phys. and Math.), Professor, Director of Center for Nanotechnology and Nanomaterials, Derzhavin Tambov State University, Tambov, Russian Federation
- Jesus Iniesta Valcarcel**, Ph.D., Associate Professor, Department of Physical Chemistry, University of Alicante, Alicante, Spain
- Ruslan Kh. Khamizov**, D. Sc. (Chem.), Professor, Director of Vernadsky Institute of Geochemistry and Analytical Chemistry of RAS, Moscow, Russian Federation
- Mikhail L. Kheifetz**, D. Sc. (Eng.), Professor, Director of Institute of Applied Physics of National Academy of Science of Belarus, Minsk, Belarus
- Roman B. Morgunov**, D. Sc. (Phys. and Math.), Professor, Leading Researcher, Institute of Problems of Chemical Physics RAS, Chernogolovka, Moscow Region, Russian Federation
- Fadei F. Komarov**, D. Sc. (Phys. and Math.), Professor, Academician of the National Academy of Sciences of Belarus, Head of Elionic Laboratory at A. N. Sevchenko Institute of Applied Physical Problems of Belarusian State University, Minsk, Belarus
- Stephane Mangin**, Ph.D., Professor, Physics of Matter and Materials Department, Institute Jean Lamour, University of Lorraine, Nancy, France
- Vladimir F. Pershin**, D. Sc. (Eng.), Professor, Professor at the Department of Technologies and Methods of Nanoproducts Manufacturing, TSTU, Tambov, Russian Federation
- Dimitar Stavrev**, D. Sc. (Eng.), Professor, Professor of Department of Materials Science at the Technical University of Varna, Varna, Bulgaria
- Alexander M. Stolin**, D. Sc. (Phys. and Math.), Professor, Head of Laboratory, ISMAN RAS, Chernogolovka, Moscow Region, Russian Federation
- Yoshifumi Tanimoto**, Ph.D., Professor, Hiroshima University, Japan
- Vener A. Valitov**, D. Sc. (Eng.), Leading Researcher, Institute for Metals Superplasticity Problems of the Russian Academy of Sciences, Ufa, Russian Federation
- Sergey M. Arakelian**, D. Sc. (Phys. and Math.), Professor, Head of the Department of Physics and Applied Mathematics, Vladimir State University, Vladimir, Russian Federation
- Arif A. Babaev**, D. Sc. (Phys. and Math.), Professor, Head of the Laboratory of Optical Phenomena in Condensed Matter, Institute of Physics of Dagestan Scientific Center of Russian Academy of Sciences, Makhachkala, Republic of Dagestan, Russian Federation
- Evgeniy I. Terukov**, D. Sc. (Eng.), Professor, Deputy Director for Science of R&D Center of Thin-Film Technology for Energetics under Ioffe Institute, St. Petersburg, Russian Federation
- Valeriy Yu. Dolmatov**, D. Sc. (Eng.), Head of Research Laboratory at the “Special Construction and Technology Bureau “Technolog”, St. Petersburg, Russian Federation
- Valeriy V. Savin**, D. Sc. (Phys. and Math.), Leading Researcher, Head of the Laboratory of Physical Materials Science, International Research Center “X-ray Coherent Optics”, Immanuel Kant Baltic Federal University, Kaliningrad, Russian Federation
- Gennady E. Selyutin**, Ph.D., Associate Professor, Senior Researcher, Federal Research Center “Krasnoyarsk Science Center” of Siberian Branch of the Russian Academy of Sciences, Krasnoyarsk, Russian Federation
- Vladimir V. Petrov**, D. Sc. (Phys. and Math.), Professor, Saratov State University, Saratov, Russian Federation
- Yury E. Kalinin**, D. Sc. (Phys. and Math.), Professor, Voronezh State Technical University, Voronezh, Russian Federation
- Vladimir S. Sevostyanov**, D. Sc. (Eng.), Professor, Head of the Department “Technological Complexes, Machines and Mechanisms”, V. G. Shukhov Belgorod State Technological University, Belgorod, Russian Federation
- Victor M. Mukhin**, D. Sc. (Eng.), Professor, D. Mendeleev University of Chemical Technology of Russia, Moscow, Russian Federation
- Vladimir D. Vermel**, D. Sc. (Eng.), Professor, Head of the Scientific and Technical Center of the Scientific and Production Complex, Central Aerohydrodynamic Institute, Zhukovsky, Moscow Region, Russian Federation
- Nadezhda V. Usoltseva**, D. Sc. (Chem.), Professor, Director of the Research Institute of Nanomaterials, Ivanovo State University, Ivanovo, Russian Federation
- Lyaylya A. Abdrakhmanova**, D. Sc. (Eng.), Professor, Kazan State University of Architecture and Engineering, Kazan, Russian Federation
- Vyacheslav A. Sergeev**, D. Sc. (Eng.), Professor, Director of the Ulyanovsk branch of Kotelnikov Institute of Radioengineering and Electronics of Russian Academy of Science, Ulyanovsk, Russian Federation
- Irina V. Zaporotzkova**, D. Sc. (Phys. and Math.), Professor, Director of the Institute of Priority Technologies, Volgograd State University, Volgograd, Russian Federation
- Vladimir E. Guterma**, Ph.D., Professor, Leading Researcher, Southern Federal University, Rostov-on-Don, Russian Federation
- Vladimir I. Kodolov**, D. Sc. (Chem.), Professor, Kalashnikov Izhevsk State Technical University, Izhevsk, Russian Federation
- Valeria S. Tafintseva**, Ph.D., Researcher, Department of Physics, Faculty of Science and Engineering, Norwegian University of Life Sciences, Norway
- Vyacheslav M. Tyutyunik**, D. Sc. (Eng.), Professor, Director General of International Nobel Information Centre (INIC), Ltd., TSTU, Tambov, Russian Federation
- Translator:** Natalia A. Gunina, Ph.D., Associate Professor, Head of Department of International Professional and Scientific Communication, TSTU, Tambov, Russian Federation

СОВЕТ РЕДАКТОРОВ

- Альмов Михаил Иванович**, д.т.н., профессор, член-корреспондент РАН, директор Института структурной макрокинетики и материаловедения им. А.Г. Мержанова РАН (ИСМАН), Черноголовка, Московская область, Россия
- Краснянский Михаил Николаевич**, д.т.н., профессор, ректор, Тамбовский государственный технический университет (ТГТУ), Тамбов, Россия
- Ткачев Алексей Григорьевич**, д.т.н., профессор, заведующий кафедрой «Техника и технологии производства нанопродуктов», ТГТУ, Тамбов, Россия
- Буракова Ирина Владимировна**, к.т.н., доцент, доцент кафедры «Техника и технологии производства нанопродуктов», ТГТУ, Тамбов, Россия
- Али Ибран**, PhD, FRSC, профессор кафедры химии, Джамяя Миллия Исламия (Центральный университет), Нью-Дели, Индия
- Бузник Вячеслав Михайлович**, д.х.н., профессор, академик РАН, Всероссийский научно-исследовательский институт авиационных материалов, Москва, Россия
- Калмыков Степан Николаевич**, д.х.н., профессор, академик РАН, декан химического факультета Московского государственного университета им. М. В. Ломоносова, Москва, Россия
- Мешалкин Валерий Павлович**, д.т.н., профессор, академик РАН, заведующий кафедрой «Логистики и экономической информатики» Российского химико-технологического университета им. Д. И. Менделеева, Москва, Россия
- Дивин Александр Георгиевич**, д.т.н., доцент, заведующий кафедрой «Мехатроника и технологические измерения», ТГТУ, Тамбов, Россия
- Дьячкова Татьяна Петровна**, д.х.н., профессор, директор центра коллективного пользования научным оборудованием «Получение и применение полифункциональных наноматериалов», ТГТУ, Тамбов, Россия
- Головин Юрий Иванович**, д.ф.-м.н., профессор, директор НИИ «Нанотехнологии и наноматериалы» Тамбовский государственный университет им. Г. Р. Державина, Тамбов, Россия
- Иньеста Хесус Валькарсель**, Ph.D., доцент кафедры физической химии Университета Аликанте, Аликанте, Испания
- Хамизов Руслан Хажсетович**, д.х.н., профессор, директор, Институт геохимии и аналитической химии им. В. И. Вернадского РАН, Москва, Россия
- Хейфец Михаил Львович**, д.т.н., профессор, директор института, Институт прикладной физики НАН Беларуси, Минск, Беларусь
- Моргунов Роман Борисович**, д.ф.-м.н., профессор, главный научный сотрудник, Институт проблем химической физики РАН, г. Черноголовка, Московская область, Россия
- Комаров Фаддей Фадеевич**, д.ф.-м.н., профессор, академик Национальной академии наук Республики Беларусь, заведующий лабораторией эллионики, Институт прикладных физических проблем им. А. Н. Севченко Белорусского государственного университета, Минск, Беларусь
- Мангин Стефан**, Ph.D., профессор кафедры физики материи и материалов Института Жана Ламура, Университет Лотарингии, Нанси, Франция
- Першин Владимир Федорович**, д.т.н., профессор, профессор кафедры «Техника и технологии производства нанопродуктов», ТГТУ, Тамбов, Россия
- Ставрев Димитр**, д.т.н., профессор, профессор кафедры «Материаловедения», Варненский технический университет, Варна, Болгария
- Столин Александр Моисеевич**, д.ф.-м.н., профессор, заведующий лабораторией, ИСМАН РАН, Черноголовка, Московская область, Россия
- Танимото Есифуми**, Ph.D., профессор, Хиросимский университет, Япония
- Валитов Венер Анварович**, д.т.н., ведущий научный сотрудник, Институт проблем сверхпластичности металлов РАН, Уфа, Республика Башкортостан, Россия
- Аракелян Сергей Мартиросович**, д.ф.-м.н., профессор, заведующий кафедрой физики и прикладной математики, Владимирский государственный университет им. А. Г. и Н. Г. Столетовых, Владимир, Россия
- Бабаев Ариф Азимович**, д.ф.-м.н., профессор, заведующий лабораторией оптических явлений в конденсированных средах Института физики им. Х. И. Амирханова ДНЦ РАН, Махачкала, Республика Дагестан, Россия
- Теруков Евгений Иванович**, д.т.н., профессор, заместитель генерального директора по научной работе ООО «НТЦ тонкопленочных технологий в энергетике при ФТИ им. А.Ф. Иоффе», Санкт-Петербург, Россия
- Долматов Валерий Юрьевич**, д.т.н., начальник научно-исследовательской лаборатории, «Специальное конструкторско-технологическое бюро «Технолог», Санкт-Петербург, Россия
- Савин Валерий Васильевич**, д.ф.-м.н., ведущий научный сотрудник, заведующий лабораторией физического материаловедения МНИЦ «Когерентная рентгеновская оптика для установок «Мегасайенс», Балтийский федеральный университет им. Иммануила Канта, Калининград, Россия
- Селютин Геннадий Егорович**, к.ф.-м.н., доцент, старший научный сотрудник, Институт химии и химической технологии Сибирского отделения Российской академии наук ФИЦ КИХ СО РАН, Красноярск, Россия
- Петров Владимир Владимирович**, д.ф.-м.н., профессор, Саратовский национальный исследовательский университет им. Н. Г. Чернышевского, Саратов, Россия
- Калинин Юрий Егорович**, д.ф.-м.н., профессор, Воронежский государственный технический университет, Воронеж, Россия
- Севостьянов Владимир Семенович**, д.т.н., профессор, заведующий кафедрой «Технологические комплексы, машины и механизмы», Белгородский государственный технологический университет им. В. Г. Шухова, Белгород, Россия
- Мухин Виктор Михайлович**, д.т.н., профессор, Российский химико-технологический университет им. Д. И. Менделеева, Москва, Россия
- Вермель Владимир Дмитриевич**, д.т.н., профессор, начальник Научно-технического центра научно-производственного комплекса, Центральный аэрогидродинамический институт им. профессора Н. Е. Жуковского, Московская область, Жуковский, Россия
- Усольцева Надежда Васильевна**, д.х.н., профессор, директор НИИ наноматериалов, Ивановский государственный университет, Иваново, Россия
- Абдрахманова Ляйля Абдулловна**, д.т.н., профессор, Казанский государственный архитектурно-строительный университет, Казань, Россия
- Сергеев Вячеслав Андреевич**, д.т.н., профессор, директор Ульяновского филиала ФГБУН «Институт радиотехники и электроники им. В. А. Котельникова» РАН, Ульяновск, Россия
- Запорожкова Ирина Владимировна**, д.ф.-м.н., профессор, директор института приоритетных технологий, Волгоградский государственный университет, Волгоград, Россия
- Гутерман Владимир Ефимович**, д.х.н., профессор, главный научный сотрудник, Южный федеральный университет, Ростов-на-Дону, Россия
- Кодолов Владимир Иванович**, д.х.н., профессор, Ижевский государственный технический университет им. М. Т. Калашникова, Ижевск, Россия
- Тафинцева Валерия Сергеевна**, Ph.D., научный сотрудник, кафедра физики, факультет науки и технологий, Норвежский университет естественных наук, Норвегия
- Тютюнник Вячеслав Михайлович**, д.т.н., профессор, генеральный директор ООО «Международный информационный Нобелевский центр» (МИНЦ), ТГТУ, Тамбов, Россия
- Переводчик:** Гунина Наталия Александровна, к.ф.н., заведующий кафедрой «Международная научная и профессиональная коммуникация», ТГТУ, Тамбов, Россия

CONTENTS

Original papers

Nanostructured, nanoscale materials and nanodevices

- Khrobak A. V., Dyachkova T. P., Chapaksov N. A., Poluboyarinov D. A.** Effect of modification of carbon nanotubes by 3-aminopropyltriethoxysilane on the properties of silicone nanocomposites 92

Materials for 3D printing and additive manufacturing

- Vozniakovskii A. A., Kidalov S. V., Voznyakovskii A. P., Podlozhnyuk N. D., Titova S. I., Auchynnika E. V.** Influence of few-layer graphene on the complex of strength and thermophysical properties of polymer composites obtained by DLP by 3D printing 103

Biological materials;

nanomedicine, and novel technologies for clinical and medical applications

- Gryaznova M. I., Lugvishchuk D. S., Gryaznov K. O., Filimonenkov I. S., Batova N. I., Mitberg E. B., Karaeva A. R., Mordkovich V. Z.** Screen-printing of electrical sensor for glucose determination with exfoliated graphite-based paste 111
- Zakharov N. A., Aliev A. D., Matveev V. V., Kiselev M. R., Koval E. M., Shelekhov E. V., Goeva L. V., Zakharova T. V.** Synthesis and properties of hydroxyapatite – fluorapatite solid solutions 120

Materials for energy and environment, next-generation photovoltaics, and green technologies

- Kadum A. H. K., Burakova I. V., Mkrtychyan E. S., Ananyeva O. A., Yarkin V. O., Burakov A. E., Tkachev A. G.** Sorption kinetics of organic dyes methylene blue and malachite green on highly porous carbon material 130
- Chichigina Ya. M., Shigabaeva G. N., Emelyanova E. A., Galunin E. V., Yakimov A. S., Isaev A. Yu., Bekker M. R.** Heavy metal contents in the Tyumen city residential area soils 141

Reviews

Manufacturing processes and systems

- Baiti A., Aldavud S. S. Yu., Algurabi A. M., Salhi H., Pershin V. F.** Modification of lubricants with graphite nanoplates 157

СОДЕРЖАНИЕ

Оригинальные статьи

Наноструктурированные, наномасштабные материалы и наноустройства

- Хробак А. В., Дьячкова Т. П., Чапаксов Н. А., Полубояринов Д. А. Влияние модифицирования углеродных нанотрубок 3-аминопропилтриэтоксисиланом на свойства силиконовых нанокompозитов 92

Материалы для 3D-печати и аддитивного производства

- Возняковский А. А., Кидалов С. В., Возняковский А. П., Подложнюк Н. Д., Титова С. И., Овчинников Е. В. Влияние малослойного графена на комплекс прочностных и теплофизических свойств полимерных композитов, полученных DLP-методом 3D-печати 103

Биологические материалы;

наномедицина и новые технологии для клинического и медицинского применения

- Грязнова М. И., Лугвищук Д. С., Грязнов К. О., Филимоненков И. С., Батова Н. И., Митберг Э. Б., Караева А. Р., Мордкович В. З. Трафаретная печать датчика для измерения глюкозы из пасты на основе терморасширенного графита 111
- Захаров Н. А., Алиев А. Д., Матвеев В. В., Киселев М. Р., Коваль Е. М., Шелехов Е. В., Гоева Л. В., Захарова Т. В. Синтез и свойства твердых растворов гидроксипатит – фторапатит 120

Материалы для энергетики и окружающей среды,

фотоэлектрическая энергия следующего поколения и зеленые технологии

- Кадум А. Х. К., Буракова И. В., Мкртчян Э. С., Ананьева О. А., Яркин В. О., Бураков А. Е., Ткачев А. Г. Кинетика сорбции органических красителей метиленового синего и малахитового зеленого на высокопористом углеродном материале 130
- Чичигина Я. М., Шигабаева Г. Н., Емельянова Е. А., Галунин Е. В., Якимов А. С., Исаев А. Ю., Беккер М. Р. Содержание тяжелых металлов в почвах селитебной зоны г. Тюмени 141

Обзоры

Производственные процессы и системы

- Баити А., Альдавуд С.С.Ю., Альгураби А., Салхи Х., Першин В.Ф. Модифицирование смазочных материалов графитовыми нанопластинами 157

Effect of modification of carbon nanotubes by 3-aminopropyltriethoxysilane on the properties of silicone nanocomposites

© Anastasia V. Khrobak^a✉, Tatyana P. Dyachkova^a, Nikolay A. Chapaksov^a, Dmitry A. Poluboyarinov^a

^a Tambov State Technical University, Bld. 2, 106/5, Sovetskaya St., Tambov, 392000, Russian Federation

✉ nastiarx@yandex.ru

Abstract: The modification of the silicone compound with carbon nanotubes (CNTs) resulted in composites with improved physical properties and thermal stability. The carbon nanotubes were functionalized with 3-aminopropyltriethoxysilane for a more uniform distribution in the matrix. Initial and pre-oxidized CNTs containing different amounts of carboxyl groups were subjected to silanization. From 0.5 to 3 wt. % of the initial or functionalized CNTs were injected into Silagerm 2111 silicone compound. The obtained samples were characterized by FTIR and Raman spectroscopy and TG/DSC analysis. The silicon content in the silanized CNTs was determined by X-ray fluorescence spectroscopy. It was shown that the pre-oxidation of CNTs slightly affects the silicon content in the silanized nanotubes, which is up to (7.69 ± 0.92) wt. %. According to Raman mapping of the surface of silicone composites, the silanized CNTs are more uniformly distributed in the surface layer of the material than the original nanotubes. This effect has a positive effect on the physical-mechanical properties of the composites. CNTs functionalized by 3-aminopropyltriethoxysilane are 1.5 times more effective in increasing the electrical conductivity than the original CNTs. The resulting composites retain their mechanical characteristics after thermal exposure and can be operated over a wider temperature range than the original silicone compound.

Keywords: nanomaterials; carbon nanotubes; nanocomposites; polymers; silicone; functionalization.

For citation: Khrobak AV, Dyachkova TP, Chapaksov NA, Poluboyarinov DA. Effect of modification of carbon nanotubes by 3-aminopropyltriethoxysilane on the properties of silicone nanocomposites. *Journal of Advanced Materials and Technologies*. 2023;8(2):092-102. DOI: 10.17277/jamt.2023.02.pp.092-102

Влияние модифицирования углеродных нанотрубок 3-аминопропилтриэтоксисиланом на свойства силиконовых нанокompозитов

© А. В. Хробак^a✉, Т. П. Дьячкова^a, Н. А. Чапаксов^a, Д. А. Полубояринов^a

^a Тамбовский государственный технический университет,
ул. Советская, 106/5, пом. 2, Тамбов 392000, Российская Федерация

✉ nastiarx@yandex.ru

Аннотация: В результате модифицирования силиконового компаунда углеродными нанотрубками (УНТ) получены композиты с улучшенными физическими свойствами и термической стабильностью. Для более равномерного распределения в матрице углеродные нанотрубки подвергались функционализации 3-аминопропилтриэтоксисиланом. Силанизации подвергались исходные и предварительно окисленные УНТ, содержащие различное количество карбоксильных групп. От 0,5 до 3 масс. % исходных или функционализированных УНТ вводили в силиконовый компаунд марки «Силагерм 2111». Полученные образцы охарактеризованы методами ИК-Фурье и КР-спектроскопии, ТГ/ДСК-анализа. Содержание кремния в силанизированных УНТ определялось методом рентгенофлуоресцентной спектроскопии. Показано, что предварительное окисление УНТ незначительно влияет на содержание кремния в силанизированных нанотрубках, которое составляет до $(7,69 \pm 0,92)$ масс. %. По данным рамановского картирования поверхности силиконовых композитов, силанизированные УНТ распределяются в поверхностном слое материала более равномерно, чем исходные нанотрубки. Функционализация способствует более равномерному распределению УНТ

в поверхностном слое материала. Данный эффект положительно сказывается на физико-механических свойствах композитов. Функционализированные 3-аминопропилтриэтоксисиланом УНТ в 1,5 раза более эффективно увеличивают электропроводность, чем исходные УНТ. Полученные композиты сохраняют механические характеристики после термического воздействия и могут эксплуатироваться в более широком интервале температур, чем исходный силиконовый компаунд.

Ключевые слова: наноматериалы; углеродные нанотрубки; нанокompозиты; полимеры; силикон; функционализация.

Для цитирования: Khrobak AV, Dyachkova TP, Chapaksov NA, Poluboyarinov DA. Effect of modification of carbon nanotubes by 3-aminopropyltriethoxysilane on the properties of silicone nanocomposites. *Journal of Advanced Materials and Technologies*. 2023;8(2):092-102. DOI: 10.17277/jamt.2023.02.pp.092-102

1. Introduction

One-dimensional carbon nanostructures are often used as fillers that impart strength [1], thermal stability [2, 3], thermal conductivity [4] and electrical conductivity [5] of polymer composites, which can subsequently be used in various fields of technology. The advantages of carbon nanotubes (CNTs) and nanofibers as a modifying additive are, in addition to outstanding characteristics, a low specific gravity [6], due to which structures made with their use are very light.

The regularities of the formation of polymer nanocomposites based on CNTs have been studied in [7, 8]. It is noted that the strength properties of composites largely depend on the quality of the fiber-matrix interface, which determines the efficiency of stress transfer between carbon nanotubes and the polymer matrix [9, 10], and also that the nonpolar and smooth surface of CNT graphene layers often cannot provide the required interfacial interactions with the polymer matrix [11]. In addition, CNTs, like other nanomaterials, are prone to aggregation in various media, which significantly reduces the efficiency of their use in composites [12].

Functionalization of the nanotube surface is most often used to enhance the interaction of CNTs with polymer matrices and facilitate the dispersion of nanotubes in the bulk of the material. In the works of scientists, numerous methods are presented for grafting functional groups to the surface of CNTs, for example, by means of plasma treatment [13], electrochemical methods, liquid-phase oxidation [14–17], and treatment in vapors of various substances [18]. In [19], the regularities of covalent functionalization of CNTs by oxygen-containing groups are presented and the behavior of oxidized nanotubes when combined with polysulfone and polyaniline is shown. The authors noted that oxidized CNTs are capable of electrostatic interaction with polymer macromolecules, which changes the structure of the polymer layer adjacent to the nanotube surface.

In various studies, to modify silicone matrices, CNTs were preliminarily combined with

molybdenum dioxide [20], carbon black [21, 22], graphene [23, 24], branched alumina [25], and titanium dioxide [26]. It was shown in [27] that the dispersibility of CNTs plays a decisive role in the thermal stability of CNT/silicone rubber composites. In addition, the material containing evenly distributed nanotubes retains elasticity after holding at 280 °C for 7 days. For deagglomeration of nanotubes, long-term ultrasonic treatment in combination with jet milling was used in the study.

In addition, oxidized CNTs [28] functionalized with polysiloxane [29], dopamine [30], and aminosilanes [31–33] were used in composites with silicone.

The latter type of modifier is much better studied in the preparation of epoxy composites. It was shown in [20] that CNTs functionalized with 3-aminopropyltrimethoxysilane improve the mechanical properties of the epoxy polymer to a greater extent than the original nanotubes.

In [7], preoxidized CNTs were modified with 3-aminopropyltriethoxysilane. It is shown that surface-modified CNTs caused an increase in the elastic modulus and tensile strength of nanocomposites by 18 and 15.8 %, respectively, better than oxidized CNTs.

The efficiency of aminosilanes is explained by their ability to participate in the curing of the epoxy matrix (by amino groups), which promotes the formation of covalent bonds between functionalized CNTs and the epoxy network and improves the properties of the material [22–25]. The efficiency of silanized CNTs in silicone composites is due to the closeness of the chemical nature of the matrix and functional groups on the surface of nanotubes.

This study aims to investigate the effect of CNTs functionalized with 3-aminopropyltriethoxysilane on the properties of the Silagerm-2111 silicone compound, as well as to establish the dependence of the effect of using silanized CNTs on the conditions of preliminary oxidation of nanotubes with nitric acid.

2. Materials and Methods

2.1. Characteristics of starting materials and reagents

In this paper, we used Taunit-M carbon nanotubes manufactured by LLC Nanotechcenter (Tambov) with a diameter of 10–30 nm and a length of more than 3 μm , obtained by the CVD method from a propane-butane mixture at a Co/Mo/Mg catalyst./Al [34].

For the oxidation of CNTs, nitric acid of chemically pure grade was used. (Khimmed, Russia). For CNT silanization we used: 1) 3-aminopropyltriethoxysilane $\text{C}_9\text{H}_{20}\text{O}_5\text{Si}$ (98 % purity) provided by Nanjing Genesis Chemical Auxiliaries Co., Ltd. (Nanjing, China); 2) glacial acetic acid (Component-Reaktiv LLC, Russia); 3) isopropyl alcohol of chemically pure grade (CJSC Laverna, Russia).

Silicone compound Silagerm 2111 (Technology-Plast Production Association, Russia) was used as a composite matrix.

2.2. CNTs functionalization method

A portion of carbon nanotubes weighing 0.5 g was dispersed in 95 mL of a solution of dilute acetic acid with $\text{pH} = 5.2$ for 10 min using an ultrasonic homogenizer. 3-aminopropyltriethoxysilane was added to the resulting suspension. The mass ratio of CNTs/3-aminopropyltriethoxysilane was 1:10. The resulting mixture was kept in a flask under reflux at 80 °C for 4 hours with constant stirring at a speed of 100 rpm. At the end of the process, the CNTs were washed with distilled water to neutral pH and then dried in a heating cabinet at 80 °C.

In a number of cases, CNTs preliminarily oxidized with nitric acid were subjected to silanization. To do this, CNTs were boiled in concentrated nitric acid (1 g of CNTs per 50 mL of acid) in a flask under reflux for 2, 5, and 10 hours, after which they were washed on a filter with distilled water to neutral pH. The resulting aqueous paste was dried in a Scientz-10N Freeze Dryer (Scientz, China).

2.3. Nanocomposite preparation method

The original and silanized CNTs were introduced into the silicone compound so that the mass fraction of nanotubes in the composite was 0.5, 1, or 3%. The resulting mixture was stirred for 3 minutes at a stirrer speed of 250 rpm. Next, the suspension was subjected to evacuation. Vulcanization took place at room temperature for 24 hours.

2.4. Characterization of CNTs samples and composites based on them

The degree of functionalization of oxidized CNTs with carboxyl, lactone, and phenol groups was determined titrimetrically according to the Boehm method [35].

The silicon concentration in functionalized CNTs was determined by energy dispersive X-ray fluorescence analysis on an ARL QUANTX spectrometer (Thermo Fisher Scientific, Switzerland).

The IR spectra of carbon nanotubes were recorded in the range from 500 to 4000 cm^{-1} with a resolution of 4 cm^{-1} on an FT/IR 6700 spectrometer (Jasco, Japan) equipped with an ATR attachment with a zinc selenide prism.

The Raman spectra of the samples with a resolution of 5 cm^{-1} were obtained at an exciting laser wavelength of 532 nm on a DXR Raman Microscope (Thermo Scientific, USA). Raman maps of silicone nanocomposites with a step of $10 \times 10 \mu\text{m}$ were recorded on the same device. The OMNIC™ AtPlus software was used to analyze Raman spectroscopy and Raman mapping data.

The TG and DSC curves of the samples in air and argon were obtained on an STA 449 F3 Jupiter synchronous thermal analysis instrument (NETZSCH-Feinmahltechnik GmbH – Selb, Germany). The temperature program included holding at 30 °C for 10 minutes and heating from 30 to 900 °C at a rate of 10 °C·min⁻¹.

The electrical resistance of silicone nanocomposites was measured using an E6-13A teraohmmeter (Punane RET, Estonia). Raman spectra were obtained on a DXR Raman Microscope (Thermo Fisher Scientific, USA) with an excitation laser wavelength of 532 nm.

3. Results and Discussion

3.1. Finding the parameters of oxidized and silanized CNTs

According to the data of titrimetric analysis (Table 1), the composition of CNTs oxidized at various durations of treatment in HNO_3 differs insignificantly. CNTs after 2 hours of treatment contain the maximum amount of phenolic groups, and CNTs after 10 hours of treatment are characterized by a higher content of carboxyl groups. The patterns of changes in the chemical composition of functional groups upon oxidation in HNO_3 generally correspond to the data presented in [36].

Table 1. The content of acidic groups in oxidized CNTs

Duration of oxidation, h	Content of functional groups, mmol·g ⁻¹		
	phenolic	lactone	-COOH
2	0.3	0.3	0.5
5	0.2	0.4	0.5
10	0.2	0.4	0.6

According to [37], phenolic groups play the greatest role in the functionalization of oxidized CNTs with aminosilanes. It is in their place that Si–O–C bonds are formed. It is also possible to form hydrogen bonds between the C=O groups and the hydrolyzed silane.

According to the data of energy dispersive X-ray fluorescence analysis (Table 2), the content of silicon in samples of silanized CNTs differs insignificantly. However, oxidized CNTs interact with 3-aminopropyltriethoxysilane somewhat more efficiently than the original ones. The CNTs subjected to silanization after 2-h oxidation of CNTs with nitric acid are characterized by the highest Si content. Recall that these CNTs contained more OH groups than other types of oxidized CNTs.

Figure 1 shows typical IR spectra of the original, oxidized, and silanized CNTs. The original CNTs contain alkyl groups, which correspond to bands at 2920 and 2850 cm⁻¹ [38]. The broad band at about 3450 cm⁻¹ refers to the stretching vibrations of the O–H bonds of water molecules [39], which can be sorbed on the CNT surface. According to [40], the peaks near 1618 and 1385 cm⁻¹ are due to vibrations of the C=C and C–H bonds.

During oxidation, due to an increase in the hydrophilicity of the CNT surface, the intensity of the band at 3450 cm⁻¹ increases. In addition, a low-intensity peak appears at 1740 cm⁻¹ due to vibrations

Table 2. Silicon content in samples of silanized CNTs according to energy dispersive X-ray fluorescence analysis

CNT pre-treatment conditions	Silicon content, wt. %
Without pretreatment	6.26 ± 0.75
2 hour oxidation	7.69 ± 0.92
5 hour oxidation	6.64 ± 0.80
10 hour oxidation	6.70 ± 0.80

of C=O bonds in carboxyl groups, the number of which was previously analyzed based on titration data. According to [41], the peak at 1136 cm⁻¹ in the spectrum of oxidized and silanized CNTs is due to vibrations of C–O bonds.

In the IR spectrum of CNTs treated with 3-aminopropyltriethoxysilane without preliminary oxidation, the band at 1385 cm⁻¹ takes the form of a narrow peak, which, according to [40], can be explained by vibrations of C–H bonds in the alkyl groups of the modifying reagent. In addition, a group of peaks is found in the region of 880–1262 cm⁻¹, which, according to [42], are characteristic of silanized CNTs. A more detailed explanation is given in [43], where it is shown that the peaks at 880, 950, and 1262 cm⁻¹ are caused by vibrations of the Si–OH, Si–O–Si, Si–O–C, and Si–CH₃ bonds. It should be noted that there is no peak at 1385 cm⁻¹ in the spectra of CNTs silanized after preliminary oxidation, which may indicate a different nature of the interaction of 3-aminopropyltriethoxysilane with the surface of oxidized CNTs.

There is some difference in the IR spectra of CNT samples silanized before and after oxidation. In the case of pre-oxidized CNTs, the peak at 1384 cm⁻¹ is weak or absent, which can be explained by a change in the nature of the interaction between CNTs and aminosilane. In the case of unoxidized ones, a modifier layer is formed that does not form covalent bonds with the CNT surface. When oxidized CNTs are used, the OH groups of the hydrolyzed silane are involved in the formation of covalent and hydrogen bonds with the oxygen-containing groups of the nanotubes.

The Raman spectra (Fig. 2) of various types of CNTs used in the work show characteristic peaks G (~1570 cm⁻¹), D (1350 cm⁻¹), D + G (~2920 cm⁻¹) and 2D (2700 cm⁻¹). According to [44], the G peak dominates in the spectra of highly crystalline graphite, while the D peak is due to the presence of amorphous carbon. The integral intensity ratio D/G is usually used to characterize the number of defects in carbon materials [45]. Peaks 2D and D + G are overtones of the main peaks.

The results of processing the Raman spectra are presented in Table 3. Peak G in the Raman spectra of oxidized CNTs is shifted to higher wavenumbers compared to the same value for the original CNTs. In this case, the values of the D/G and 2D/G ratios for oxidized and silanized CNTs are practically the same as for the original CNTs. Consequently, functional groups are formed during oxidation at the site of defects in the original nanotubes, and new defects are formed to an extremely small extent.

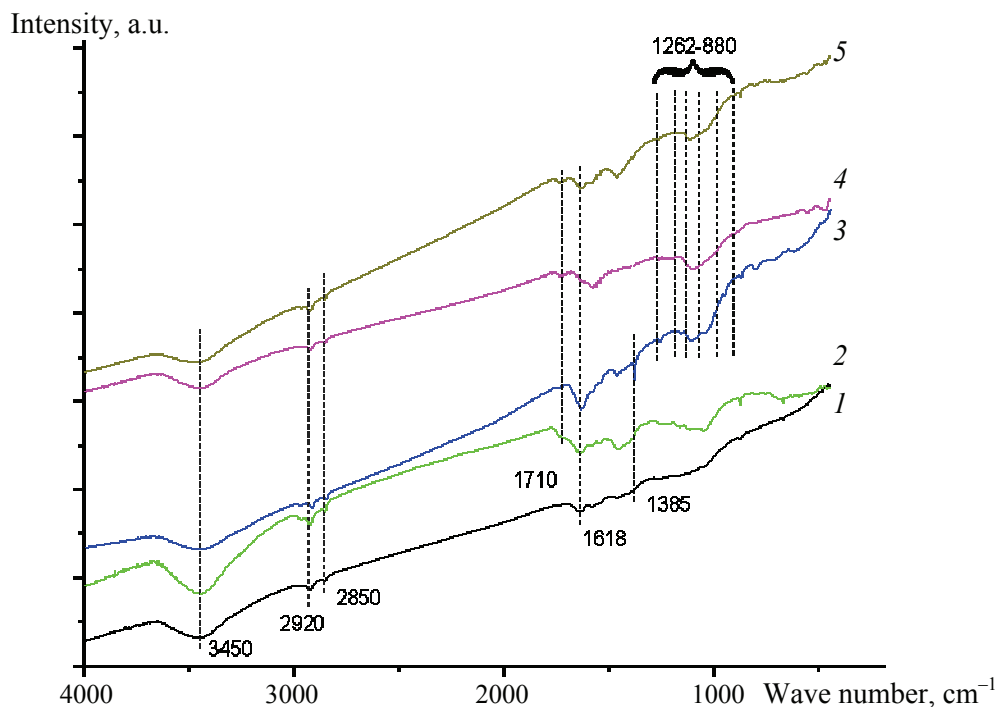


Fig. 1. IR spectra of the original (1) oxidized with nitric acid for 2 hours (2), silanized without pre-oxidation (3) and after pre-oxidation for 2 (4) and 10 (5) hours

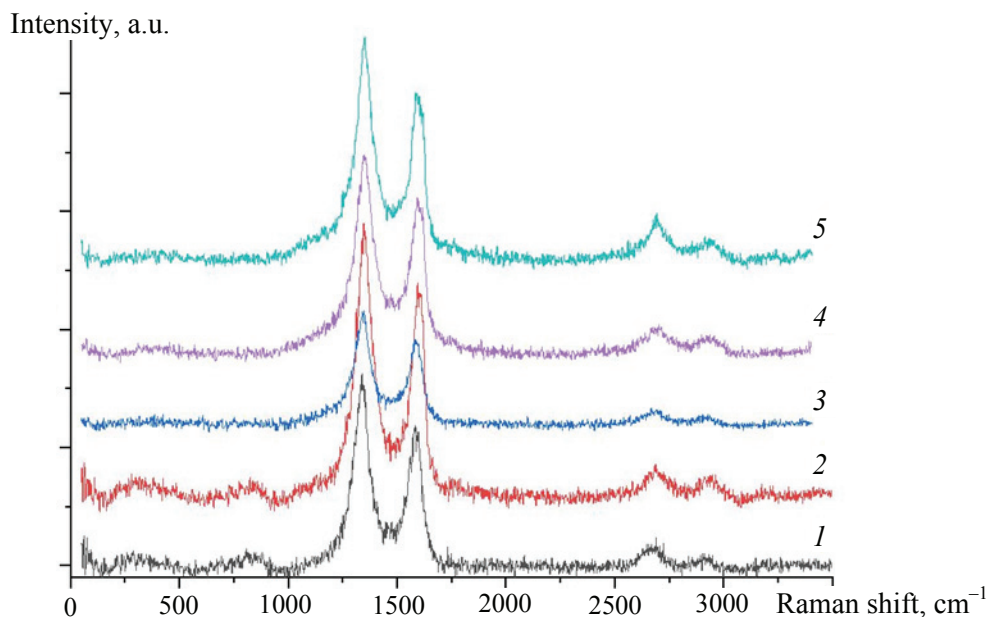


Fig. 2. Raman scattering spectra of CNTs: original (1); silanized without preliminary preparation (2); oxidized for 2 (3), and 10 (4) hours; silanized after preliminary oxidation for 5 (5) hours

In some cases, silanization contributes to an increase in the value of 2D/G due to the formation of a modifying layer of silanes or functional groups containing alkyl fragments.

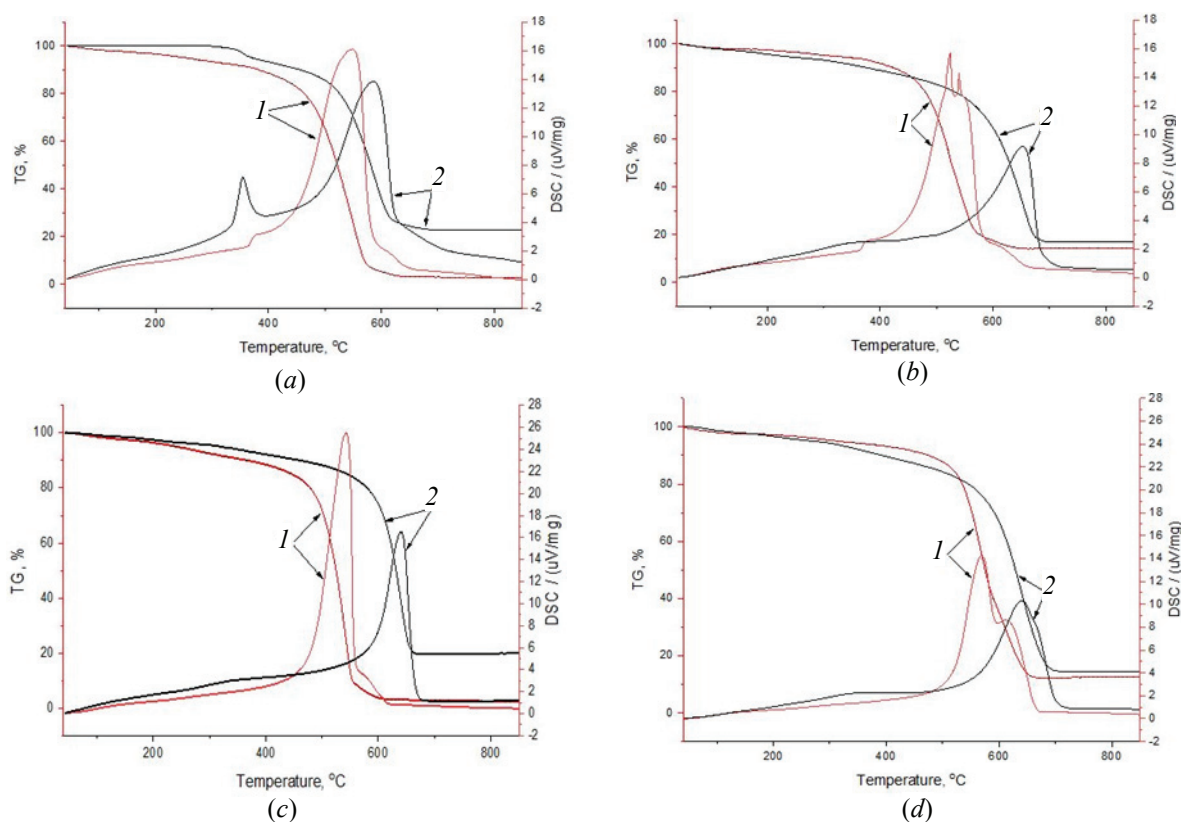
The data of TG/DSC analysis (Fig. 3) shows that the nature of the interaction between CNTs and 3-aminopropyltriethoxysilane and the behavior of the modified form upon thermal treatment depend on the

duration of the preliminary oxidation of CNTs. The behavior of the original CNTs (Fig. 3a, curves 1) is typical and was previously explained in detail in other papers [19].

Silanization in some cases contributes to an increase in the value of 2D/G due to the formation of a modifying layer of silanes or functional groups containing alkyl fragments.

Table 3. Results of processing of Raman spectra of original, oxidized and silanized CNTs

Sample	G Peak position, cm^{-1}	D/G	2D/G
Original CNTs	1584	0.85	1.69
CNTs oxidized for 2 hours	1599	0.84	1.68
CNTs oxidized for 5 hours	1592	0.85	1.69
CNTs oxidized for 10 hours	1610	0.84	1.67
CNTs silanized without pre-oxidation	1586	0.85	1.69
CNTs silanized after oxidation for 2 hours	1593	0.85	1.69
CNTs silanized after oxidation for 5 hours	1584	0.85	1.70
CNTs silanized after oxidation for 10 hours	1593	0.85	1.69

**Fig. 3.** TG and DSC-curves in air of original (a) and oxidized CNTs for 2 (b), 5 (c) and 10 (d) hours before (1) and after (2) silanization

The data of TG/DSC analysis (Fig. 3) show that the nature of the interaction between CNTs and 3-aminopropyltriethoxysilane and the behavior of the modified CNTs upon thermal treatment depend on the duration of the preliminary oxidation of CNTs. The behavior of the original CNTs (Fig. 3a, curves 1) is typical and was previously explained in detail in other studies [19].

The TG/DSC curves of the sample obtained by silanization of the original CNTs (Fig. 3a, curves 2)

contain 2 separate regions corresponding to the decomposition of CNTs and 3-aminopropyltriethoxysilane. The silanized CNTs are noticeably more thermally stable than the original ones; however, it can be assumed that in this case the modifier (3-aminopropyltriethoxysilane) does not form covalent bonds with the nanotube surface, but non-covalent modification takes place.

As a result of silanization of oxidized CNTs, we obtained materials whose intense thermal

decomposition begins 100–150 °C later than the corresponding nanotubes before modification (Fig. 3*b–d*). The change in the nature of the TG/DSC curves indicates a change in the nature of the interaction between CNTs and 3-aminopropyltriethoxysilane and the formation of chemical bonds between them. The best thermal stability is shown by the sample obtained by silanization of CNTs preliminarily oxidized for 5 hours.

3.2. Investigation of the properties of silicone nanocomposites

To find out the nature of the distribution of CNTs in the silicone matrix, Raman maps of nanocomposites were recorded (Fig. 4) and the intensity of the G-peak signal at different points of the surface was analyzed.

There is no G-peak signal on the Raman map of the surface of the nanocomposite obtained by adding

0.5 wt. % of the original CNTs to silicone (Fig. 4*a*). This indicates that the nanotubes are located in the bulk of the polymer matrix, at a considerable distance from the surface layer.

Regions up to 20 × 20 μm in size with a high intensity of the G-peak signal are found on the Raman map of the sample obtained by introducing the same amount of silanized CNTs into silicone (Fig. 4*b*). This indicates the tendency of this type of CNT to be localized in the surface layer of the composite.

A comparison of the Raman maps of samples containing 1 wt. % of the original (Fig. 4*c*) and silanized (Fig. 4*d*) CNTs shows that in the second case, the surface layer of the nanocomposite contains a larger amount of CNTs. As in the previous case, they form “islands” with transverse dimensions up to 20 μm.

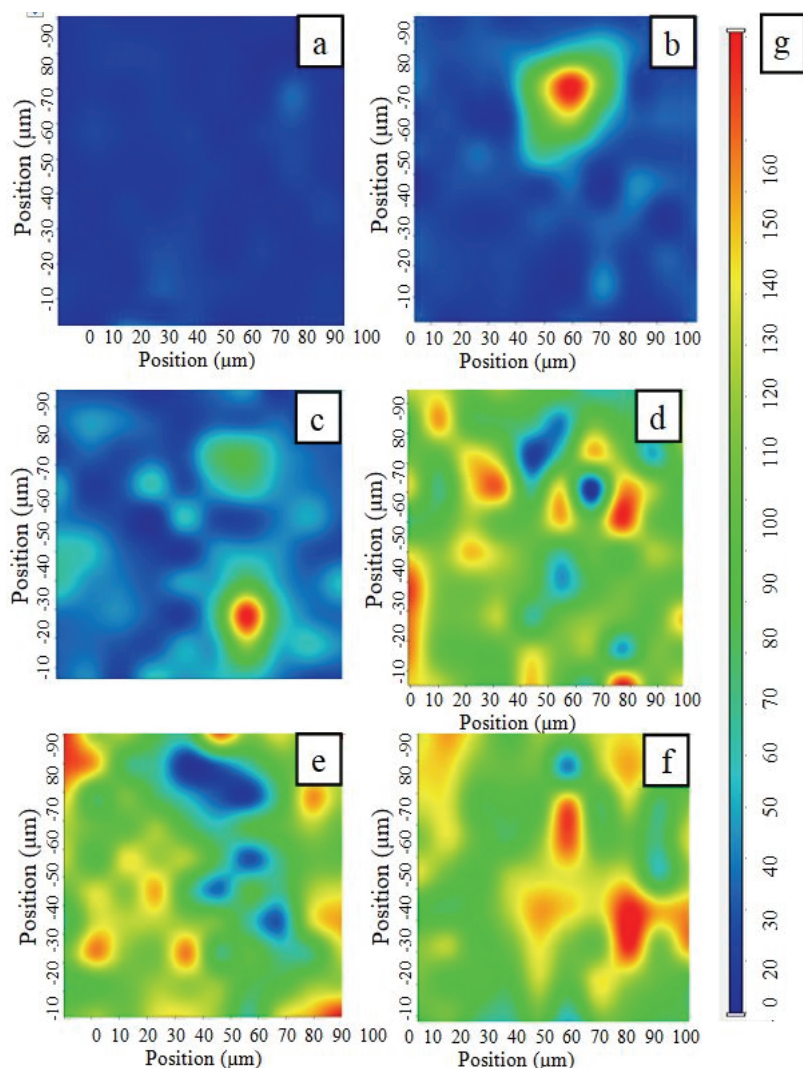


Fig. 4. Raman maps of the surface of silicone nanocomposites containing 0.5 (*a, b*), 1 (*c, d*) and 3 (*e, f*) original (*a, c, e*) and silanized (*b, d, f*) CNTs and the G-peak signal intensity scale (*g*)

When comparing the composition of the surface of composites containing 3 wt. % of original (Fig. 4e) and silanized (Fig. 4f) CNTs, it can be concluded that the area of areas without CNTs in the second case is noticeably smaller.

Thus, silanization contributes to a more uniform distribution of CNTs in the surface layer of silicone composites.

Figure 5 shows the TG curves of the original silicone and nanocomposites containing 0.5–3 wt. % silanized CNTs. It should be noted that the original Silagerm 2111 silicone compound is quite thermally stable. Up to 300 °C, its weight remains unchanged, and intensive destruction begins after 400 °C. The introduction of silanized CNTs practically does not change the behavior of the material in the temperature range up to 300 °C, but makes it somewhat more stable at temperatures above 400 °C. It should also be noted that the original silicone after holding at a temperature of 300 °C for 3–4 hours, according to visual observations, loses its elasticity, becomes brittle, and crumbles, while the appearance and mechanical characteristics of the nanocomposites remain unchanged. A similar effect was previously described in [46].

Also, by the TG curves, one can notice a significant difference in the residual mass of the composites and the original silicone. Given that the composites contain no more than 3 wt. % CNTs, the residual mass of these materials should not differ from the corresponding parameter of the unmodified material by almost 20 wt. %. It can be assumed that the introduction of silanized CNTs form chemical bonds with the silicone matrix, contributing to the formation of a material with a much higher thermal stability in an inert atmosphere.

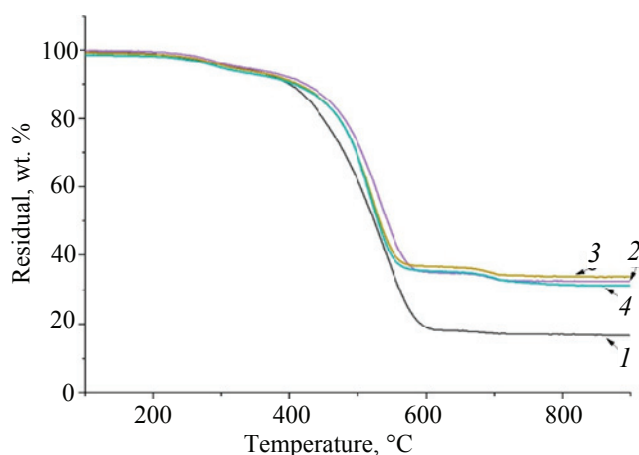


Fig. 5. TG curves in argon of the original silicone (1) and nanocomposites containing 0.5 (2), 1 (3) and 3(4) wt. % silanized CNTs

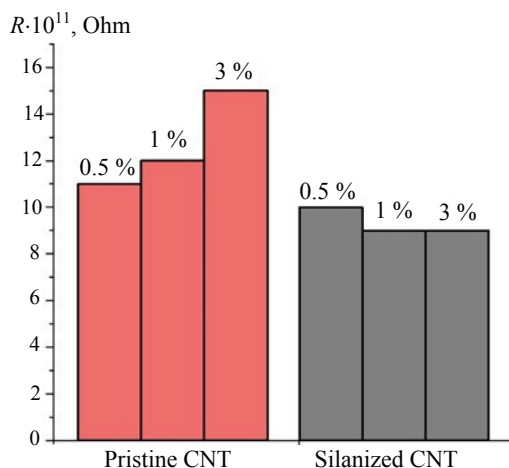


Fig. 6. Electrical resistance of nanocomposites containing original and silanized CNTs

Figure 6 shows data on the electrical resistance of the obtained nanocomposites. All obtained materials are dielectrics. According to [47], to achieve the percolation threshold and a noticeable increase in the electrical conductivity, more than 5 wt. % CNTs should be introduced into various polymer matrices. Possibly, in this case, too, a larger amount of conductive filler should have been introduced. We plan to obtain and study such nanocomposites in the future. However, a number of effects should also be noted here.

Thus, due to the significant agglomeration of the original CNTs in the silicone matrix, an increase in their concentration, contrary to expectations, leads not to a decrease, but to an increase in the electrical resistance of the material. Nanocomposites containing silanized CNTs, in general, have a lower resistance value than materials of a similar composition with original CNTs. With an increase in the concentration of silanized CNTs, there is a trend towards an increase in the electrically conductive properties of the nanocomposite due to the saturation of its surface layer with a conductive component. As a result, the electrical resistance of the nanocomposite containing 3 wt. % silanized CNTs is 1.5 times lower than that of the composite containing the same amount of original nanotubes.

4. Conclusion

The functionalization of the original and preliminarily oxidized carbon nanotubes with concentrated nitric acid for various times with 3-aminopropyltriethoxysilane was carried out. It is shown that the content of silicon in functionalized samples weakly depends on the oxidation conditions; however, CNTs containing the

largest amount of phenolic groups are silanized more efficiently. The presence of silanol groups in the composition of modified CNTs is proved by IR spectroscopy data. According to TG/DSC analysis, 3-aminopropyltriethoxysilane is not chemically bonded to the surface of unoxidized CNTs, while covalent bonds are formed with oxidized nanotubes. Raman mapping of the surface of silicone nanocomposites made it possible to establish that silanization contributes to a more uniform distribution of CNTs in the surface layer of the material. Introduction 0.5–3.0 wt. % silanized CNTs with silicone compound Silagerm 2111 contributed to an increase in its thermal stability and retention of the mechanical properties of the binder after exposure at a temperature of 300 °C. The resulting nanocomposites were dielectrics; however, composites containing 3 wt. % silanized CNTs had a 1.5 times higher electrical conductivity compared to composites containing a similar amount of original CNTs. The studies performed have shown the promise of using silanized CNTs as part of silicone nanocomposites in order to expand the operating temperature range, maintain mechanical properties after thermal exposure, and increase electrical conductivity.

5. Funding

This research received no external funding.

6. Acknowledgments

The study has been done using facilities of the shared access center “Production and application of multifunctional nanomaterials” (Tambov State Technical University).

7. Conflicts of Interest

The authors declare no conflict of interest.

References

1. Behera RP, Rawat P, Tiwari SK, Singh KK. A brief review on the mechanical properties of carbon nanotube reinforced polymer composites. *Materials Today: Proceedings*. 2020;22:2109-2117. DOI:10.1016/j.matpr.2020.03.277
2. Zakaria MR, Akil HM, Kudus MH, Ullah FA, Javed F, Nosbi N. Hybrid carbon fiber-carbon nanotubes reinforced polymer composites: A review. *Composites Part B: Engineering*. 2019;176:107313. DOI:10.1016/j.compositesb.2019.107313
3. Kondrashov SV, D'yachkova TP, Bogatov VA, Mansurova IA, Marakhovskii PS, Mokretsova IA, Fokin AS. Utilization of carbon nanotubes for enhancing the heat resistance of epoxy binders. *Inorganic Materials: Applied Research*. 2013;4(5):394-399. DOI:10.1134/s2075113313050092
4. Bokai L, Nam V, Xiaoying Z, Xiaolong F, Rabczuk T. Stochastic integrated machine learning based multiscale approach for the prediction of the thermal conductivity in carbon nanotube reinforced polymeric composites. *Composites Science and Technology*. 2022;224. DOI:10.1016/j.compscitech.2022.109425.
5. Matos MAS, Tagarielli VL, Pinho ST. On the electrical conductivity of composites with a polymeric matrix and a non-uniform concentration of carbon nanotubes. *Composites Science and Technology*. 2020;188:108003. DOI:10.1016/j.compscitech.2020.108003
6. Jackson EM, Laibinis PE, Collins WE, Ueda A, Wingard CD, Penn B. Development and thermal properties of carbon nanotube-polymer composites. *Composites Part B: Engineering*. 2016;89:362-373. DOI:10.1016/j.compositesb.2015.12.018
7. Mozaffarinasab H, Jamshidi M. Surface modification of carbon nanotubes by a bifunctional amine silane; effects on physical/mechanical/thermal properties of epoxy nanocomposite. *Progress in Organic Coatings*. 2023;179:107521. DOI:10.1016/j.porgcoat.2023.107521
8. Lotfi M, Yari H, Ganjaee MS, Azizi A. Fabrication of a highly hard yet tough epoxy nanocomposite coating by incorporating graphene oxide nanosheets dually modified with aminosilane coupling agent and hyperbranched polyester-amide. *Progress in Organic Coatings*. 2022;162:106570:0300-9440. DOI:10.1016/j.porgcoat.2021.106570
9. Yari H, Rostami M. Enhanced weathering performance of epoxy/ZnO nanocomposite coatings via functionalization of ZnO UV blockers with amino and glycidoxysilane coupling agents. *Progress in Organic Coatings*. 2020;147:105773. DOI:10.1016/j.porgcoat.2020.105773
10. Merkulova YI, Kondrashov SV, D'yachkova TP, Marakhovskii PS, Yurkov GY. Effect of carbon nanotubes dispersed in binder on properties of epoxy nanocomposite. *Russian Journal of Applied Chemistry*. 2015;88(11):1848-1854. DOI:10.1134/s10704272150110166
11. Xiguang L, Xuejun C, Chunxu Z, Xiandong Z, Guangshun W. Effects of different silanization followed via the sol-gel growing of silica nanoparticles onto carbon fiber on interfacial strength of silicone resin composites. *Chemical Physics Letters*. 2018;707:1-7. DOI:10.1016/j.cplett.2018.07.034
12. Gerasimova A, Dyachkova T, Memetov N, Chapaksov N, Melezhik A, Smirnova A, Usol'tseva N. Stabilization of pristine and oxidized carbon nanotubes dispersions in acidic and alkaline solutions. *Fullerenes, Nanotubes and Carbon Nanostructures*. 2022;30(1):191-198. DOI:10.1080/1536383X.2021.1961132
13. Zhangping W, Cheng X, Xin Q, Yonggang Z, Xuefei W, Shulin S, Mingzhi D, Cheng Z. A two-step carbon fiber surface treatment and its effect on the interfacial properties of CF/EP composites: The electrochemical oxidation followed by grafting of silane coupling agent. *Applied Surface Science*. 2019;486:546-554. DOI:10.1016/j.apsusc.2019.04.248
14. Osbeck S, Bradley RH, Liu C, Idriss H, Ward S. Effect of an ultraviolet/ozone treatment on the surface

texture and functional groups on polyacrylonitrile carbon fibres. *Carbon*. 2011;49(13):4322-4330. DOI:10.1016/j.carbon.2011.06.005

15. Boudou J, Paredes J, Cuesta A, Martínez-Alonso A, Tascón JM. Oxygen plasma modification of pitch-based isotropic carbon fibres. *Carbon*. 2003;41(1):41-56. DOI:10.1016/s0008-6223(02)00270-1

16. Xu Z, Chen L, Huang Y, Li J, Wu X, Li X, Jiao Y. Wettability of carbon fibers modified by acrylic acid and interface properties of carbon fiber/epoxy. *European Polymer Journal*. 2008;44(2):494-503. DOI:10.1016/j.eurpolymj.2007.11.021

17. Wen Z, Xu C, Qian X, Zhang Y, Wang X, Song S, Zhang C. A two-step carbon fiber surface treatment and its effect on the interfacial properties of CF/EP composites: The electrochemical oxidation followed by grafting of silane coupling agent. *Applied Surface Science*. 2019;486:556-554. DOI:10.1016/j.apsusc.2019.04.248

18. Dyachkova TP, Khan YA, Orlova NV, Kondrashov SV. Oxidation of multiwalled carbon nanotubes by hydrogen peroxide vapor: laws and effects. *Vestnik Tambovskogo gosudarstvennogo tekhnicheskogo universiteta*. 2016;22(2):323-333. DOI:10.17277/vestnik.2016.02.pp.323-333 (In Russ.)

19. Dyachkova TP, Melezhyk AV, Gorsky SYu, Anosova IV, Tkachev AG. Some aspects of functionalization and modification of carbon nanomaterials. *Nanosystems: Physics, Chemistry, Mathematics*. 2013;4:605-621.

20. Alam MN, Kumar V, Lee DJ, Choi J. Synergistically toughened silicone rubber nanocomposites using carbon nanotubes and molybdenum disulfide for stretchable strain sensors. *Composites Part B: Engineering*. 2023;259:110759. DOI:10.1016/j.compositesb.2023.110759

21. Nabeel M, Kuzsella L, Viskolcz B, Kollar M, Fiser B, Vanyorek L. Synergistic effect of carbon nanotubes and carbon black as nanofillers of silicone rubber pressure sensors. *Arabian Journal of Chemistry*. 2023;16(4):104594. DOI:10.1016/j.arabjc.2023.104594

22. Song P, Song J, Zhang Y. Stretchable conductor based on carbon nanotube/carbon black silicone rubber nanocomposites with highly mechanical, electrical properties and strain sensitivity. *Composites Part B: Engineering*. 2020;107979. DOI:10.1016/j.compositesb.2020.107979

23. Yang H, Yuan L, Yao X, Zheng Z, Fang D. Monotonic strain sensing behavior of self-assembled carbon nanotubes/graphene silicone rubber composites under cyclic loading. *Composites Science and Technology*. 2020;108474. DOI:10.1016/j.compscitech.2020.108474

24. Hu H, Zhao L, Liu J, Liu Y, Cheng J, Luo J, Zhao J. Enhanced dispersion of carbon nanotube in silicone rubber assisted by graphene. *Polymer*. 2012;53(15):3378-3385. DOI:10.1016/j.polymer.2012.05.039

25. Ouyang Y, Zongxian Y, Tianyang L, Huafeng T, Liuyang B, Xiaofei L, Fangli Y. Preparation of branched Al₂O₃ and its synergistic effect with carbon nanotubes on the enhancement of thermal conductive and electrical insulation properties of silicone rubber composites.

Materials Today Communications. 2022;34:105239. DOI:10.1016/j.mtcomm.2022.105239

26. Kumar V, Kumar A, Han SS, Park SS. RTV silicone rubber composites reinforced with carbon nanotubes, titanium-di-oxide and their hybrid: Mechanical and piezoelectric actuation performance. *Nano Materials Science*. 2021;3(3):233-240. DOI:10.1016/j.nanoms.2020.12.002

27. Shimizu T, Kishi R, Kobashi K, Morimoto T, Okazaki T, Yamada T, Hata K. Improved thermal stability of silicone rubber nanocomposites with low filler content, achieved by well-dispersed carbon nanotubes. *Composites Communications*. 2020;22:100482. DOI:10.1016/j.coco.2020.100482

28. Chen H, Wei H, Chen M, Meng F, Li H, Li Q. Enhancing the effectiveness of silicone thermal grease by the addition of functionalized carbon nanotubes. *Applied Surface Science*. 2013;283:525-531. DOI:10.1016/j.apsusc.2013.06.139

29. Liu Y, Shao Y, Wang Y, Wang J. An abrasion-resistant, photothermal, superhydrophobic anti-icing coating prepared by polysiloxane-modified carbon nanotubes and fluorine-silicone resin. *Colloids and Surfaces A: Physicochemical and Engineering Aspects*. 2022;648:129335. DOI:10.1016/j.colsurfa.2022.129335

30. Song Y, Phule AD, Yu Z, Zhang X, Du A, Wang H, Zhang ZX. Lightweight and flexible silicone rubber foam with dopamine grafted multi-walled carbon nanotubes and silver nanoparticles using supercritical foaming technology: Its preparation and electromagnetic interference shielding performance. *European Polymer Journal*. 2021;161:110839. DOI:10.1016/j.eurpolymj.2021.110839

31. Vast L, Mekhalif Z, Fonseca A, Nagy BJ, Delhalle J. Preparation and electrical characterization of a silicone elastomer composite charged with multi-wall carbon nanotubes functionalized with 7-octenyltrichlorosilane. *Composites Science and Technology*. 2007;67(5):880-889. DOI:10.1016/j.compscitech.2005.12.033

32. Jiang MJ, Dang ZM, Xu HP. Enhanced electrical conductivity in chemically modified carbon nanotube/methylvinyl silicone rubber nanocomposite. *European Polymer Journal*. 2007;43(12):4924-4930. DOI:10.1016/j.eurpolymj.2007.09.022

33. Vast L, Mekhalif Z, Fonseca A, Nagy JB, Delhalle J. Preparation and electrical characterization of a silicone elastomer composite charged with multi-wall carbon nanotubes functionalized with 7-octenyltrichlorosilane. *Composites Science and Technology*. 2007;67(5):880-889. DOI:10.1016/j.compscitech.2005.12.033

34. Melezhyk AV, Romantsova IV, D'yachkova TP, Bychkov ON, Shlykova AA, Smykov MA, Tkachev AG, Golovin YuI. Effect of the matrix composition on activity of metal oxide catalysts in CVD synthesis of carbon nanotubes. *Russian Journal of Applied Chemistry*. 2012;85(5):782-787. DOI:10.1134/s1070427212050175

35. Boehm HP. Chemical identification of surface groups. *Advances in Catalysis and Related Subjects*. 1996;16:179-274. DOI:10.1016/S0360-0564(08)60354-5

36. Dyachkova TP, Rukhov AV, Tkachev AG, Tugolukov EN. Functionalization of carbon nanotubes:

methods, mechanisms and technological realization. *Advanced Materials and Technologies*. 2018;2:18-41. DOI:10.17277/amt.2018.02.pp.018-041

37. Shanmugaraj A, Bae J, Lee K, Noh W, Lee S, Ryu S. Physical and chemical characteristics of multiwalled carbon nanotubes functionalized with aminosilane and its influence on the properties of natural rubber composites. *Composites Science and Technology*. 2007;67(9):1813-1822. DOI:10.1016/j.compscitech.2006.10.021

38. Avilés F, Sierra-Chi CA, Nistal AMP, Rubio AF, Rubio J. Influence of silane concentration on the silanization of multiwall carbon nanotubes. *Carbon*. 2013;57:520-529. DOI:10.1016/j.carbon.2013.02.031

39. Mozaffarinasab H, Jamshidi M. Surface modification of carbon nanotubes by a bifunctional amine silane; effects on physical/mechanical/thermal properties of epoxy nanocomposite. *Progress in Organic Coating*. 2023;179:107521. DOI:10.1016/j.porgcoat.2023.107521

40. Murugesan S, Myers K, Subramanian V. Amino-functionalized and acid treated multi-walled carbon nanotubes as supports for electrochemical oxidation of formic acid. *Applied Catalysis B: Environmental*. 2011;103(3-4):266-274. DOI:10.1016/j.apcatb.2010.07.038

41. Prasad K, Kyung H. Modification of β -cyclodextrin-carbon nanotube-thermally reduced graphite oxide by using ambient plasma for electrochemical sensing of ascorbic acid. *Chemical Physics Letters*. 2019;730:306-11. DOI:10.1016/j.cplett.2019.06.032

42. Vennerberg D, Hall R, Kessler MR. Supercritical carbon dioxide-assisted silanization of multi-walled carbon

nanotubes and their effect on the thermo-mechanical properties of epoxy nanocomposites. *Polymer*. 2014;55(16):4156-4163. DOI:10.1016/j.polymer.2014.06.020

43. Lavorgna M, Romeo V, Martone A, Zarrelli M, Giordano M, Buonocore GG, Xia HS. Silanization and silica enrichment of multiwalled carbon nanotubes: Synergistic effects on the thermal-mechanical properties of epoxy nanocomposites. *European Polymer Journal*. 2013;49(2):428-438. DOI:10.1016/j.eurpolymj.2012.10.003

44. Keszler AM, Nemes L, Ahmad SR, Fang X. Characterization of carbon nanotube materials by Raman spectroscopy and microscopy – A case study of multiwalled and singlewalled samples. *Journal of Optoelectronics and Advanced Materials*. 2004;6(4):1269-1274.

45. Pimenta MA, Dresselhaus G, Dresselhaus MS, Cançado LG, Jorio A, Saito R. Studying disorder in graphite-based systems by Raman spectroscopy. *Physical Chemistry Chemical Physics*. 2007;9(11):1276-1290. DOI:10.1039/b613962k

46. Kong J, Tong Y, Sun J, Wei Y, Thitsartarn W, Jayven CCY, He C. Electrically conductive PDMS-grafted CNTs-reinforced silicone elastomer. *Composites Science and Technology*. 2018;159:208-215. DOI:10.1016/j.compscitech.2018.02.018

47. Punetha VD, Rana S, Yoo HJ, Chaurasia A, McLeskey JT, Ramasamy MS, Cho JW. Functionalization of carbon nanomaterials for advanced polymer nanocomposites: A comparison study between CNT and graphene. *Progress in Polymer Science*. 2017;67:1-47. DOI:10.1016/j.progpolymsci.2016.12.010

Information about the authors / Информация об авторах

Anastasia V. Khrobak, Graduate Student, Tambov State Technical University (TSTU), Tambov, Russian Federation; ORCID 0000-0001-9732-763X; e-mail: nastiarx@yandex.ru

Tatyana P. Dyachkova, D. Sc. (Chem.), Professor, TSTU, Tambov, Russian Federation; ORCID 0000-0002-4884-5171; e-mail: dyachkova_tp@mail.ru

Nikolay A. Chapaksov, Senior Assistant, TSTU, Tambov, Russian Federation; ORCID 0000-0001-9076-9400; e-mail: tchapaxov.nikolaj@yandex.ru

Dmitry A. Poluboyarinov, Master's Student, TSTU, Tambov, Russian Federation; e-mail: poluboiarinow@yandex.ru

Хробак Анастасия Витальевна, аспирант, Тамбовский государственный технический университет (ТГТУ), Тамбов, Российская Федерация; ORCID 0000-0001-9732-763X; e-mail: nastiarx@yandex.ru

Дьячкова Татьяна Петровна, доктор химических наук, профессор, ТГТУ, Тамбов, Тамбов, Российская Федерация; ORCID 0000-0002-4884-5171; e-mail: dyachkova_tp@mail.ru

Чапаксов Николай Андреевич, ассистент, ТГТУ, Тамбов, Российская Федерация; ORCID 0000-0001-9076-9400; e-mail: tchapaxov.nikolaj@yandex.ru

Полубояринов Дмитрий Алексеевич, магистрант, ТГТУ, Тамбов, Российская Федерация; e-mail: poluboiarinow@yandex.ru

Received 05 May 2023; Accepted 14 June 2023; Published 06 July 2023



Copyright: © Khrobak AV, Dyachkova TP, Chapaksov NA, Poluboyarinov DA, 2023. This article is an open access article distributed under the terms and conditions of the Creative Commons Attribution (CC BY) license (<https://creativecommons.org/licenses/by/4.0/>).

Influence of few-layer graphene on the complex of strength and thermophysical properties of polymer composites obtained by DLP by 3D printing

© Aleksei A. Vozniakovskii^a, Sergey V. Kidalov^a, Alexander P. Voznyakovskii^b,
Nikita D. Podlozhnyuk^a, Sofia I. Titova^a, Evgenii V. Auchynnika^c

^a Ioffe Institute, 26, Politekhnikeskaya St., St. Petersburg, 194021, Russian Federation,

^b Scientific Research Institute of Synthetic Rubber, 1, Gapsalskaya St., St. Petersburg, 198035, Russian Federation,

^c Yanka Kupala State University of Grodno, 22, Eliza Ozheshko St., Grodno, 230023, Belarus

✉ alexey_inform@mail.ru

Abstract: The digital light processing method (DIGITAL LIGHT PROCESSING or DLP) is one of the most affordable 3D printing methods, which allows you to obtain high-precision products, which, however, are inferior in their characteristics to products obtained by other 3D printing methods. Due to their high characteristics, graphene nanostructures can solve this problem by acting as effective modifying additives. However, despite all the promise of this approach, the introduction of graphene nanostructures into actual practice has not yet occurred due to their high cost due to the imperfection of the methods of their synthesis. The paper considers the effectiveness of using few-layer graphene synthesized according to the author's method under conditions of self-propagating high-temperature synthesis from cellulose as a modifying additive to improve the complex strength and thermophysical properties of products from photopolymer resins obtained by DLP 3D printing. It was found that adding few-layer graphene makes it possible to increase Brinell hardness up to 1.8 times, bending strength up to 1.5 times, and thermal conductivity up to 2.2 times compared to the original polymer when using no more than two wt. % few-layer graphene. The data obtained indicate the high efficiency of the synthesized few-layer graphene as a modifying additive in creating products from photopolymer resins using the DLP 3D printing method.

Keywords: polymer composites; digital light processing; few-layer graphene; hardness; bending strength; thermal conductivity; heat capacity.

For citation: Vozniakovskii AA, Kidalov SV, Voznyakovskii AP, Podlozhnyuk ND, Titova SI, Auchynnika EV. Influence of few-layer graphene on the complex of strength and thermophysical properties of polymer composites obtained by DLP by 3D printing. *Journal of Advanced Materials and Technologies*. 2023;8(2):103-110. DOI: 10.17277/jamt.2023.02.pp.103-110

Влияние малослойного графена на комплекс прочностных и теплофизических свойств полимерных композитов, полученных DLP-методом 3D-печати

© А. А. Возняковский^a✉, С. В. Кидалов^a, А. П. Возняковский^b,
Н. Д. Подложнюк^a, С. И. Титова^a, Е. В. Овчинников^c

^a Физико-технический институт им. А.Ф. Иоффе РАН,
ул. Политехническая, 26, Санкт-Петербург, 194021, Российская Федерация,

^b Научно-исследовательский институт синтетического каучука имени академика С. В. Лебедева,
ул. Гапсальская, 1, Санкт-Петербург, 198035, Российская Федерация,

^c Гродненский государственный университет им. Янки Купалы,
ул. Элизы Ожешко, 22, Гродно, 230023, Республика Беларусь

✉ alexey_inform@mail.ru

Аннотация: Рассмотрена эффективность применения малослойного графена (число слоев не более 5), синтезированного по авторской методике в условиях самораспространяющегося высокотемпературного синтеза из целлюлозы в качестве модифицирующей добавки для повышения комплекса прочностных и теплофизических

свойств изделий из фотополимерных смол, полученных методом DLP 3D-печати. Несмотря на высокие характеристики графеновых наноструктур, к которым относится и малослойный графен, данный класс материалов до сих пор не применяется в промышленности из-за невозможности синтеза больших объемов материала высокого качества и с приемлемой себестоимостью. Предложенный метод синтеза позволяет получать большие объемы малослойного графена, не содержащего в своей структуре дефекты Стоуна–Уэйлса. Установлено, что добавление малослойного графена позволяет добиться роста твердости по Бринеллю до 1,8 раз, прочности на изгиб до 1,5 раз и теплопроводности до 2,2 раз по сравнению с исходным полимером при использовании не более 2 масс. % малослойного графена. Дальнейшее увеличение концентрации малослойного графена не привело к дальнейшему росту свойств конечного композита. Полученные данные свидетельствуют о высокой эффективности синтезированного малослойного графена в качестве модифицирующей добавки при создании изделий из фотополимерных смол методом DLP 3D-печати.

Ключевые слова: полимерные композиты; DLP; малослойный графен; твердость; прочность на изгиб; теплопроводность; теплоемкость.

Для цитирования: Vozniakovskii AA, Kidalov SV, Voznyakovskii AP, Podlozhnyuk ND, Titova SI, Auchynnikau EV. Influence of few-layer graphene on the complex of strength and thermophysical properties of polymer composites obtained by DLP by 3D printing. *Journal of Advanced Materials and Technologies*. 2023;8(2):103-110. DOI: 10.17277/jamt.2023.02.pp.103-110

1. Introduction

Over the past 10 years, 3D printing as a technique for creating finished polymer products has come a long way in development and has become available to a wide range of both researchers and ordinary consumers [1]. One of the varieties of 3D printing technique is the digital light processing method (DIGITAL LIGHT PROCESSING or DLP). This technique is based on the layer-by-layer polymerization of resins under the influence of light [2]. Compared to other 3D printing techniques, such as Fused Deposition Modeling (FDM), DLP produces end products with precise dimensions and shapes. Also, this method is more productive (has a higher printing speed) [3].

The main disadvantage of the DLP method is the relatively low strength of the final products compared to products obtained, for example, by the FDM method. One of the most promising ways to solve this problem is the creation of composite materials using graphene nanostructures as filler. The reason for this is their superior performance. Considering the properties of single-layer graphene, it should be noted that its thermal conductivity is up to $5000 \text{ W} \cdot (\text{m} \cdot \text{K})^{-1}$ [4], Young's modulus is up to 1 TPa [5], while its specific surface is estimated at $2630 \text{ m}^2 \cdot \text{g}^{-1}$ [6]. However, obtaining a “true” single-layer graphene in the form of a powder, even in gram quantities, is an extremely difficult task; therefore, the so-called graphene nanostructures, which are particles consisting of 2–10 layers of graphene [7]. Despite the fact that the properties of graphene nanostructures decrease with an increase in the number of graphene layers [8], many studies, including [9–11], noted the high efficiency of graphene nanostructures when creating products from polymer composites using DLP 3D printing. At the same time, graphene

nanostructures make it possible to obtain a higher increase in properties at the same concentrations compared to classical fillers such as carbon black [12, 13] or graphite [14]. For example, in [15], the authors noted that the addition of even large volumes of carbon black (up to 50 wt. %) does not lead to a significant increase in the thermal conductivity of the polymer matrix at temperatures up to 70 °C.

However, the researchers also note that the experimental results of using graphene nanostructures do not match the theoretical estimates. The main reasons for this discrepancy include the presence of various structural defects in graphene nanostructures, which can significantly reduce their characteristics [16]. One of the types of structural defects in graphene nanostructures are the Stone-Wales defects. The Stone-Wales defect, which occurs due to a 90° rotation of adjacent carbon atoms about their center, is a connected carbon ring with five and seven carbon atoms. It was shown in [17] that such defects reduce the efficiency of using graphene nanostructures in polymer composites.

In previous papers [18, 19], we described the developed procedure for the synthesis of few-layer graphene (FLG), containing no more than 5 graphene layers in its structure, from cyclic biopolymers under conditions of self-propagating high-temperature synthesis (SHS). At the same time, such MGs were devoid of Stone–Wales defects in their structure [20]. In [21], we showed that synthesized FLG can significantly improve the complex of strength and thermal properties of nitrile butadiene rubber.

The purpose of this paper is to study the effect of FLG synthesized from cellulose under SHS conditions on the complex of strength and thermophysical properties of products made of polymer composites based on photopolymer resins obtained by DLP 3D printing.

2. Materials and Methods

2.1. Materials

A commercial photopolymer resin of the Anycubic brand (405 nm, Anycubic, China) was taken as the starting material for the creation of polymer composites. FLG synthesized from cellulose under the conditions of the SHS process was taken as a modifying additive. The procedure for synthesizing FLG was described in detail in [18].

2.2. Methods

2.2.1. Synthesis of polymer composites

Powdered portions of FLG were added to the original photopolymer resin with constant stirring (500 rpm) using an overhead stirrer. Samples were added in portions of 1/10 of the mass of the entire sample. The FLG concentration was 0.25–4.00 wt. %. After adding the entire sample, the resulting suspension was additionally stirred for 30 minutes at 1000 rpm and the resulting suspensions were treated in the ultrasonic field (ultrasonic bath, 22 kHz) for 30 minutes. From the resulting suspensions, samples were printed using the DLP 3D printing method (Anycubic Photon S printer, China). The thickness of each of the successive layers subjected to irradiation for curing was 0.1 mm, exposure time 8 seconds. Figure 1 shows various variants of the samples obtained in the study.

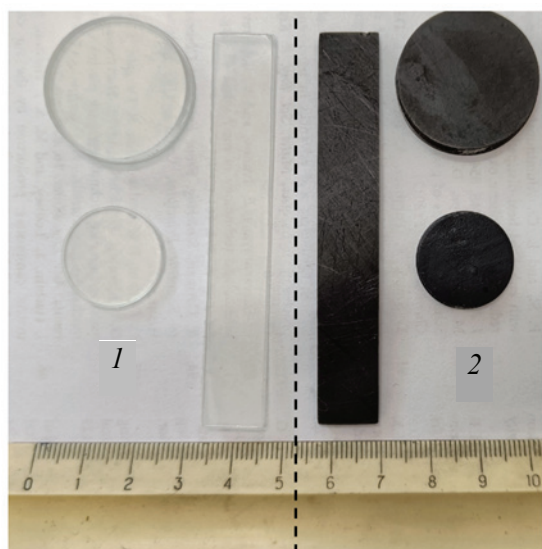


Fig. 1. The appearance of products made of polymer composites based on photopolymer resins obtained by DLP by 3D printing: 1 – obtained from unmodified resin (transparent samples); 2 – from modified resin at an FLG concentration of 2 wt. % (black samples)

The resulting samples after 3D printing were additionally processed with a UV lamp with a wavelength of 405 nm for 30 minutes (UV radiation power 50 W). This exposure time was due to the cessation of changes in the properties of the samples at a longer exposure.

2.2.2. Study of few-layer graphene parameters

Electronic images of FLG were obtained with a Tescan Mira 3M scanning electron microscope (SEM) (Tescan, Brno, Czech Republic). The accelerating voltage was 20 kV. The diffraction pattern of the FLG sample was obtained on an XRD-7000 X-ray diffractometer (Shimadzu, Kyoto, Japan). The shooting speed was 0.5 degrees/min, $\text{CuK}\alpha = 0.154051$ nm. The Raman spectrum (RSS) of FLG was obtained on a Confotec NR500 instrument (SOL Instruments, Minsk, Belarus). The laser length was 532 nm. The dispersion of FLG particles was measured by laser diffraction using a Malvern Mastersizer 2000 instrument (Malvern Instruments, Malvern, UK). For measurements, a sample of FLG (0.25 wt. %) was dispersed in water by ultrasonic treatment (ultrasonic bath, 22 kHz) for 30 minutes.

2.2.3. Study of the properties of polymer composites

Hardness measurements were carried out by the Brinell method on an ITB 3000 AM hardness tester (Metrotest, Neftekamsk, Russia). For measurements, a ball of 2.5 mm was used; the load was 62.5 kgf, in accordance with Russian Standard 23677-79. The samples were disks 5 mm thick and 20 mm in diameter. The measurement error was 5%. Measurements of bending strength were carried out on a hydraulic press PM-FLG4 (Stroypribor, Chelyabinsk, Russia) in accordance with Russian Standard 4648-2014. The samples were plates 80 mm long, 10 mm wide and 3 mm thick. The measurement error was 6%. The thermal conductivity and heat capacity were measured by the monotonic cooling method on a KITT Polymer instrument (Teplofon Design Bureau, Novomoskovsk, Russia) in accordance with Russian Standard 23630.1-79. The samples were disks 10 mm in diameter and 2 mm thick.

3. Results and Discussion

Figure 2 shows a micrograph of the FLG surface obtained by SEM. As can be seen from Fig. 2, the few-layer graphene used as a modifying additive consisted of aggregates of flat particles with linear sizes up to several tens of microns, which is confirmed by the results of measuring the dispersion presented in Fig. 3.

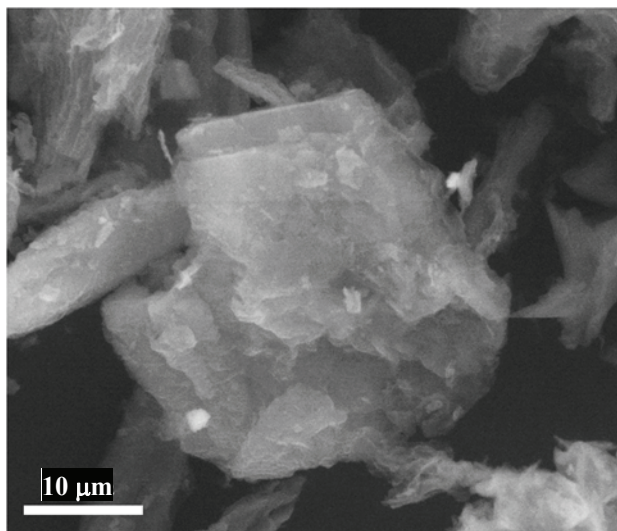


Fig. 2. Electronic image of few-layer graphene. Linearscale – 10 μm

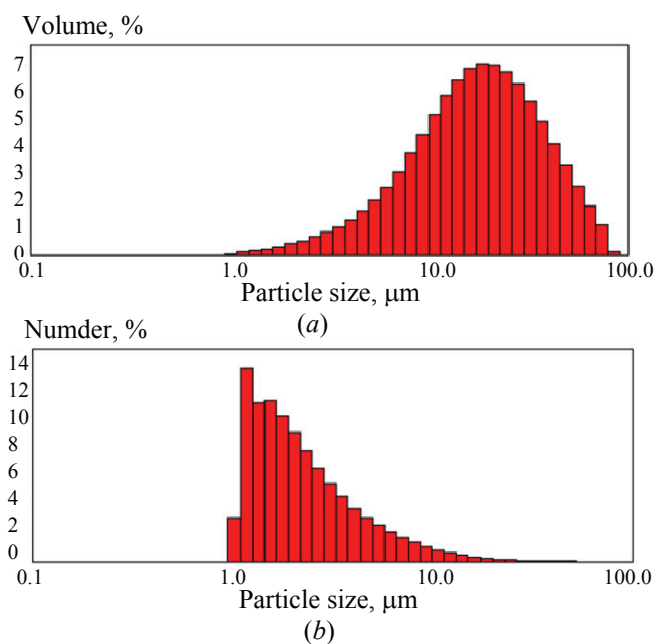


Fig. 3. Results of particle dispersion measurement:
a particle dispersion distribution by volume;
b particle dispersion distribution by the number of particles

As can be seen from Fig. 3, despite the fact that the sample contains particles with a dispersion of up to several tens of microns, the number of such particles is small, and most of the particles have a dispersion of 1–5 microns.

Figure 4 shows the results of the FLG study by Raman spectroscopy.

As can be seen from Fig. 4, the FLG sample spectrum contains peaks D 1391 cm^{-1} , G 1586 cm^{-1} typical for graphene nanostructures and a region $2250\text{--}3250\text{ cm}^{-1}$ (2D region) with a superposition of

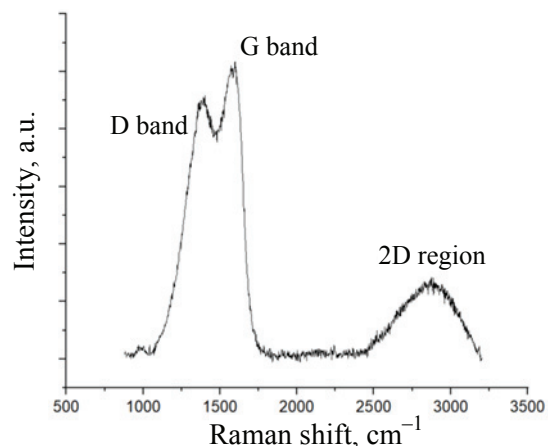


Fig. 4. Raman spectrum of FLG sample

many peaks characteristic of graphene structures (D*, 2D, D+D' and 2D') [22]. As noted in [23], such Raman spectra are characteristic of graphene nanostructures with various folds, which are not point defects. Since, due to the broadening of the 2D region, it is impossible to determine the number of layers in the sample based on the position and shape of the 2D peak [24], we additionally conducted FLG studies using the X-ray diffraction method.

Figure 5 shows the diffraction pattern of the FLG sample in the 2θ range of angles from 10 to 35 degrees.

Based on the position of the 002 peak, as well as the FWHM of the 002 peak, the crystallite size (L) was calculated using the Scherrer formula [25], which, together with the data on the interplanar distance (d), made it possible to determine the number of layers in the synthesized sample (N) using the formula $L = N/d$ (Table 1).

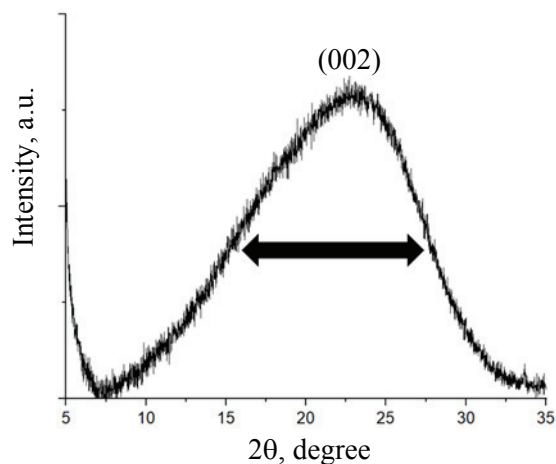


Fig. 5. Diffraction pattern of the few-layer graphene

Table 1. Results of calculating the number of layers

Crystallite size L , nm	Interplanar spacing d , nm	Number of layers N
1.50	0.38	4

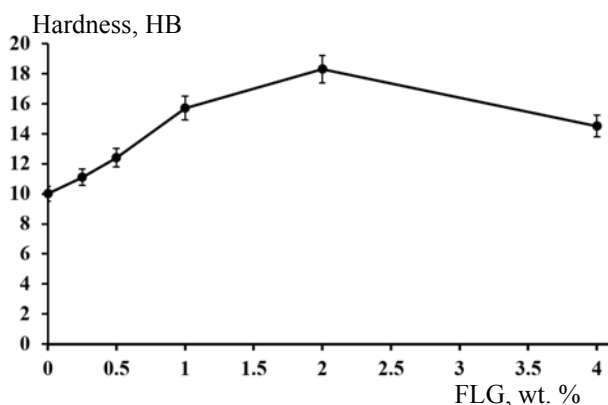
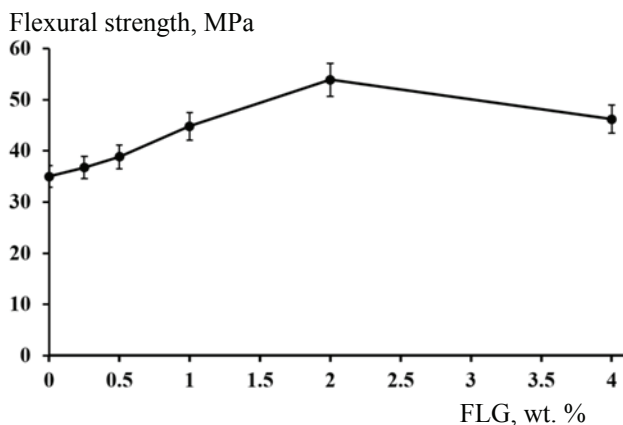
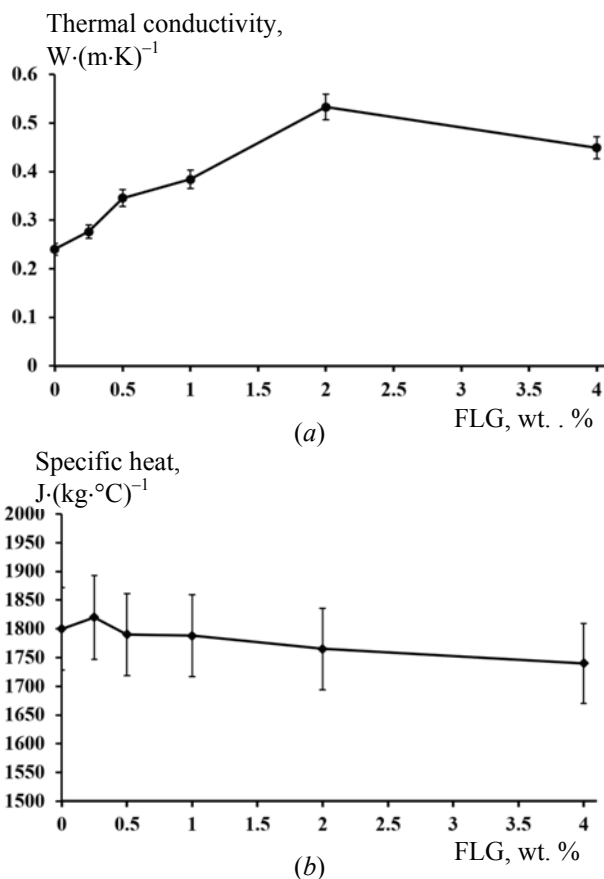
As can be seen from Table 4, the synthesized FLG particles consist of no more than 4 layers of graphene.

We consider the FLG influence on the complex of strength and thermophysical properties of final polymer composites.

Figures 6 and 7 show the results of a study of Brinell hardness and bending strength of synthesized polymer resin samples.

As can be seen from Figs. 6 and 7, the introduction of FLG in small amounts makes it possible to increase the Brinell hardness up to 1.8 times and the bending strength up to 1.5 times at a FLG concentration of not more than 2 wt. %.

Figure 8 shows the thermal conductivity measurements and specific heat capacity of polymer samples.

**Fig. 6.** Dependence of sample hardness on FLG concentration**Fig. 7.** Dependence of the flexural strength of samples on the concentration of FLG**Fig. 8.** Dependence of thermal conductivity (a) and specific heat (b) of samples on the concentration of FLG

As can be seen from Fig. 8, the introduction of FLG in small amounts makes it possible to increase the thermal conductivity of the samples up to 2.2 times compared to the initial polymer.

At the same time, the specific heat capacity of the samples is practically independent of the FLG concentration (change within the measurement error).

The increase in the strength and thermophysical properties of polymer composites with the addition of graphene nanostructures is primarily due to the high properties of graphene nanostructures, which is clearly demonstrated by the results of measuring the properties of the composite. As noted earlier, the thermal conductivity of graphene can reach up to $5000 W \cdot (m \cdot K)^{-1}$, which leads to an increase in thermal conductivity (Fig. 8a). However, the specific heat capacity of graphene is about $700 J \cdot (kg \cdot ^\circ C)^{-1}$ [26], so that the addition of FLG has almost no effect on the specific heat capacity of the polymer composite at relatively low (up to 4 wt. %) concentrations of the additive (Fig. 8b).

However, despite a significant increase in the properties of the final composites, the obtained values are still significantly inferior to the theoretically

expected results. In review [27], the authors note that the efficiency of using graphene nanostructures is greatly reduced when they are used in the form of powders (i.e., aggregates of particles), as well as under the influence of other factors such as the defectiveness of particles, the degree of their interaction with the polymer matrix, etc. Since FLG particles are actually distributed throughout the polymer in the form of aggregates (see Figs. 2 and 3), their efficiency is much lower than the expected theoretical assumptions. A similar mechanism was observed in [20].

It should also be noted that with an increase in the FLG concentration in the composite from 2 to 4 wt. %, no further increase in the properties of the composite is observed, and even a slight drop in characteristics occurs. This fact may be due to the fact that at 4 wt. % due to the large number of FLG particles, they interact with each other with the formation of secondary aggregates, which negatively affects the properties of the composite [28].

4. Conclusion

A few-layer graphene synthesized from cellulose under the conditions of the SHS process has shown its high efficiency as a filler for increasing the complex of strength and thermophysical properties when creating composite products from polymer resins using the DLP 3D printing method. It was found that the addition of low-layer graphene makes it possible to achieve an increase in Brinell hardness up to 1.8 times, bending strength up to 1.5 times and thermal conductivity up to 2.2 times compared to the original polymer when using no more than 2 wt. % low-layer graphene. A further increase in the concentration of few-layer graphene did not lead to a further increase in the properties of the final composite, which may be due to the formation of secondary aggregates. However, in order to fully exploit the potential of using FLG as a builder in polymer resins, it is necessary to further improve the methods for dispersing FLG in the original polymer resin in order to avoid secondary aggregation of FLG particles.

5. Funding

The study was funded by the Russian Foundation for Basic Research and BRFFR No. 20-53-04026

6. Conflict of interests

The authors declare no conflict of interest.

References

1. Shahrubudin N, Lee TC, Ramlan R. An overview on 3D printing technology: Technological, materials, and applications. *Procedia Manufacturing*. 2019;35:1286-1296. DOI:10.1016/j.promfg.2019.06.089
2. Zhao Z, Tian X, Song X. Engineering materials with light: recent progress in digital light processing based 3D printing. *Journal of Materials Chemistry C*. 2020; 8(40):13896-13917. DOI:10.1039/D0TC03548C
3. Ngo TD, Kashani A, Imbalzano G et. al. Additive manufacturing (3D printing): A review of materials, methods, applications and challenges. *Composites Part B: Engineering*. 2018;143:172-196. DOI:10.1016/j.compositesb.2018.02.012
4. Balandin AA, Ghosh S, Bao W et. al. Superior thermal conductivity of single-layer graphene. *Nano Letters*. 2008;8(3):902-907. DOI:10.1021/nl0731872
5. Lee C, Wei X, Kysar JW et. al. Measurement of the elastic properties and intrinsic strength of monolayer graphene. *Science*. 2008;321(5887):385-388. DOI:10.1126/science.1157996
6. Zhu Y, Murali S, Cai W et. al. Graphene and graphene oxide: synthesis, properties, and applications. *Advanced Materials*. 2010;22(35):3906-3924. DOI:10.1002/adma.201001068
7. ISO/TS 80004-13:2017(en) Nanotechnologies – Vocabulary – Part 13: *Graphene and related two-dimensional (2D) materials*. Available from: <https://www.iso.org/standard/64741.html> [Accessed 20 April 2023]
8. Zhang YY, Gu YT. Mechanical properties of graphene: Effects of layer number, temperature and isotope. *Computational Materials Science*. 2013;71:197-200. DOI:10.1016/j.commatsci.2013.01.032
9. Zheng Y, Huang X, Chen J et. al. A review of conductive carbon materials for 3D printing: Materials, technologies, properties, and applications. *Materials*. 2021;14(14):3911. DOI:10.3390/ma14143911
10. Hanon MM, Ghaly A, Zsidai L et. al. Investigations of the mechanical properties of DLP 3D printed graphene/resin composites. *Acta Polytechnica Hungarica*. 2021;18(8):143-161. DOI:10.12700/APH.18.8.2021.8.8
11. Joo H, Cho S. Comparative studies on polyurethane composites filled with polyaniline and graphene for DLP-type 3D printing. *Polymers*. 2020;12(1):67. DOI:10.3390/polym12010067
12. Vidakis N, Petousis M, Velidakis E et. al. Fused filament fabrication three-dimensional printing Multi-Functional of polylactic acid/carbon black nanocomposites. *C*. 2021;7(3):52. DOI:10.3390/c7030052
13. Zheng Y, Huang X, Chen J et. al. A review of conductive carbon materials for 3D printing: Materials, technologies, properties, and applications. *Materials*. 2021;14(14):3911. DOI: 10.3390/ma14143911
14. Przekop RE, Kujawa M., Pawlak W et. al. Graphite modified polylactide (PLA) for 3D printed (FDM/FFF) sliding elements. *Polymers*. 2020;12(6):1250. DOI:10.3390/polym12061250

15. Ram R, Soni V, Khastgir D. Electrical and thermal conductivity of polyvinylidene fluoride (PVDF) – Conducting Carbon Black (CCB) composites: Validation of various theoretical models. *Composites Part B: Engineering*. 2020;185:107748. DOI:10.1016/j.compositesb.2020.107748
16. Bhatt MD, Kim H, Kim G. Various defects in graphene: a review. *RSC Advances*. 2022;12(33):21520-21547. DOI:10.1039/D2RA01436J
17. Haghghi M, Khodadadi A, Golestanian H et. al. Effects of defects and functional groups on graphene and nanotube thermoset epoxy-based nanocomposites mechanical properties using molecular dynamics simulation. *Polymers and Polymer Composites*. 2021;29(6):629-639. DOI:10.1177/0967391120929075
18. Voznyakovskii AA, Vozniakovskii AP, Kidalov SV. New way of synthesis of few-layer graphene nanosheets by the self propagating high-temperature synthesis method from biopolymers. *Nanomaterials*. 2022;12(4):657. DOI:10.3390/nano12040657
19. Voznyakovskii AA, Vozniakovskii AP, Kidalov S.V. Phenomenological model of synthesis of few-layer graphene (FLG) by the selfpropagating high-temperature synthesis (SHS) method from biopolymers. *Fullerenes, Nanotubes and Carbon Nanostructures*. 2022;30(1):59-65. DOI:10.1080/1536383X.2021.1993831
20. Voznyakovskii AP, Neverovskaya A, Vozniakovskii A et. al. A Quantitative chemical method for determining the surface concentration of stone-wales defects for 1D and 2D carbon nanomaterials. *Nanomaterials*. 2022;12(5):883. DOI:10.3390/nano12050883
21. Vozniakovskii AA, Vozniakovskii AP, Kidalov SV et. al. Characteristics and mechanical properties of composites based on nitrile butadiene rubber using graphene nanoplatelets. *Journal of Composite Materials*. 2020;54(23):3351-3364. DOI:10.1177/0021998320914366
22. Muzyka R, Drewniak S, Pustelny T et. al. Characterization of graphite oxide and reduced graphene oxide obtained from different graphite precursors and oxidized by different methods using Raman spectroscopy. *Materials*. 2018;11(7):1050. DOI:10.3390/ma11071050
23. Kaniyoor A, Ramaprabhu S. A Raman spectroscopic investigation of graphite oxide derived graphene. *AIP Advances*. 2012;2(3):032183. DOI:10.1063/1.4756995
24. Silva DL, Campos, JLE, Fernandes TF et. al. Raman spectroscopy analysis of number of layers in mass-produced graphene flakes. *Carbon*. 2020;161:181-189. DOI:10.1016/j.carbon.2020.01.050
25. Kumar V, Kumar A, Lee DJ et. al. Estimation of number of graphene layers using different methods: a focused review. *Materials*. 2021;14(16):4590. DOI:10.3390/ma14164590
26. Li QY, Xia K, Zhang J et. al. Measurement of specific heat and thermal conductivity of supported and suspended graphene by a comprehensive Raman optothermal method. *Nanoscale*. 2017;9(30):10784-10793. DOI: 10.1039/C7NR01695F
27. Kumar A, Sharma K, Dixit AR. A review on the mechanical properties of polymer composites reinforced by carbon nanotubes and graphene. *Carbon Letters*. 2021;31(2):149-165. DOI:10.1007/s42823-020-00161-x
28. Sun X, Huang C, Wang L et. al. Recent progress in graphene/polymer nanocomposites. *Advanced Materials*. 2021;33(6):2001105. DOI:10.1002/adma.202001105

Information about the authors / Информация об авторах

Aleksei A. Vozniakovskii, Cand. Sc. (Chem.), Researcher, Ioffe Institute, St. Petersburg, Russian Federation; ORCID 0000-0001-6482-172X; e-mail: alexey_inform@mail.ru

Sergey V. Kidalov, Cand. Sc. (Phys. and Math.), Leading Researcher, Ioffe Institute, St. Petersburg, Russian Federation; ORCID 0000-0002-5685-9899; e-mail: kidalov@mail.ioffe.ru

Alexander P. Voznyakovskii, D. Sc. (Chem.), Sector Manager, Research Institute of Synthetic Rubber S.V. Lebedev, St. Petersburg, Russian Federation; ORCID 0000-0002-5979-3661; e-mail: voznap@mail.ru

Nikita D. Podlozhniuk, Acting Junior Researcher, Ioffe Institute, St. Petersburg, Russian Federation; ORCID 0000-0002-4414-6066; e-mail: nikigod.1@gmail.com

Возняковский Алексей Александрович, кандидат химических наук, научный сотрудник, Физико-технический институт им. А. Ф. Иоффе (ФТИ им. А. Ф. Иоффе), Санкт-Петербург, Российская Федерация; ORCID 0000-0001-6482-172X; e-mail: alexey_inform@mail.ru

Кидалов Сергей Викторович, кандидат физико-математических наук, ведущий научный сотрудник, ФТИ им. А. Ф. Иоффе, Санкт-Петербург, Российская Федерация; ORCID 0000-0002-5685-9899; e-mail: kidalov@mail.ioffe.ru

Возняковский Александр Петрович, доктор химических наук, заведующий сектором, Научно-исследовательский институт синтетического каучука им. академика С. В. Лебедева, Санкт-Петербург, Российская Федерация; ORCID 0000-0002-5979-3661; e-mail: voznap@mail.ru

Подложнюк Никита Денисович, и.о. младшего научного сотрудника, ФТИ им. А. Ф. Иоффе, Санкт-Петербург, Российская Федерация; ORCID 0000-0002-4414-6066; e-mail: nikigod.1@gmail.com

Sofya I. Titova, Laboratory Assistant, Ioffe Institute, St. Petersburg, Russian Federation; ORCID 0009-0007-5176-7892; e-mail: rus.sofiatitova@gmail.com

Evgenii V. Auchynnikau, D. Sc. (Eng.), Associate Professor, Professor of the Department of Mechanical Engineering and Technical Operation of Vehicles, Yanka Kupala State University of Grodno, Grodno, Belarus; ORCID 0000-0003-1454-7341; e-mail: ovchin_1967@mail.ru

Титова Софья Ивановна, лаборант, ФТИ им. А. Ф. Иоффе, Санкт-Петербург, Российская Федерация; ORCID 0009-0007-5176-7892; e-mail: rus.sofiatitova@gmail.com

Овчинников Евгений Витальевич, доктор технических наук, доцент, профессор кафедры машиностроения и технической эксплуатации автомобилей, Гродненский государственный университет имени Янки Купалы, Гродно, Республика Беларусь; ORCID 0000-0003-1454-7341; e-mail: ovchin_1967@mail.ru

Received 26 April 2023; Accepted 29 May 2023; Published 06 July 2023



Copyright: © Vozniakovskii AA, Kidalov SV, Voznyakovskii AP, Podlozhnyuk ND, Titova SI, Auchynnikau EV, 2023. This article is an open access article distributed under the terms and conditions of the Creative Commons Attribution (CC BY) license (<https://creativecommons.org/licenses/by/4.0/>).

Screen-printing of electrical sensor for glucose determination with exfoliated graphite-based paste

© Marina I. Gryaznova^a✉, Dmitry S. Lugvishchuk^a, Kirill O. Gryaznov^a, Ivan S. Filimonenkov^a, Natalia I. Batova^a, Edward B. Mitberg^a, Aida R. Karaeva^a, Vladimir Z. Mordkovich^a

^a *Technological Institute for Superhard and Novel Carbon Materials, 7A, Tsentralnaya St., Moscow, Troitsk, 108840, Russian Federation*

✉ mig@tisnum.ru

Abstract: In this paper, the properties of electrochemical sensor made of screen-printing technology application with graphite-base paste were investigated. The main electrically conductive component in the original paste developed in this study is exfoliated graphite. The electrodes were studied using optical and scanning electron microscopy methods to confirm the quality and integrity of the screen-printing process results. Electrochemical measurements (chronoamperometry and cyclic voltammetry) of printed electrodes show that the performance of this exfoliated graphite-based paste is similar to that of a commercially available graphite paste despite the radically lower content of carbon. The biosensor prototype manufactured in this work is characterized by anisotropic surface morphology formed by mixed carbon black with milled carbon particles (exfoliated graphite and microcrystalline graphite). This prototype has a very good linearity of response to glucose in a wide range from 1 to 40 mM, while manifesting the values of currents and sensitivity comparable to a commercially available analogue.

Keywords: electrochemical measurements; exfoliated graphite; glucose biosensor; graphite electrode; graphite paste; screen-printing.

For citation: Gryaznova MI, Lugvishchuk DS, Gryaznov KO, Filimonenkov IS, Batova NI, Mitberg EB, Karaeva AR, Mordkovich VZ. Screen-printing of electrical sensor for glucose determination with exfoliated graphite-based paste. *Journal of Advanced Materials and Technologies. 2023;8(2):111-119. DOI: 10.17277/jamt.2023.02.pp.111-119*

Трафаретная печать датчика для измерения глюкозы из пасты на основе терморасширенного графита

© М. И. Грязнова^a✉, Д. С. Лугвищук^a, К. О. Грязнов^a, И. С. Филимоненков^a, Н. И. Батова^a, Э. Б. Митберг^a, А. Р. Караева^a, В. З. Мордкович^a

✉ mig@tisnum.ru

^a *Технологический институт сверхтвердых и новых углеродных материалов, ул. Центральная, 7А, Москва, Троицк, 108840, Российская Федерация*

Аннотация: Исследованы свойства электрохимического датчика, изготовленного с помощью технологии трафаретной печати графитовой пасты. Основным электропроводящим компонентом пасты является терморасширенный графит. Для подтверждения качества и целостности результатов трафаретной печати электроды исследованы методами оптической и сканирующей электронной микроскопии. Электрохимические измерения (хроноамперометрия и циклическая вольтамперометрия) печатных электродов показали, что характеристики пасты на основе терморасширенного графита аналогичны характеристикам коммерчески доступной графитовой пасты, несмотря на радикально меньшее содержание углерода. Прототип биосенсора, изготовленный в данной работе, характеризуется анизотропной морфологией поверхности, образованной смесью технического углерода с измельченными частицами углерода (терморасширенный и микрокристаллический графит). Данный прототип обладает хорошей линейностью реакции на глюкозу в широком диапазоне от 1 до 40 мм, проявляя при этом значения токов и чувствительности, сравнимые с коммерчески доступным аналогом.

Ключевые слова: электрохимические измерения; терморасширенный графит; датчик глюкозы; графитовый электрод; графитовая паста; трафаретная печать.

Для цитирования: Gryaznova MI, Lugvishchuk DS, Gryaznov KO, Filimonenkov IS, Batova NI, Mitberg EB, Karaeva AR, Mordkovich VZ. Screen-printing of electrical sensor for glucose determination with exfoliated graphite-based paste. *Journal of Advanced Materials and Technologies*. 2023;8(2):111-119. DOI: 10.17277/jamt.2023.02.pp.111-119

1. Introduction

Graphite pastes are used for screen-printing and are the main material for the manufacture of electrodes in biosensors [1–4]. The search for inexpensive and reliable solutions to meet the growing demand for electrochemical biosensors with which quantitative measurement of glucose concentration in human blood can be carried out quickly remains relevant. Over the years, a large number of different materials have been tested in graphite paste formulations for screen-printing. However, only a few compositions have been partially disclosed and presented in the public domain.

There are several manufacturers in the research area reporting successful implementation of commercial graphite pastes: Acheson Colloids Company (UK), Gwent Electronic Materials (UK), DuPont (USA), Ercon (USA) and Nippon Graphite Industries Ltd (Japan). As found in the literature, the products of Gwent Electronic Materials demonstrate good reproducibility of the electrical conductivity of the electrodes and the best characteristics of sensitivity to a wide range of detectable substances [5–7], in particular, to glucose [8, 9]. This is often used as a reference in the research related to the creation of the original formulations of graphite paste and printed electrodes based on it.

Most of the recent works are devoted to modification of a commercially available graphite paste by adding various materials to its composition [10–12]. These modifications can change rheological behavior of a graphite paste and improve physicochemical properties of printed electrodes. For example, such modification may increase electrode surface area or sensitivity; it may also influence the kinetics of electronic transport. The most common nonmetallic conductive fillers of conductive pastes are carbon black, glassy carbon, graphite, carbon nanotubes and graphene [13–17].

From this point of view, exfoliated graphite (EG) is a promising material for the manufacture of graphite electrodes obtained by screen-printing [18]. EG is characterized by low electrical resistivity, thermal stability and chemical inertness [19, 20]. However, due to the low density of EG, it is difficult to maintain the high-quality level of printed electrodes. A solution to this problem may be the co-

introduction of additional carbon materials into the EG-based paste, such as microcrystalline graphite (MG) and carbon black (CB) [21].

The purpose of this work is to develop, manufacture and investigate the properties of EG-based printed electrodes for electrochemical biosensors for determining glucose concentration.

2. Materials and Methods

2.1. Source materials

Suspension polyvinyl chloride (PVC) grade C-7059 M (CAUSTIC, Russia), 1,2,3,4-tetrahydronaphthalene (THN) (qualification "Purified", LLC "VitaChem Kazan", Russia), N-methylpyrrolidone (N-MP) (qualification "Purified", ECOS-1, Russia), 3-glycidoxy-propyltrimethoxy-silane (LT560, Jiangxi Chenguang New Materials Co., Ltd., China) were used to prepare the polymer base for exfoliated graphite paste (referred to as EGP below in the text). The main electrically conductive component is EG (UNICHIMTEK, Russia). Additional carbon materials were also used: MG grade "MG-1" (NIIgrafit, Russia) and CB brand "N375" ("YATU named after V.U. Orlov", Russia).

The EGP has been tested in comparison with the commercially available analogue of GWENT C2130814D2 (referred to as CGP below in the text) (Gwent Electronic Materials, UK).

2.2. Production of graphite paste

The use of a screen mesh when printing graphite electrodes imposes a limit on the size of the solid components of the paste. In this work, their size should not exceed 40 μm , so the original carbon materials were ground. The grinding of EG particles was carried out using an Ultrasonic Disperser Vibracell VCX750 (Sonics & Materials, Inc., USA) in acetone medium. A PULVERISETTE 7 premium line planetary ball mill (FRITSCH GmbH, Germany) was used to grind MG. The CB consists of nanoscale particles (~ 50 nm), so it does not require pre-grinding. The finished carbon components were introduced into a liquid polymer base and stirred until a visually homogeneous mass was obtained. The mass content of solid and liquid components of graphite pastes is presented in Table 1.

Table 1. Solid and liquid components of graphite pastes

Component, wt. %	CGP	EGP
Solid components, total	34–38	16
Liquid components, total	62–66	84

Manufacture of graphite electrodes

The screen printing of the studied graphite pastes was carried out on an automatic machine WSC-160 B (WINON Industrial Co., Ltd., China). Sheets of polyethylene terephthalate (PET) were used as a substrate. The heat treatment conditions of graphite electrodes in the drying oven for their fixation on the PET substrate for EGP were 90 °C for 45 min, CGP – 100 °C for 3 h. The conditions are selected so as to minimize the effect of temperature on the original shape of the substrates. Geometric parameters of the finished electrodes: length – 38 mm, width – 1 mm, thickness – 11 µm.

2.3. Preparation and characterization of biosensors

The morphology and surface defects of the graphite electrodes, as well as the size of the conductive particles, were investigated by scanning electron microscopy (SEM) using a TESCAN Vega 3 electron microscope (TESCAN, Czech Republic). Print quality control (geometry of the pattern, through pores, etc.) was carried out by high-resolution optical microscopy using an Olympus BX-51M optical microscope (Olympus Corporation, Japan).

The thickness of printed electrode was evaluated based on the average of five measurements by MITUTOYO digital indicator ID-F125E with stand (MITUTOYO, Japan).

The electrode resistivity was evaluated by means of a four-probe method on a Keithley 2400 Standard Series Source Measuring Unit instrument (Keithley Instruments Inc., USA) at room temperature (~300 K).

Electrochemical measurements were performed according to a three-electrode circuit using printed graphite electrodes. EmStat3 potentiostat (PalmSens BV, Netherlands) was used to register electrode signals. Buffer and aqueous solutions were prepared using pure deionized water purified at Milli-Q (Millipore, USA).

Cyclic voltamperograms (CV) were recorded in a potassium-phosphate buffer solution (pH 7.4) with a potential scanning rate of 40 mV·s⁻¹ in the range from -0.40 to 0.75 V. The printed electrode of the sample under study was used as a working electrode, a silver chlorine electrode was used as a reference electrode (Ag/AgCl), a graphite rod was used as an

auxiliary electrode. All electrodes were immersed in glass containing a working solution. The area of the submerged part of the working electrode was 0.07 cm². To verify the reproducibility, measurements were made on at least two independently printed electrodes.

Chronoamperograms (CA) were recorded at a potential of 0.3 V in a potassium-phosphate buffer solution with the addition of sodium chloride (10 mM KH₂PO₄, 40 mM K₂HPO₄, 184 mM NaCl, pH 7.4) containing glucose at concentrations 0.6 to 50.0 mM. A printed graphite working electrode, an auxiliary electrode and a reference electrode were used to detect currents. The enzyme immobilization was carried out in such a way: an aqueous solution (0.9 µL) of glucose oxidase (10 mg·mL⁻¹) and potassium hexacyanoferrate (III) (113 mg·mL⁻¹) were placed to the working area by means of microdozer and then left to stabilize at a room temperature. The printed electrodes with a substrate were fixed horizontally and a portion of the working electrolyte with a volume of 2 µL was applied to the working area using a microdozer. At least three CA were recorded for each glucose concentration, a new printed electrode was used for each measurement.

3. Results and Discussion

The original EG powder consisted of macroparticles of various shapes and sizes formed from interconnected ~150–250 µm graphite plates. Ultrasonication of the original EG led to their destruction to separate, predominantly flat particles of irregular shape. By the means of SEM method the particle sizes of the EG after the US was estimated (Fig. 1).

According to Fig. 1, based on the established parameters of the screen mesh of 40 µm, 84 % of the EG particles pass threshold. The size of a third of all particles after ultrasonication (33 %) is 20 – 25 µm.

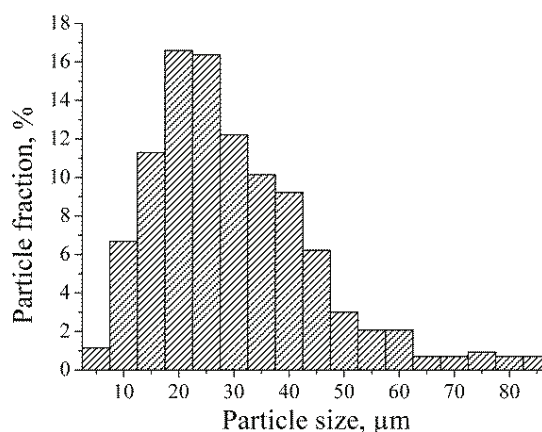


Fig. 1. Distribution histogram of the EG particle size after ultrasonication

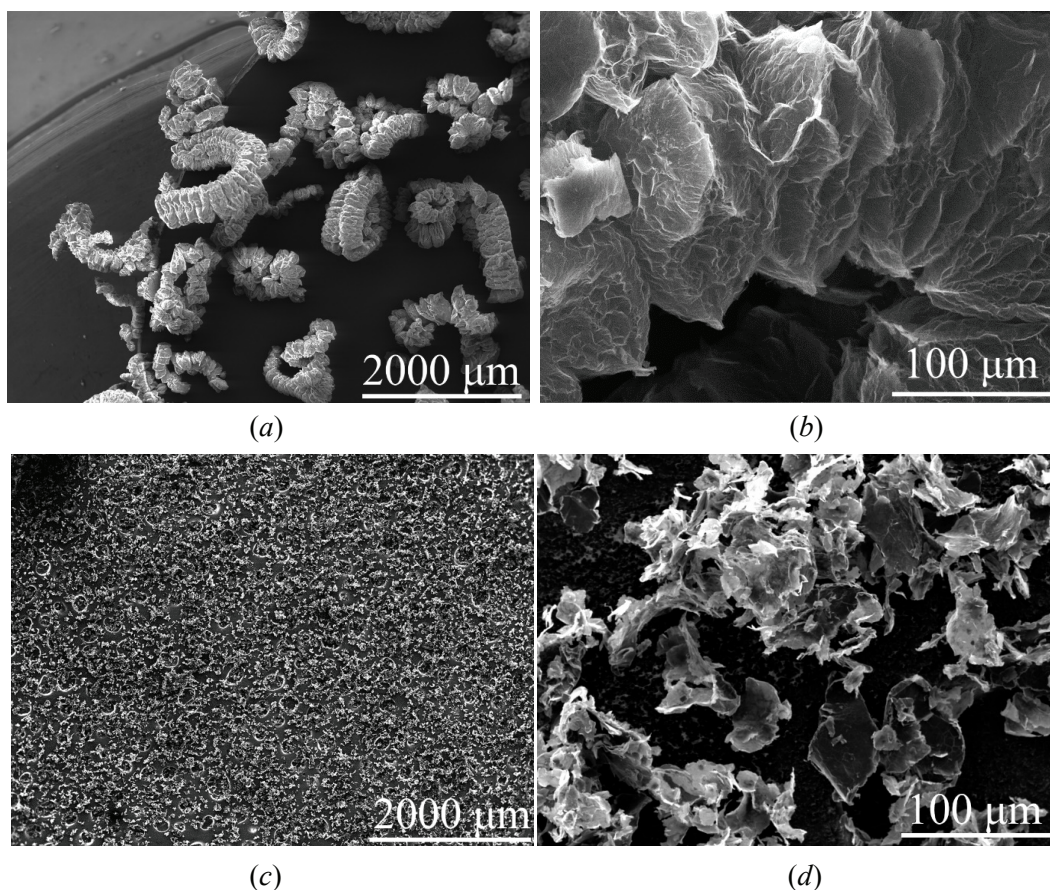


Fig. 2. SEM micrographs of the EG particles: (a, b) initial particles; (c, d) particles after ultrasonication

The result of the ultrasonication of the original EG powder is presented in Fig. 2.

The original MG powder consisted of individual particles ranging in size from 0.1 to 2.0 mm. As a result of grinding in a planetary mill, the size of most MG particles (91 %) did not exceed 40 μm, while particles ranging in size from 5 to 15 μm made up the main share (67 %) (Fig. 3).

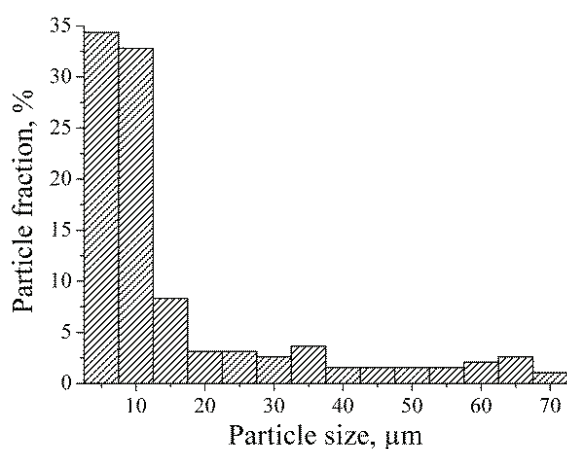


Fig. 3. Distribution histogram of the MG particles size after grinding in a planetary mill

The SEM micrographs for the MG powder before and after grinding in a ball mill are presented in Fig. 4.

The physical properties of the graphite electrode depend on the number of defects that can emerge during the process of screen-printing or be formed due to the incompatibility of the materials that make up the graphite paste with each other. The most common defects of printed electrodes are uneven thickness, unfilled areas due to blockage of mesh cells, lack of reproducibility when measuring electrical resistance, and breakdowns between the working, auxiliary, and reference electrodes due to the spread of the paste immediately during printing.

According to the passport data, CGP graphite paste contains 34–38 wt. % of solid components (Table 1). Fig. 5 shows the results of optical microscopy and SEM of CGP paste-based printed graphite electrode.

As can be seen from the microphotographs, the electrode surface is uniformly smoothed and completely filled with carbon particles (Fig. 5b). There is almost no separation of the polymer base (Fig. 5a) along the entire perimeter of the electrode, and there are no spreads either. The boundaries of the electrode have a clear shape, close to rectangular, but its contour is slightly blurred.

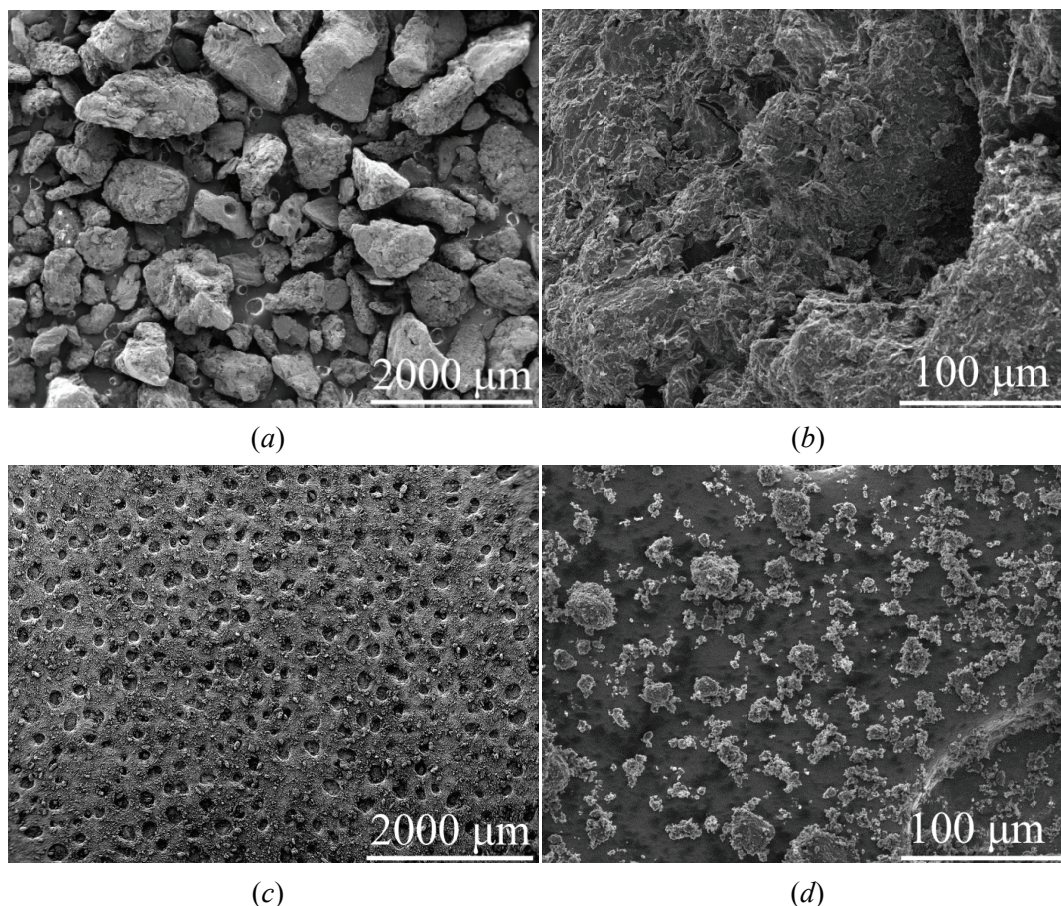


Fig. 4. Scanning electron micrographs of the particles MG: (a, b) original particles; (c, d) particles after ball milling

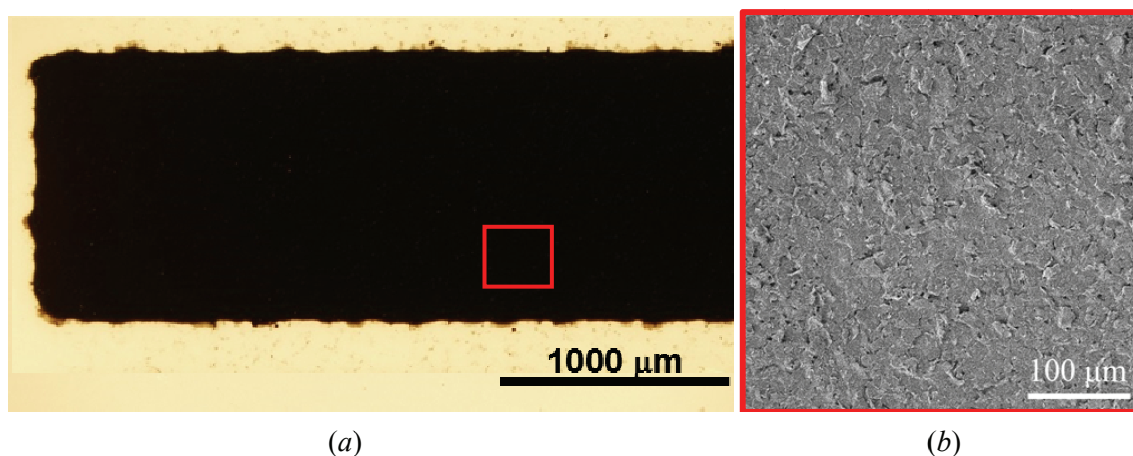


Fig. 5. Images of a printed graphite electrode based on CGP paste:
(a) optical micrograph of the edge; (b) scanning electron micrograph of the surface

Fig. 6a presents a graphite electrode manufactured with the original EGP.

It can be seen from microphotographs that the electrode surface looks loose, but the edges of the EG particles are smoothed by the polymer base, and the filling of the electrode volume with graphite paste components is uniform (Fig. 6b). The separation of the polymer base (Fig. 6c) at the electrode boundaries

is practically absent, there is no spreading, and the electrode border has a wave-like shape.

As a result, the obtained graphite electrodes based on EGP had a rectangular shape with a wave-like contour, without traces of spreading, with a weak separation of the polymer base around the perimeter and uniform filling of the volume with conductive components. The specific electrical resistance values

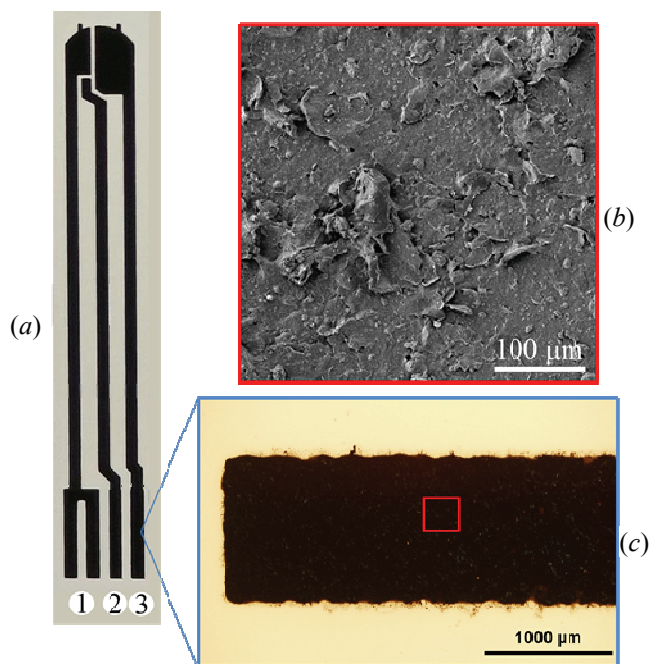


Fig. 6. (a) printed graphite electrode, (1) auxiliary, (2) reference and (3) working electrodes; (b) scanning electron micrograph of the EGP surface; (c) optical micrograph of the EGP edge

of the CGP and EGP are different but similar to each other (Table 2).

Compared to CGP graphite paste, the use of EG as the main electrically conductive component of EGP can reduce the content of solid components by almost two times (see Table 1). It was found that the reduction in the specific electrical resistance of graphite electrodes was influenced by the use of nanoscale CB in the paste [22]. The addition of crushed MG facilitated the passage through the screen mesh of more EG particles up to 40 μm in size (Fig. 7). Corresponding EGP paste volume resistivity value is performing at the same level as EtOH1-5, HMP1-5 and PVP1-5 graphite ink samples with 35 wt. % conductive carbon components, it should be noted that comparable samples may have a lower roughness as in this work it was not investigated [21].

Table 2. Physical characteristics of graphite electrodes

Paste	Electrode thickness, μm	Electrical resistance of the working electrode, Ω	Specific electrical resistance, (Ω×mm ²)·m ⁻¹
CGP	10	1000	270
EGP	11	1500	440

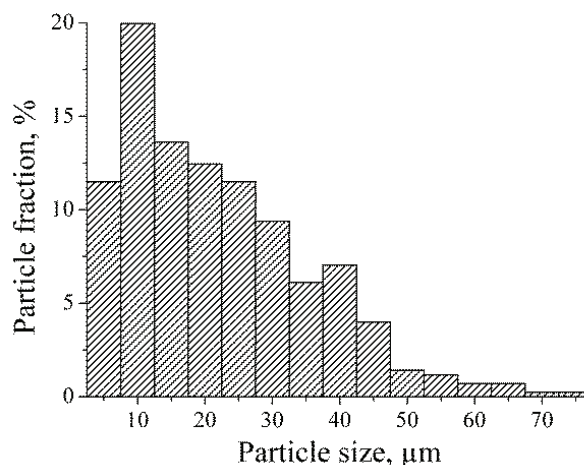


Fig. 7. Histogram of particle size distribution in EGP sample after screen-printing

The chosen ratio between EG, MG and CB in graphite paste led to the formation of an effective electrically conductive network in the printed electrodes.

To compare the electrochemical characteristics of the printed electrodes, voltamperometric and chronoamperometric studies were carried out.

Figure 8 shows the CV of graphite electrodes based on CGP and EGP.

In both cases the CV have a smooth shape without ohmic defects and do not contain extraneous redox peaks. CV are reproduced uniformly for all the printed electrodes. In the case of CGP-based electrodes, the CV is slightly more symmetric and has a slightly wider dual electric layer recharge region than for EGP-based electrodes.

Figures 9 and 10 show the calibration dependencies obtained from the corresponding CA of the samples under study.

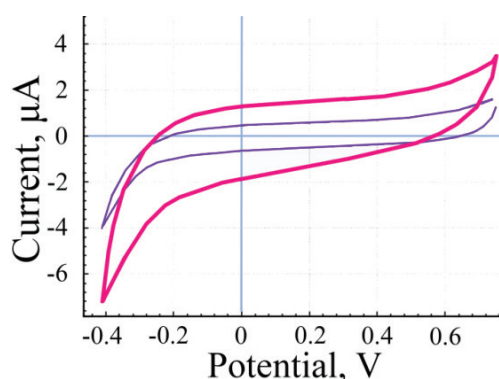


Fig. 8. CV of printed electrodes: graphite electrode based on CGP (purple line); graphite electrode based on EGP (pink line)

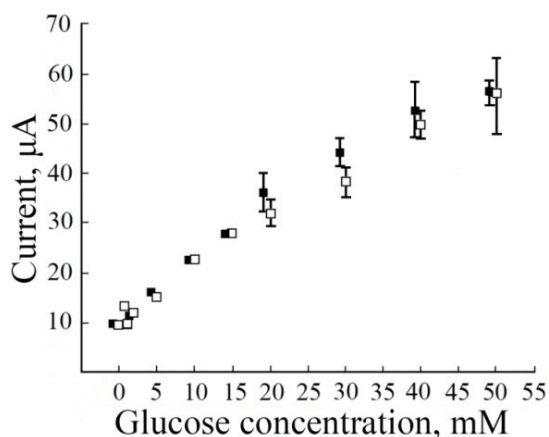


Fig. 9. Calibration dependencies “current – glucose concentration” for graphite electrodes: ■ – CGP; □ – EGP

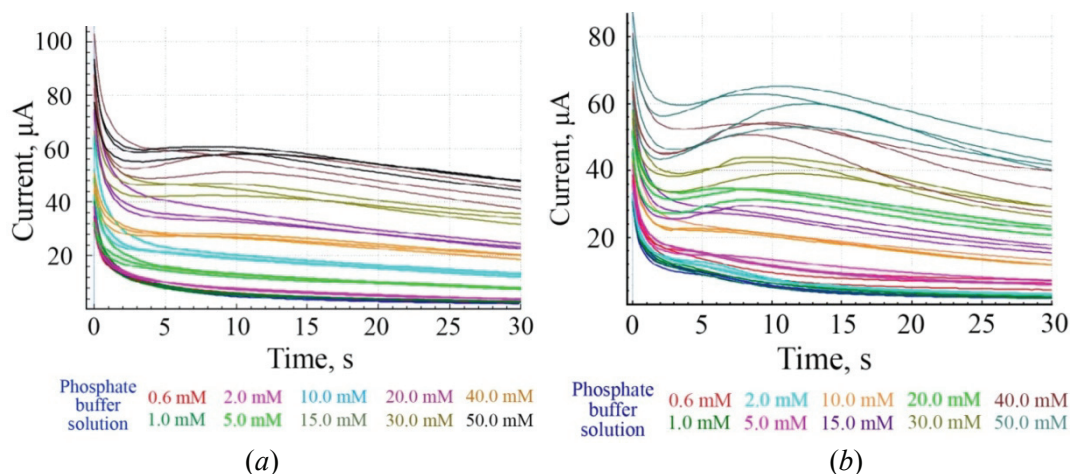


Fig. 10. Chronoamperometry results at different glucose concentrations for graphite electrode based on (a) CGP; (b) EGP

Table 3. Calibration dependency parameters for electrodes based on CGP and EGP pastes

Paste	Sensitivity at 30 mM, $\mu\text{A}/\text{mM}$	Current density at 30 mM, mA/cm^2	Linear range, mM
CGP	1.50	0.7	1–40
EGP	1.30	0.6	

The studied electrodes manifest similar currents and current densities at glucose concentrations of up to 30 mM, as well as the same linear range and similar sensitivity (Table 3). It can be concluded that with the enzymatic oxidation of glucose on printed electrodes based on EGP are not inferior to electrodes obtained on the basis of CGP. It should be noted that such a wide linear range of glucose detection is not presented among chemical sensors screen-printed by nanomaterials based inks, which are better suited for low concentration glucose detection [4].

4. Conclusion

The EG-based graphite paste studied in this research is suitable for creating electrochemical biosensors manufactured by screen-printing technology. The EG addition into the graphite paste allows the content of carbon-conductive particles to be reduced by up to 16 wt. %, maintaining a low sheet resistivity of the resulting electrodes, and thus reducing the cost of its manufacture. Analysis of the electrode surface by optical microscopy and SEM, as

well as the results of electrochemical tests on the enzymatic oxidation of glucose, shows that the EG-based paste with basic properties is not inferior to the commercially available analogues and is suitable for screen-printing of electrodes that work as a biosensor for glucose quantitative determination in a wide linear arrangement with good reproducibility.

5. Funding

This research received no external funding.

6. Acknowledgments

The authors are grateful to ELTA Company LLC and personally to Yu.F. Glukhov and Z.Y. Nikanorov for their contribution to the research.

The present work was carried out on FSBI TISNCM Shared-Use Equipment Center “Research of Nanostructured, Carbon and Superhard Materials” equipment.

7. Conflicts of Interest

The authors declare no conflict of interest.

References

1. Švancara I, Vytrás K, Kalcher K, Walcarius A, Wang J. Carbon paste electrodes in facts, numbers, and notes: A review on the occasion of the 50-years jubilee of carbon paste in electrochemistry and electroanalysis. *Electroanalysis*. 2009;21:7-28. DOI:10.1002/elan.200804340
2. Švancara I, Walcarius A, Kalcher K, Vytrás K. Carbon paste electrodes in the new millennium. *Open Chemistry*. 2009;7:598-656. DOI:10.2478/s11532-009-0097-9
3. Renedo OD, Alonso-Lomillo MA, Martínez MJA. Recent developments in the field of screen-printed electrodes and their related applications. *Talanta*. 2007;73:202-19. DOI:10.1016/j.talanta.2007.03.050
4. Chu Z, Peng J, Jin W. Advanced nanomaterial inks for screen-printed chemical sensors. *Sensors and Actuators, B: Chemical*. 2017;243:919-26. DOI:10.1016/j.snb.2016.12.022
5. Potts SJ, Phillips C, Claypole T, Jewell E. The effect of carbon ink rheology on ink separation mechanisms in screen-printing. *Coatings*. 2020;10:1-17. DOI:10.3390/coatings10101008
6. Rao VK, Sharma MK, Pandey P, Sekhar K. Comparison of different carbon ink based screen-printed electrodes towards amperometric immunosensing. *World Journal of Microbiology and Biotechnology*. 2006;22:1135-43. DOI:10.1007/s11274-006-9154-0
7. Sys M, Khaled E, Metelka R, Vytrás K. Electrochemical characterisation of novel screen-printed carbon paste electrodes for voltammetric measurements. *Journal of the Serbian Chemical Society*. 2017;82:865-77. DOI:10.2298/JSC170207048S
8. Melios N, Tsouti V, Chatzandroulis S, Tsekenis G. Development of an all-carbon electrochemical biosensor on a flexible substrate for the sensitive detection of glucose. *Engineering Proceedings*. 2022;4-9. DOI:10.3390/IECB2022-12273
9. Tang Y, Petropoulos K, Kurth F, Gao H, Migliorelli D, Guenat O, et al. Screen-printed glucose sensors modified with cellulose nanocrystals (CNCs) for Cell Culture Monitoring. *Biosensors*. 2020;10. DOI:10.3390/BIOS10090125
10. Mazzaracchio V, Tomei MR, Cacciotti I, Chiodoni A, Novara C, Castellino M, et al. Inside the different types of carbon black as nanomodifiers for screen-printed electrodes. *Electrochimica Acta*. 2019;317:673-683. DOI:10.1016/j.electacta.2019.05.117
11. Kava AA, Henry CS. Exploring carbon particle type and plasma treatment to improve electrochemical properties of stencil-printed carbon electrodes. *Talanta*. 2021;221:121553. DOI:10.1016/j.talanta.2020.121553
12. Wang K, Frewin CL, Esrafilzadeh D, Yu C, Wang C, Pancrazio JJ, et al. High-performance graphene-fiber-based neural recording microelectrodes. *Advanced Materials*. 2019;31:1805867. DOI:10.1002/adma.201805867
13. Potts S-J, Korochkina T, Holder A, Jewell E, Phillips C, Claypole T. The influence of carbon morphologies and concentrations on the rheology and electrical performance of screen-printed carbon pastes. *Journal of Materials Science*. 2022;57(4):2650-2666. DOI:10.1007/s10853-021-06724-1
14. Phillips C, Al-Ahmadi A, Potts SJ, Claypole T, Deganello D. The effect of graphite and carbon black ratios on conductive ink performance. *Journal of Materials Science*. 2017;52:9520-30. DOI:10.1007/s10853-017-1114-6
15. Kitova A, Tarasov S, Plekhanova Y, Bykov A, Reshetilov A. Direct bioelectrocatalytic oxidation of glucose by gluconobacter oxydans membrane fractions in PEDOT:PSS/TEG-modified biosensors. *Biosensors*. 2021;11:144. DOI:10.3390/bios11050144
16. Scognamiglio V. Nanotechnology in glucose monitoring: Advances and challenges in the last 10 years. *Biosensors and Bioelectronics*. 2013;47:12-25. DOI:10.1016/J.BIOS.2013.02.043
17. Hwang HS, Jeong JW, Kim YA, Chang M. Carbon nanomaterials as versatile platforms for biosensing applications. *Micromachines*. 2020;11:814. DOI:10.3390/mi11090814
18. Suresh RR, Lakshmanakumar M, Arockia Jayalatha JBB, Rajan KS, Sethuraman S, Krishnan UM, et al. Fabrication of screen-printed electrodes: opportunities and challenges. *Journal of Materials Science*. 2021;56:8951-9006. DOI:10.1007/s10853-020-05499-1
19. Plekhanova Y, Tarasov S, Kitova A, Kolesov V, Kashin V, Sundramoorthy AK, et al. Modification of thermally expanded graphite and its effect on the properties of the amperometric biosensor. *3 Biotech*. 2022;12:42. DOI:10.1007/s13205-021-03107-w
20. Debelak B, Lafdi K. Use of exfoliated graphite filler to enhance polymer physical properties. *Carbon*. 2007;45:1727-34. DOI:10.1016/j.carbon.2007.05.010

21. Hatala M, Gemeiner P, Hvojnik M, Mikula M. The effect of the ink composition on the performance of carbon-based conductive screen printing inks. *Journal of Materials Science: Materials in Electronics*. 1234;30:1034-44. DOI:10.1007/s10854-018-0372-7

22. Griaznova MI, Lugvishchuk DS, Gryaznov KO, Mitberg EB, Karaeva AR, Mordkovich VZ. Electroconductive paste based on thermally expanded graphite for screen printed electrodes of medical applications. *Nanobiotechnology Reports*. 2022;17:500-6. DOI:10.1134/S2635167622040115

Information about the authors / Информация об авторах

Marina I. Gryaznova, Junior Research Scientist, Technological Institute for Superhard and Novel Carbon Materials (TISNCM), Moscow, Troitsk, Russian Federation; ORCID 0000-0002-9141-1934; e-mail: mig@tisnum.ru

Dmitry S. Lugvishchuk, Cand. Sc. (Eng.), Research Associate, TISNCM, Moscow, Troitsk, Russian Federation; ORCID 0000-0001-9589-6206; e-mail: lugvishchuk.d@tisnum.ru

Kirill O. Gryaznov, Cand. Sc. (Eng.), Senior Researcher, TISNCM, Moscow, Troitsk, Russian Federation; ORCID 0000-0001-9360-3326; e-mail: gryaznovkirill@tisnum.ru

Ivan S. Filimonenkov, Cand. Sc. (Chem.), Research Associate, TISNCM, Moscow, Troitsk, Russian Federation; ORCID 0000-0003-2766-1709; e-mail: filimonenkov@tisnum.ru

Natalia I. Batova, Cand. Sc. (Eng.), Leading Engineer, TISNCM, Moscow, Troitsk, Russian Federation; ORCID 0000-0001-9183-3662; e-mail: nat59bat@tisnum.ru

Edward B. Mitberg, Cand. Sc. (Chem.), Leading Researcher, TISNCM, Moscow, Troitsk, Russian Federation; ORCID 0000-0001-6499-7274; e-mail: mitbergeb@tisnum.ru

Aida R. Karaeva, Cand. Sc. (Eng.), Leading Researcher, TISNCM, Moscow, Troitsk, Russian Federation; ORCID 0000-0002-9728-354X; e-mail: karaevaar@tisnum.ru

Vladimir Z. Mordkovich, D. Sc. (Chem.), Deputy Director for Scientific Work, TISNCM, Moscow, Troitsk; ORCID 0000-0002-9553-7657; e-mail: mordkovich@tisnum.ru

Грязнова Марина Игоревна, младший научный сотрудник, Технологический институт сверхтвердых и новых углеродных материалов (ТИСЧУМ), Москва, Троицк, Российская Федерация; ORCID 0000-0002-9141-1934; e-mail: mig@tisnum.ru

Лугвищук Дмитрий Сергеевич, кандидат технических наук, научный сотрудник, ТИСЧУМ, Москва, Троицк, Российская Федерация; ORCID 0000-0001-9589-6206; e-mail: lugvishchuk.d@tisnum.ru

Грязнов Кирилл Олегович, кандидат технических наук, старший научный сотрудник, ТИСЧУМ, Москва, Троицк, Российская Федерация; ORCID 0000-0001-9360-3326; e-mail: gryaznovkirill@tisnum.ru

Филимоненков Иван Сергеевич, кандидат химических наук, научный сотрудник, ТИСЧУМ, Москва, Троицк, Российская Федерация; ORCID 0000-0003-2766-1709; e-mail: filimonenkov@tisnum.ru

Батова Наталья Ивановна, кандидат технических наук, ведущий инженер, ТИСЧУМ, Москва, Троицк, Российская Федерация; ORCID 0000-0001-9183-3662; e-mail: nat59bat@tisnum.ru

Митберг Эдуард Борисович, кандидат химических наук, ведущий научный сотрудник, ТИСЧУМ, Москва, Троицк, Российская Федерация; ORCID 0000-0001-6499-7274; e-mail: mitbergeb@tisnum.ru

Караева Аида Разимовна, кандидат технических наук, ведущий научный сотрудник, ТИСЧУМ, Москва, Троицк, Российская Федерация; ORCID 0000-0002-9728-354X; e-mail: karaevaar@tisnum.ru

Мордкивич Владимир Зальманович, доктор химических наук, профессор, заместитель директора по научной работе, ТИСЧУМ, Москва, Троицк, Российская Федерация; ORCID 0000-0002-9553-7657; e-mail: mordkovich@tisnum.ru

Received 18 April 2023; Accepted 15 May 2023; Published 06 July 2023



Copyright: © Gryaznova MI, Lugvishchuk DS, Gryaznov KO, Filimonenkov IS, Batova NI, Mitberg EB, Karaeva AR, Mordkovich VZ, 2023. This article is an open access article distributed under the terms and conditions of the Creative Commons Attribution (CC BY) license (<https://creativecommons.org/licenses/by/4.0/>).

Synthesis and properties of hydroxyapatite – fluorapatite solid solutions

© Nikolay A. Zakharov^a✉, Ali D. Aliev^b, Vladimir V. Matveev^b, Michail R. Kiselev^b, Elena M. Koval^a, Evgeniy V. Shelekhov^c, Ludmila V. Goeva^a, Tatiana V. Zakharova^d

^a Kurnakov Institute of General and Inorganic Chemistry RAS, 31, Leninskii Pr., Moscow, 119991, Russian Federation,

^b Institute of Physical Chemistry and Electrochemistry RAS, 31/4, Leninskii Pr., Moscow, 119071, Russian Federation,

^c University of Science and Technology MISIS, 4/1, Leninskii Pr., Moscow, 119049, Russian Federation,

^d Russian University of Transport MIIT, 9/9, Obraztsova St., Moscow, 127994, Russian Federation

✉ zakharov@igic.ras.ru

Abstract: Solid solutions of $\text{Ca}_{10}(\text{PO}_4)_6(\text{OH})_{2-x}\text{F}_x$, $x = 0.0; 0.2; 0.5; 1.0; 1.5; 2.0$ were obtained by reacting $\text{Ca}_{10}(\text{PO}_4)_6(\text{OH})_2$, $\text{Ca}_3(\text{PO}_4)_2$ and CaF_2 in the course of a solid-state synthesis reaction at 1200 °C for 3 h in air. Synthesis products were identified using X-ray phase and X-ray fluorescence analysis, infrared and impedance spectroscopy. According to the results of X-ray phase analysis, the synthesized solid solutions had the structure of hexagonal apatite, the extreme members of the series of solid solutions corresponded to the JCPDS standards ($\text{Ca}_{10}(\text{PO}_4)_6(\text{OH})_2$ – No. 9-0432; $\text{Ca}_{10}(\text{PO}_4)_6\text{F}_2$ – No. 00-003-0736). Vibrational spectra of solid solutions corresponded to the apatite structure with characteristic absorption bands of tetrahedra of PO_4^{3-} , OH^- groups. An increase in the fluorine content in solid solutions was accompanied by a typical shift of the 631 cm^{-1} band to the region of large values of wave numbers, and its intensity successively decreased. With an increase in the fluorine content in solid solutions at a frequency of 1 kHz, the dielectric loss tangent did not undergo significant changes, and the permittivity slightly decreased. Based on the results of physicochemical analysis, the fundamental relationships “composition – structure – properties” for the studied synthesis products were determined. The influence of the composition and synthesis conditions on the crystallographic (elementary cell parameters) and electrical (dielectric permittivity, dielectric loss tangent, conductivity) characteristics of the synthesized solid solutions was assessed. Solid solutions of fluorine-substituted calcium hydroxyapatite are promising for use in medical practice.

Keywords: hydroxyapatite; fluorapatite; solid solutions; solid-phase synthesis; properties; characterization.

For citation: Zakharov NA, Aliev AD, Matveev VV, Kiselev MR, Koval EM, Shelekhov EV, Goeva LV, Zakharova TV. Synthesis and properties of hydroxyapatite – fluorapatite solid solutions. *Journal of Advanced Materials and Technologies*. 2023;8(2):120-129. DOI: 10.17277/jamt.2023.02.pp.120-129

Синтез и свойства твердых растворов гидроксиапатит – фторапатит

© Н. А. Захаров^a✉, А. Д. Алиев^b, В. В. Матвеев^b, М. Р. Киселев^b,
Е. М. Коваль^a, Е. В. Шелехов^c, Л. В. Гоева^a, Т. В. Захарова^d

^a Институт общей и неорганической химии РАН, Ленинский пр., 31, Москва, 119991, Российская Федерация,

^b Институт физической химии и электрохимии РАН,

Ленинский пр., 31, корп. 4, Москва, 119071, Российская Федерация,

^c Университет науки и технологий МИСИС, Ленинский пр., 4, стр. 1., Москва, 119049, Российская Федерация,

^d Российский университет транспорта (МИИТ),

ул. Образцова, 9, стр. 9, Москва, 127994, ГСП-4, Российская Федерация

✉ zakharov@igic.ras.ru

Аннотация: Твердые растворы фторзамещенного гидроксиапатита кальция составов $\text{Ca}_{10}(\text{PO}_4)_6(\text{OH})_{2-x}\text{F}_x$, $x = 0,0; 0,2; 0,5; 1,0; 1,5; 2,0$ получены при взаимодействии $\text{Ca}_{10}(\text{PO}_4)_6(\text{OH})_2$, $\text{Ca}_3(\text{PO}_4)_2$ и CaF_2 в ходе твердофазной реакции синтеза при 1200 °C в течение 3 ч на воздухе. Продукты синтеза идентифицировали с использованием рентгенофазового и рентгенофлуоресцентного анализов, инфракрасной и импедансной спектроскопии. По результатам рентгенофазового анализа синтезированные твердые растворы обладали структурой

гексагонального апатита, крайние члены ряда твердых растворов отвечали стандартам JCPDS ($\text{Ca}_{10}(\text{PO}_4)_6(\text{OH})_2$ – № 9-0432; $\text{Ca}_{10}(\text{PO}_4)_6\text{F}_2$ – № 00-003-0736). Колебательные спектры твердых растворов соответствовали структуре апатита с характерными полосами поглощения тетраэдров PO_4^{3-} , OH^- -групп; рост содержания фтора в твердых растворах сопровождался типичным смещением полосы 631 см^{-1} в область больших значений волновых чисел, а интенсивность ее последовательно снижалась. С ростом содержания фтора в твердых растворах на частоте 1 кГц тангенс угла диэлектрических потерь не претерпевал значительных изменений, а диэлектрическая проницаемость незначительно снижалась. На основе результатов физико-химического анализа определены фундаментальные взаимосвязи «состав – структура – свойства» для исследованных продуктов синтеза, проведена оценка влияния состава и условий синтеза на кристаллографические (параметры элементарной ячейки) и электрические (диэлектрическая проницаемость, тангенс угла диэлектрических потерь, проводимость) характеристики синтезированных твердых растворов. Твердые растворы фторзамещенного гидроксиапатита кальция перспективны для использования в медицинской практике.

Ключевые слова: гидроксиапатит; фторапатит; твердые растворы; твердофазный синтез; свойства; характеристикация.

Для цитирования: Zakharov NA, Aliev AD, Matveev VV, Kiselev MR, Koval EM, Shelekhov EV, Goeva LV, Zakharova TV. Synthesis and properties of hydroxyapatite – fluorapatite solid solutions. *Journal of Advanced Materials and Technologies*. 2023;8(2):120-129. DOI: 10.17277/jamt.2023.02.pp.120-129

1. Introduction

Calcium phosphates (CPs) are an inorganic component of mineralized bone and dental tissues of mammals [1]. The growing interest in biocompatible CPs in recent years is largely due to their characteristics of biocompatibility, bioactivity, and the absence of toxic and allergenic properties. This opens up broad prospects for the use of such compounds as materials for medical preparations: implants, dental materials, drug delivery systems, etc. Practice has already proven the effectiveness of using such materials in orthopedics and reconstructive medicine, for coating implants, as composite components, bone cements in maxillofacial and orthopedic surgery and dental preparations in the form of toothpastes and mouth rinses [2–4].

The use of synthetic CPs was first shown for the regeneration of bone tissue defects in experimental animals in 1920 [2]. Later, CP-based bioceramics were successfully used for the reconstruction of bone defects in medicine [3]. Biocompatible synthetic CPs with an apatite structure are a crystal-chemical analogue of the inorganic component of mineralized tissues of mammals and form a large group of crystalline and amorphous compounds [5–7]. Typical representatives of this group of compounds are calcium hydroxyapatite $\text{Ca}_{10}(\text{PO}_4)_6(\text{OH})_2$ (HA) and calcium fluorapatite $\text{Ca}_{10}(\text{PO}_4)_6\text{F}_2$ (FA).

Fluorine is an important constituent element in the human diet, essential for the growth of bones and teeth [8–10]. The mineralized phase of native hard tissues contains a certain amount of fluorine, which replaces OH groups in the apatite structure (Fig. 1) [11]. FA is characterized by properties of

biocompatibility, bioactivity, antibacterial behavior, high stability, and good strength characteristics [12–16]. The substitution of OH groups of HA for fluorine ions F increases the strength of the ceramic material, reduces the rate of its dissolution, increasing the stability in the biological environment [17–19]. The presence of fluorine in bone tissue and tooth enamel, saliva and blood plasma has been proven [20]. The incorporation of fluorine into the HA composition in mineralized tissues has a positive effect associated with an increase in the response of osteoblasts, promotes their differentiation and proliferation [18, 19], and accelerates the process of biomineralization and growth of bone tissue [16, 17]. At the same time, fluorine ions, showing extraordinary chemical and biological activity, are able to easily penetrate into various types of body cells, cause metabolic disorders, leading to the destruction of liver, kidney, and brain tissues [10].

There is a continuous series of $\text{Ca}_{10}(\text{PO}_4)_6(\text{OH})_{2-x}\text{F}_x$ (FHA) solid solutions [21], which can be synthesized using various processes [22]. A number of methods for the synthesis of FHA are known, including precipitation from aqueous solutions, hydrolysis, hydrothermal, sol-gel, etc. [23–26]. At the same time, the problem of finding effective methods with reproducible results that allow scaling up the production of FHA-based materials for medical use is still relevant.

In this paper, we present the results of using the solid-phase synthesis of FHA solid solutions and analyze the relationships between composition, synthesis conditions, structure, and properties for materials of this type.

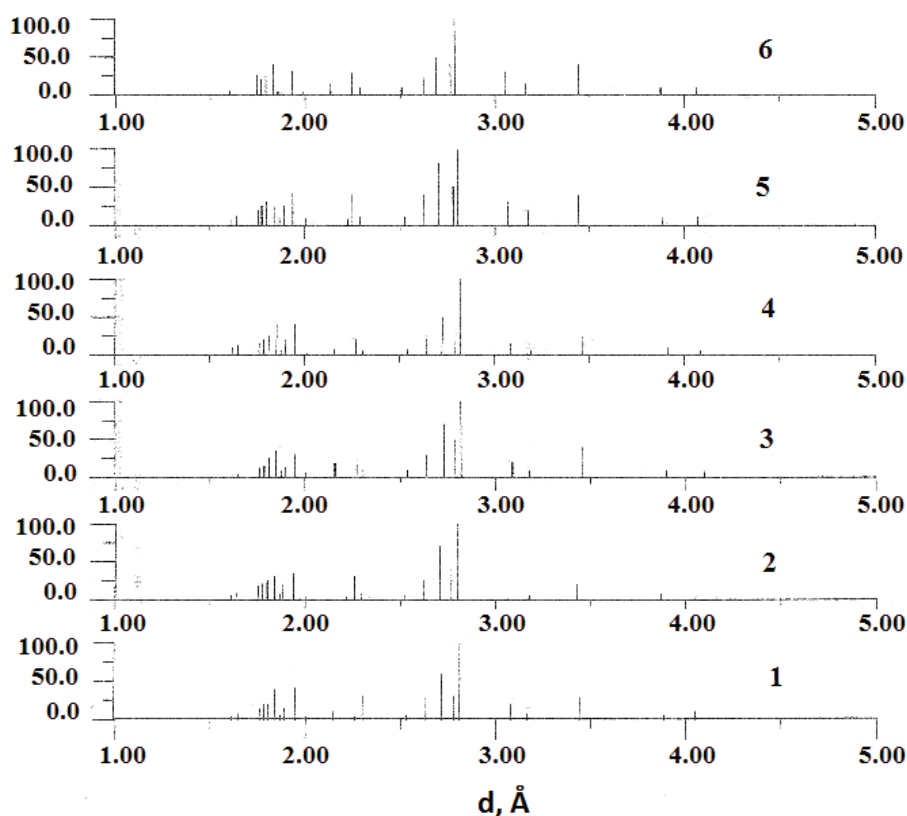
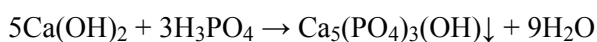


Fig. 1. X-ray reflections of solid solutions of composition $\text{Ca}_{10}(\text{PO}_4)_6(\text{OH})_{2-x}\text{F}_x$, $x = 0.0$ (1); 0.2 (2); 0.5 (3); 1.0 (4); 1.5 (5); 2.0 (6)

2. Materials and Methods

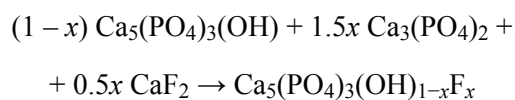
2.1. Materials, synthesis, sample preparation

$\text{Ca}(\text{OH})_2$, $\text{Ca}_3(\text{PO}_4)_2$ and CaF_2 (crystalline) of analytical purity (Merck, Germany), H_3PO_4 , and distilled water were used as starting reagents for FHA synthesis. The reagents $\text{Ca}(\text{OH})_2$, $\text{Ca}_3(\text{PO}_4)_2$ were preliminarily dried (200°C , 1 h), the CaF_2 preparation underwent the procedure of additional grinding. HA was obtained in accordance with the neutralization reaction



in air conditions at 37°C according to previously described procedures [21]. The precipitate was kept for 1 day and then filtered off with a Buchner funnel. The resulting HA powder was dried in air (room temperature, 12 h), then calcined at 900°C for 1 h and left to cool in an oven.

Fluorine-substituted FHA of $\text{Ca}_{10}(\text{PO}_4)_6(\text{OH})_{2-x}\text{F}_x$, $x = 0.0$; 0.2 ; 0.5 ; 1.0 ; 1.5 ; 2.0 , designated as FHA00, FHA10, FHA25, FHA50, FHA75 and FHA100, respectively, were obtained from a mixture of uniaxially compressed mixtures of preformed HA, $\text{Ca}_3(\text{PO}_4)_2$ and CaF_2 during the synthesis reaction



in air conditions at a temperature of 1200°C for 3 hours. Reagents for a sample with a total weight of 8 g were calculated for each degree (x) of fluorination. The sintered synthesis products were cooled together with the furnace, then crushed to obtain samples for physicochemical analysis.

2.2. Methods of analysis and characterization

X-ray phase analysis and determination of crystallographic characteristics were performed using a DRON-4 automatic diffractometer (LNPO Burevestnik, RF) ($\text{CuK}\alpha$ -radiation, graphite monochromator). X-ray diffraction of powders was observed in the range of angles $2\theta = 20 - 85^\circ$ with a step of 0.02 degrees and a counting time of 1 s for each step.

Spectroscopic data in the IR region $400-4000\text{ cm}^{-1}$ on powdered samples in suspension in paraffin oil at room temperature were obtained using a SPECORD-80M spectrometer (Karl Zeisse, Germany).

The chemical analysis of the synthesized samples was carried out using the X-ray fluorescence method, VRA-33 spectrometer (Karl Zeisse, Germany).

Dielectric permittivity (ϵ), dielectric loss tangent ($\text{tg}\delta$), and electrical conductivity (σ) of the synthesized samples were measured in air in the dynamic mode with a temperature change at a rate of $\sim 0.5 \text{ deg}\cdot\text{s}^{-1}$ and a measuring voltage of $< 15 \text{ V}$ using an automatic AC bridge. For research, the samples were prepared in the form of cylindrical tablets without adding a binder during uniaxial pressing of powdered synthesis products. The tablets were fired in air at a temperature of $\sim 800 \text{ }^\circ\text{C}$. Measuring electrodes were applied by burning silver paste at $600 \text{ }^\circ\text{C}$.

3. Results and Discussion

The diffraction patterns of the synthesized samples corresponded to the structural type of apatite (see Fig. 1). The presence of foreign phases (CaCO_3 , CaO , $\text{Ca}_3(\text{PO}_4)_2$) in the obtained synthesis products was not detected. The synthesis at elevated temperatures provided the synthesis products with a high degree of crystallinity. An increase in the content of fluorine ions in the composition of solid solutions $\text{Ca}_{10}(\text{PO}_4)_6(\text{OH})_{2-x}\text{F}_x$ was accompanied by a decrease in the values of the unit cell parameters a and c (Table 1). This decrease was not linear (Fig. 2): up to $x=1.6$, the unit cell parameters a and c remained at the level of the values for HA ($x=0$), decreasing to lower values only for FA ($x=2.0$). The Ca/P ratio in the synthesis products changed insignificantly (Table 2) and corresponded to the values given in [28] for stoichiometric HA, FA, and bone tissue apatite (Table 3).

The deviation from the linear behavior of the lattice parameters a and c of the apatite structure (Fig. 2) can be associated with the effect of carbonization during synthesis at high temperatures. In this case, the formation of a francolite type phase $(\text{Ca}, \text{Mg}, \text{Na}, \text{K})_5[(\text{P}, \text{C})\text{O}_4]_3(\text{F}, \text{OH})$ is possible (Fig. 3) [29]. This assumption is supported by the presence in the X-ray diffraction patterns of FHA solid solutions ($x=0.5; 1.0$) of reflections that are not characteristic of the apatite structure. The formation of the francolite phase seems to be characteristic of solid-phase synthesis at elevated temperatures and does not take place during the synthesis during precipitation from aqueous solutions [22]. In the structure of francolite, B-type substitutions are most likely, associated with the substitution of PO_4^{3-} groups by CO_3^{2-} ions and leading to a decrease in the a/c ratio of the apatite lattice parameters.

Table 1. The unit cell parameters of the synthesized solid solutions of $\text{Ca}_{10}(\text{PO}_4)_6(\text{OH})_{2-x}\text{F}_x$, $x = 0.0; 0.2; 0.5; 1.0; 1.5; 2.0$

Composition x	Unit cell parameters, Å	
	a	c
0.0	9.420(6)	6.892(9)
0.2	9.383(7)	6.876(7)
0.5	9.440(4)	6.903(6)
1.0	9.432(5)	6.927(7)
1.5	9.381(7)	6.896(10)
2.0	9.341(5)	6.865(8)

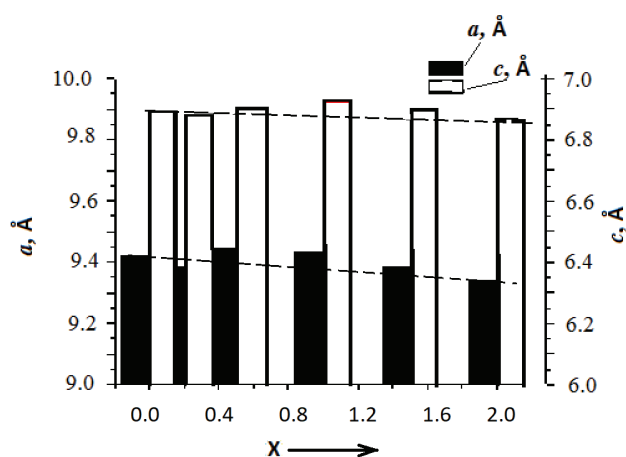


Fig. 2. Unit cell a parameters of the synthesized $\text{Ca}_{10}(\text{PO}_4)_6(\text{OH})_{2-x}\text{F}_x$, $x = 0.0; 0.2; 0.5; 1.0; 1.5; 2.0$

Table 2. Content of elements (experimental, calculated) in $\text{Ca}_{10}(\text{PO}_4)_6(\text{OH})_{2-x}\text{F}_x$ solid solutions according to X-ray fluorescence analysis data

Composition x	Content of elements in $\text{Ca}_{10}(\text{PO}_4)_6(\text{OH})_{2-x}\text{F}_x$, wt. %			
	Ca		P	
	exp.	calc.	exp.	calc.
0.0	39.9	39.89	18.5	18.50
0.2	39.9	39.88	18.9	18.49
0.5	39.6	39.86	18.9	18.48
1.0	40.0	39.82	18.9	18.46
1.5	39.8	39.78	18.6	18.44
2.0	39.4	39.74	18.4	18.43

Table 3. Composition and parameters of unit cells of native and synthesized calcium phosphates

Lattice Composition/Parameters	Dimension	Type of material		
		Bone [28]	HA	FA
Calcium (Ca)	wt. %	34.80 – 36.60	39.6	39.4
Phosphorus (P)		15.2 – 17.10	18.5	18.4
Lattice Parameters				
<i>a</i>		9.410	9.421	9.342
<i>c</i>		6.890	6.892	6.866
JCPDS data				
No. 9-432, Ca ₁₀ (PO ₄) ₆ (OH) ₂				
<i>a</i>	Å		9,418	
<i>c</i>			6,884	
No. 15-0876 Ca ₁₀ (PO ₄)F ₂				
<i>a</i>				9.368
<i>c</i>				6.884

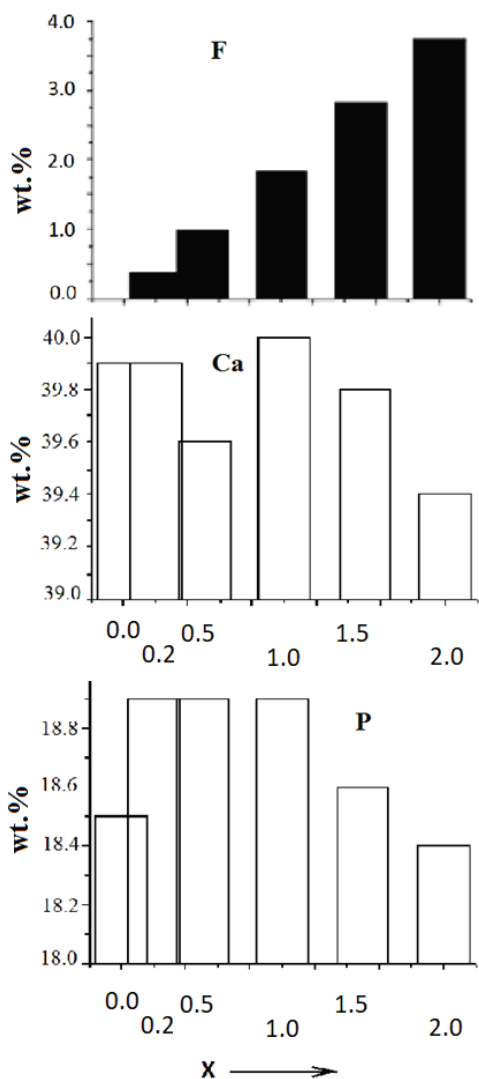


Fig. 3. Content of elements (F, Ca, P) in solid solutions Ca₁₀(PO₄)₆(OH)_{2-x}F_x, x = 0.0; 0.2; 0.5; 1.0; 1.5; 2.0 according to X-ray fluorescence analysis

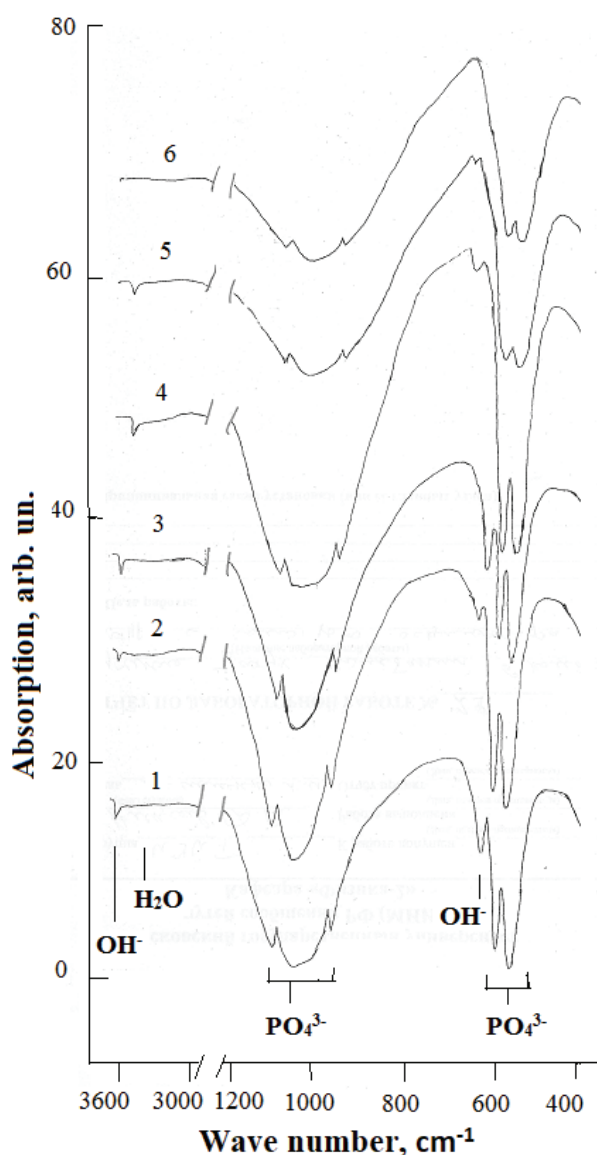
Vibrational spectra in the IR range of the synthesized solid solutions were typical of compounds with the apatite structure [30] (Table 4, Fig. 4). In the region of 3573 cm⁻¹, there was a band of stretching vibrations of the OH⁻ hydroxyl group, the intensity of which decreased as the content of fluorine ions in Ca₁₀(PO₄)₆(OH)_{2-x}F_x solid solutions increased (Table 4). It was absent in the vibrational spectra of FHA100, which agrees with the literature data for FHA100 [31, 32]. The vibrational spectra in the range of 500–800 cm⁻¹ are characterized by two strong bands in the range of 571 and 601 cm⁻¹, which belong to the ν₄ mode of the PO₄³⁻ tetrahedron of the apatite. The band at 631 cm⁻¹ corresponds to the libration mode of OH⁻ groups in Ca-channels. The position and intensity of this band depend on the degree of incorporation of fluorine ions into linear OH⁻ chains [33]. With an increase in the fluorine content, this band shifted to the region of high wave numbers, and its intensity successively decreased.

Specific values of the electrical characteristics (permittivity ε, dielectric loss tangent tan δ, electrical conductivity σ) of the studied samples of FHA solid solutions could vary slightly depending on the conditions of sample preparation. However, the general nature of the dependences on the composition and frequency of the electromagnetic field, which is determined by the structural characteristics, composition, and typical types of defects that arise during the preparation of FHA samples, was generally repeated.

The analysis of the results of electrical measurements (Figs. 5 and 6) seems to be possible on the basis of the crystal structure, composition, and

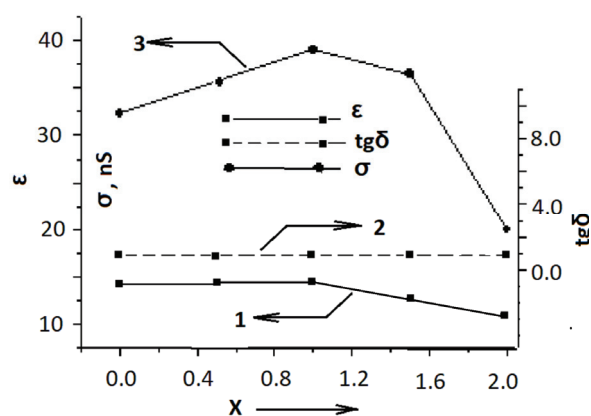
Table 4. Wave numbers (cm^{-1}) and assignment of absorption bands of IR spectra of synthesized apatites with compositions $\text{Ca}_{10}(\text{PO}_4)_6(\text{OH})_{2-x}\text{F}_x$, $x = 0.0$ (FHA0); 1.0 (FHA50); 2.0 (FHA100)

Assignment [31]	Apatite (wave numbers cm^{-1})		
	HA	FHA50	FA
OH^- (libration)	744	741	–
OH^- (stretching)	3546	3546	–
$\nu_3 \text{PO}_4^{3-}$ (stretching)	1040	1048	1048
$\nu_1 \text{PO}_4^{3-}$ (stretching)	966	970	971
$\nu_4 \text{PO}_4^{3-}$ (bending)	568, 606	568, 606	571, 606
CO_3^{2-}	1473	1470	1470

**Fig. 4.** Infrared spectra of solid solutions of composition $\text{Ca}_{10}(\text{PO}_4)_6(\text{OH})_{2-x}\text{F}_x$, $x = 0.0$ (1); 0.2 (2); 0.5 (3); 1.0 (4); 1.5 (5); 2.0 (6)

emerging defects in the structure of the investigated FHA solid solutions. In accordance with the structural data [34], the features of the dependences of ϵ , $\text{tg}\delta$, and σ on the FHA composition and the frequency of the electromagnetic field are determined to the greatest extent by the presence in the HA structure of weakly bound hydroxyl OH^- groups located perpendicular to the Ca-triangles that form channels in the apatite structure. [34]. With an increase in the content of fluorine ions in the FHA composition, conditions for easier reorientation of OH^- groups are created in the apatite structure, which leads to a decrease in the dielectric permittivity ϵ of FHA solid solutions. For FHA100 ϵ have the smallest values.

A slight change in ϵ at a frequency of 1 kHz (Fig. 5) in the course of changing the FHA composition was not accompanied by a change in dielectric losses. The values of $\text{tg}\delta$ throughout the range of changes remained practically unchanged.

**Fig. 5.** Dependences of permittivity ϵ (1), dielectric loss tangent $\text{tg}\delta$ (2), and conductivity σ (3) at a frequency $f = 1 \text{ kHz}$ on the composition of solid solutions $\text{Ca}_{10}(\text{PO}_4)_6(\text{OH})_{2-x}\text{F}_x$, $x = 0.0$; 0.2; 0.5; 1.0; 1.5; 2.0

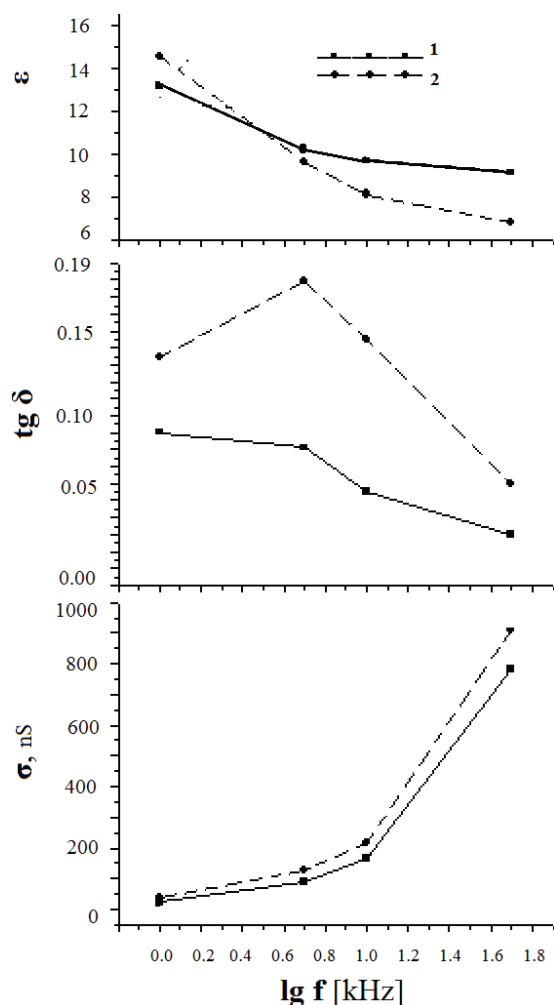


Fig. 6. Frequency dependences f of permittivity ϵ , dielectric loss tangent $\text{tg} \delta$, and conductivity σ of solid solutions $\text{Ca}_{10}(\text{PO}_4)_6(\text{OH})_{2-x}\text{F}_x$ compositions FHA100 ($x = 2.0$) (1), FHA50 ($x = 1.0$) (2)

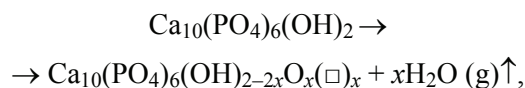
Only the conductivity σ of FHA solid solutions underwent a rather significant change. In the range of $x = 1.0$, FHA50 had a conductivity maximum (Fig. 5).

The general mechanism of conduction in HA and its solid solutions is still not fully elucidated. So far, only the fact that Ca^{2+} ions do not contribute to the conductivity seems quite certain [35, 36]. It is assumed [37] that the electrical conductivity in HA-based materials may be due to the migration of OH^- groups in the center of the Ca^{2+} triangles along the c -axis.

Measurements in an alternating electric field give grounds to assume that the charge carriers are OH^- groups [36]. However, a number of authors [38] suggest a protonic (H^+) character of conduction along OH^- chains in the apatite structure, as well as participation of O^{2-} ions in the conduction processes. The validity of the first of the listed assumptions is confirmed, for example, by the sensory moisture

characteristic of HA. Proton conductivity between neighboring OH^- ions is considered [39, 40] according to the scheme $\text{OH}^- + \text{OH}^- \rightarrow \text{O}^{2-} + \text{HOH}$ or as proton jumps between OH^- groups through neighboring PO_4^{3-} ions. In this case, since the distance between neighboring OH^- ions seems to be too large (0.344 nm) [35, 38], proton interaction with neighboring PO_4^{3-} ions is preferable (0.307 nm).

The character of conductivity is influenced to a certain extent by the prehistory of the samples. In particular, the dehydroxylation and nonstoichiometry of HA that occur during thermal treatment during the synthesis of FHA and form vacancies at the hydroxyl position as a result of the reaction in accordance with the equation [38]:



where $x < 1$, \square – vacancy.

In a number of cases [41], both H^+ and OH^- ions were considered responsible for the conductivity in different temperature ranges. Thus, the conductivity at room temperature was assumed to be due to the migration of H^+ from adsorbed water, and OH^- ions contributing at an elevated temperature. In particular, OH^- vacancies formed during dehydration can prevent H^+ conduction and facilitate conduction at the expense of OH^- [35].

Accounting for these factors greatly complicates the unambiguous interpretation of the frequency dependences of the electrical characteristics of the FHA (Fig. 6). In accordance with the results obtained, FA does not show significant changes in ϵ with frequency. To the greatest extent, the effect of the electric field frequency affects ϵ in FHA50.

Samples FHA50 and FHA100 showed dielectric losses with a maximum in the region of $f = 5$ kHz. As the field frequency increased to 50 kHz, the FHA50 and FHA100 losses began to decrease after $f = 5$ kHz (Fig. 5). In this case, the conductivity of both samples (FHA50, FHA100) with an increase in the frequency of the applied electric field increased at first not very significantly in the frequency range $f = 1$ –10 kHz, then it increased significantly in the range from 10 to 50 kHz.

The obtained results of electrical measurements of FHA solid solutions, among other applications, can be used, for example, to identify materials based on FHA solid solutions and implants based on them, as well as to determine the optimal modes of electrical stimulation of the implantation processes.

4. Conclusion

Under the conditions of solid-phase synthesis (1200 °C, 3 h) by the interaction of $\text{Ca}_{10}(\text{PO}_4)_6(\text{OH})_2$, $\text{Ca}_3(\text{PO}_4)_2$ and CaF_2 , solid solutions of the compositions $\text{Ca}_{10}(\text{PO}_4)_6(\text{OH})_{2-x}\text{F}_x$ (FHA), $x = 0.0$; 0.2; 0.5; 1.0; 1.5; 2.0 (designation: FHA00, FHA10, FHA25, FHA50, FHA75 and FHA100).

The X-ray diffraction patterns of the synthesized FHA corresponded to the structural type of apatite; there were no foreign phases in the synthesis products. The structural characteristics of the obtained hydroxyapatite (FHA00) and fluorapatite (FHA100) corresponded to the data of JCPDS nos. 09-0432 (HA) and 15-0876 (FA), respectively.

The results of vibrational IR spectroscopy are consistent with X-ray data and correspond to the structural type of apatite; all the bands characteristic of apatite (PO_4^{3-} , OH^- , CO_3^{2-}) were present in the FHA spectra.

In the frequency range of an electromagnetic field of 1 kHz, the dielectric loss tangent $\text{tg}\delta$ with an increase in the content of fluorine ions F^- in FHA solid solutions remained practically unchanged, the values of the permittivity ϵ decreased in the region $x > 1.0$, and the electrical conductivity σ at $x = 1.0$ had a maximum, decreasing then with increasing values of x up to $x = 2$.

In the frequency range of the electromagnetic field up to 100 kHz, for the compositions of the FHA100 ($x = 2$) and FHA50 ($x = 1$) solid solutions, there is a slight decrease in the permittivity ϵ and a multiple increase in the conductivity σ . The frequency value of 60 kHz corresponds to anomalies in the behavior of the frequency dependence of the dielectric loss tangent $\text{tg}\delta$: for FHA50 this is a characteristic maximum, and for FHA100 it is a break in the frequency dependence of $\text{tg}\delta$.

The results obtained can be used for directed synthesis of FHA solid solutions for medical use, identification of synthesis products, and selection of conditions for electrical action on such materials in the composition of medical preparations.

5. Funding

The work was carried out within the framework of the state task of the IGIC RAS in the field of fundamental scientific research.

6. Conflict of interest

The authors declare no conflict of interest.

References

1. Kitaev VM, Kitaev SV, Bronov OYu. *Radiation diagnostics of bone tissue pathology*. Moscow: MEDpress-inform, 2022. 184 p. (In Russ.)

2. Vallet-Regi M. *Bio-ceramics with clinical applications*. USA: John Wiley & Sons; 2014. p. 17-22.

3. Bairo F, Novajra G, Vitale-Brovarone C. Bioceramics and scaffolds: a winning combination for tissue engineering. *Frontiers in Bioengineering and Biotechnology*. 2015;3:202-222. DOI:10.3389/fbioe.2015.00202

4. Pajor K, Pajchel L, Kolmas J. Hydroxyapatite and fluorapatite in conservative dentistry and oral implantology – a review. *Materials*. 2019;12(17):2683-2699. DOI:10.3390/ma12172683

5. Dorozhkin SV. Calcium orthophosphate (CaPO_4)-based bioceramics: preparation, properties, and applications. *Coatings*. 2022;12(10):1-89. DOI:10.3390/coatings12101380

6. Ippolitov YA, Plotnikova YA, Seredin PV. Hygienic aspects of endo- and exogenic methods of prevention of caries and their efficiency in the remineralization of teeth enamel. *Gigiyena i Sanitariya*. 2018;97(8):710-713. DOI: 10.18821/0016-9900-2018-97-8-710-713 (In Russ.)

7. de Groot K. Bioceramics consisting of calcium phosphate salts. *Biomaterials*. 1980;1(1):47-50. DOI:10.1016/0142-9612(80)90059-9

8. Feroz S, Khan AS. Fluoride-substituted hydroxyapatite. In: Khan AS, Chaudhry AA. (eds.) *Handbook of Ionic Substituted Hydroxyapatites*. Woodhead Publishing; 2020. p. 175-196. DOI:10.1016/b978-0-08-102834-6.00007-0

9. World Health Organization, *Guidelines for drinking-water quality*. Geneva; 2011. 564 p. Available from: https://apps.who.int/iris/bitstream/handle/10665/44584/9789241548151_eng.pdf?sequence=1 [Accessed 15 February 2023]

10. Borisova EG, Komova AA, Ermolovich AA, et al. Caries resistance of enamel. Modern view on prevention of dental caries. *Mediko-farmatsevticheskiy zhurnal "Puls" = Medical & Pharmaceutical Journal "Pulse"*. 2019;21(12):16-21. DOI:10.26787/nydha-2686-6838-2019-21-12-16-21 (In Russ.)

11. Shchapova YV, Votyakov SL, Mikhalevsky GB, et al. Impurity luminescence centers in fluorapatite from quartz-bearing paragenesis according to photo-, cathode- and synchrotron-induced luminescence. *Geodynamics & Tectonophysics*. 2022;13(3):0610. DOI:10.5800/GT-2022-13-2s-0610

12. Stanić V, Dimitrijević S, Antonović DG, Jokić BM, Zec SP, Tanasković ST, Raičević S. Synthesis of fluorine substituted hydroxyapatite nanopowders and application of the central composite design for determination of its antimicrobial effects. *Applied Surface Science*. 2014;290:346-352. DOI: 10.1016/j.apsusc.2013.11.081

13. Wang L, He S, Wu X, Liang S, Mu Z, Wei J, Deng F, Deng Y, Wei S. Polyetheretherketone/nano-fluorohydroxyapatite composite with antimicrobial activity and osseointegration properties. *Biomaterials*. 2014;35:6758-6775. DOI:10.1016/j.biomaterials.2014.04.085

14. Youness RA, Taha MA, Ibrahim M. In vitro bioactivity, physical and mechanical properties of carbonated-fluoroapatite during mechanochemical

- synthesis. *Ceramics International*. 2018;44(17):21323-21329. DOI:10.1016/j.ceramint.2018.08.184
15. Milligan RS. *Feature of apatite in kimberlite from ekaite mine diamond and lake: modeling kimberlite composition*. Dalhousie University: Halifax, Nova Scotia; 2017. p. 1-86.
16. Pan Y, Fleet ME. Compositions of the apatite-group minerals: substitution mechanisms and controlling factors. *Reviews in Mineralogy and Geochemistry*. 2002;48(1):13-49. DOI:10.2138/rmg.2002.48.2
17. Ptáček P. Rare-earth element-bearing apatites and oxyapatites. *Apatites and their Synthetic Analogues*. 2016;475:408-414. DOI:10.5772/62209
18. Stockli D, Boyd P, Galster F. Intra-grain common Pb correction in apatite by LA-ICP-MS depth profiling and implications for detrital apatite U-Pb dating. *EGU General Assembly*. 2017;19:2017-12225. DOI: 10.1016/j.ceramint.2010.02.033
19. Evis Z, Sun ZP. Structural and mechanical investigations of magnesium and fluoride doped nanosize calcium phosphates. *Journal of Ceramic Processing Research*. 2010;11:701-715.
20. Akhmedbeyli RM. Microhardness of enamel and dentine on temporary and permanent teeth formed with fluoride-iodine deficiency. *Kazanskiy meditsinskiy zhurnal*. 2018;99(4):22-32. DOI:10.17816/KMJ2018-625 (In Russ.)
21. Hussin MS, Abdullah HZ, Izwana Idris MI. Extraction of natural hydroxyapatite for biomedical applications – a review. *Heliyon*. 2022;8(8):1-11. DOI:10.1016/j.heliyon.2022.e10356
22. Pajor K, Pajchel L, Kolmas J. Hydroxyapatite and fluorapatite in conservative dentistry and oral implantology – A Review. *Materials*. 2019;12(17):2683-2689. DOI:10.3390/ma12172683
23. Eliaz N, Metoki N. Calcium phosphate bioceramics: a review of their history, structure, properties, coating technologies and biomedical applications. *Materials*. 2017;10:334-337. DOI:10.3390/ma10040334
24. Ptáček P. Substituents and dopants in the structure of apatite. *Materials Science, Geology*. 2016;13:19-33. DOI:10.5772/62213
25. Okazaki M, Miake Y, Tohda H, Yanagisawa T, Matsumoto T, Takahashi J. Functionally graded fluoridated apatites. *Biomaterials*. 1999;20:1421-1426. DOI:10.1016/s0142-9612(99)00049-6
26. Seyedmajidi S, Seyedmajidi S, Alaghehmand H. Synthesis and characterization of hydroxyapatite/bioactive glass nanocomposite foam and fluorapatite/bioactive glass nanocomposite foam by gel casting method as cell scaffold for bone tissue. *Eurasian Journal of Analytical Chemistry*. 2018;13(2):1-15. DOI:10.29333/ejac/85078
27. Gytoku H, Azuma Y, Furuzono T. Evaluation of fluorinated hydroxyapatite nanoparticles as an antibacterial material for catheter coating. *Renal Replacement Therapy*. 2020;6(3):2-8. DOI:10.1186/s41100-019-0251-6
28. Dorozhkin SV. Nanometric calcium orthophosphates (CaPO₄): preparation, properties and biomedical applications. *Advanced Nano-Bio-Materials and Devices*. 2020;3(4):421-513.
29. Rodicheva GV, Orlovsky VP, Romanova NM. Synthesis and physicochemical study of carbonate hydroxyapatites. *Zhurnal neorganicheskoy khimii = Russian Journal of Inorganic Chemistry*. 1996;41(5):754-757. (In Russ.)
30. Massit A, Yacoubi A, Rezzouk A, et al. Thermal behavior of Mg-doped calcium-deficient apatite and stabilization of β tricalcium phosphate. *Biointerface Research in Applied Chemistry*. 2020;10(6):6837-6845. DOI:10.33263/BRIAC106.68376845
31. Shafiei F, Behroozbakhsh M, Moztafzadeh F. Nanocrystalline fluorine-substituted hydroxyapatite [Ca₅(PO₄)₃(OH)_{1-x}F_x(0≤x≤1)] for biomedical applications: preparation and characterization. *Micro & Nano Letters*. 2013;7(2):109-114. DOI:10.1049/mnl.2011.0533
32. Gao Y, Karpukhina N, Law RV. Phase segregation in hydroxyfluorapatite solid solution at high temperatures studied by combined XRD/solid state NMR. *RSC Advances*. 2016;6:103782-103790. DOI:10.1039/c6ra17161c
33. Elliott JC. Structure and chemistry of the apatites and other calcium orthophosphates. *Studies in Organic Chemistry*. 1994;18:94008066-94008066.
34. Smolegovsky AM. *History of crystal chemistry of phosphates*. Moscow: Nauka; 1986. p. 49–98. (In Russ.)
35. Avakyan LA, Paramonova EA, Coutinho J. Optoelectronics and defect levels in hydroxyapatite by first-principles. *Electronic*. 2018;26:1-14. DOI:10.1063/1.5025329
36. Takahashi T, Tanase S, Yamamoto O. Electrical conductivity of some hydroxyapatites. *Electrochimica Acta*. 1978;23(4):369-373. DOI:10.1016/0013-4686(78)80076-0
37. Alkhalzali A, Etier M, Aljarrah M, Momani HA, Salman F. Structural, thermal and electrical properties of ionic conductors (AgPO₃)_{1-x}(Ag₂SO₄)_x glass systems. *International Journal of Microstructure and Materials Properties*. 2019;14(6):536. DOI:10.1504/IJMMP.2019.103182
38. Demirel B, Saban E, Yaras A, Akkurt F. Synthesis of Gd⁺³ doped hydroxyapatite ceramics: optical, thermal and electrical properties. *Journal of Asian Ceramic Societies*. 2021;9(3):865-873. DOI:10.1080/21870764.2021.1920160
39. Bystrova A, Dekhtyar Y, Sapronova A, Bystrov VS, Pullar RC, et al. Study of polar and electrical properties of Hydroxyapatite: Modeling and data analysis. *2013 Joint IEEE International Symposium on Applications of Ferroelectric and Workshop On Piezoresponse Force Microscopy (ISAF/PFM)*. 2013;100-103. DOI:10.1109/ISAF.2013.6748702
40. Aljerf L, Choukaife AE. Hydroxyapatite and fluoroapatite behavior with pH change. *International Medical Journal*. 2017;24(5):407-410. DOI:10.1006/jssc.2000.8958
41. Doi K, Abe Y, Kobatake R, Okazaki Y, Oki Y, et al. Novel development of phosphate treated porous hydroxyapatite. *Materials*. 2017;10(12):1405. DOI:10.3390/ma10121405

Information about the authors / Информация об авторах

Nikolay A. Zakharov, D. Sc. (Phys. and Math.), Chief Research Officer, Kurnakov Institute of General and Inorganic Chemistry, Moscow, Russian Federation; ORCID 0000-0002-2326-408X; e-mail: zakharov@igic.ras.ru

Ali D. Aliev, Cand. Sc. (Phys. and Math.), Senior Researcher, The Institute of Physical Chemistry and Electrochemistry RAS, Moscow, Russian Federation; ORCID 0000-0001-9736-78869; e-mail: ali_aliev1948@mail.ru

Vladimir V. Matveev, Cand. Sc. (Phys. and Math.), Senior Researcher, The Institute of Physical Chemistry and Electrochemistry RAS, Moscow, Russian Federation; ORCID 0000-0002-5221-8488; e-mail: matveev46@jandex.ac.ru

Michail R. Kiselev, Cand. Sc. (Phys. and Math.), Senior Researcher, The Institute of Physical Chemistry and Electrochemistry RAS, Moscow, Russian Federation; ORCID 0000-0003-2309-257X; e-mail: Kisselev@phyche.ac.ru

Elena M. Koval, Research Officer, Kurnakov Institute of General and Inorganic Chemistry, Moscow, Russian Federation; ORCID 0000-0002-3145-3753; e-mail: Elena375Lavok@jandex.ru

Evgeni V. Shelekhov, Cand. Sc. (Phys. and Math.), Senior Researcher, National University of Science and Technology (MISiS), Moscow, Russian Federation; ORCID 0000-0002-7294-8197; e-mail: radish13@yandex.ru

Ludmila V. Goeva, Cand. Sc. (Chem.), Senior Researcher, Kurnakov Institute of General and Inorganic Chemistry, Moscow, Russian Federation; ORCID 0000-0002-7294-8197; e-mail: lydmila_goeva@mail.ru

Tatiana V. Zakharova, Cand. Sc. (Phys. and Math.), Senior Researcher, Russian University of Transport (MIIT), Moscow, Russian Federation; ORCID 0000-0002-6688-3163; e-mail: rathatvz@mail.ru

Захаров Николай Алексеевич, доктор физико-математических наук, главный научный сотрудник, Институт общей и неорганической химии РАН, Москва, Российская Федерация; ORCID 0000-0002-2326-408X; e-mail: zakharov@igic.ras.ru

Алиев Али Джавадович, кандидат физико-математических наук, старший научный сотрудник, Институт физической химии и электрохимии РАН, Российская Федерация; ORCID 0000-0001-9736-78869; e-mail: ali_aliev1948@mail.ru

Матвеев Владимир Васильевич, кандидат физико-математических наук, старший научный сотрудник, Институт физической химии и электрохимии РАН, Москва, Российская Федерация; ORCID 0000-0002-5221-8488; e-mail: matveev46@jandex.ac.ru

Киселев Михаил Романович, кандидат физико-математических наук, старший научный сотрудник, Институт физической химии и электрохимии РАН, Москва, Российская Федерация; ORCID 0000-0003-2309-257X; e-mail: Kisselev@phyche.ac.ru

Коваль Елена Михайловна, научный сотрудник, Институт общей и неорганической химии РАН, Москва, Российская Федерация; ORCID 0000-0002-3145-3753; e-mail: Elena375Lavok@jandex.ru

Шелехов Евгений Владимирович, кандидат физико-математических наук, старший научный сотрудник, Национальный исследовательский технологический университет МИСИС, Москва, Российская Федерация; ORCID 0000-0002-7294-8197; e-mail: radish13@yandex.ru

Гоева Людмила Викторовна, кандидат химических наук, старший научный сотрудник, Институт общей и неорганической химии РАН, Москва, Российская Федерация; ORCID 0000-0002-7294-8197; e-mail: lydmila_goeva@mail.ru

Захарова Татьяна Владимировна, кандидат физико-математических наук, старший научный сотрудник, Российский университет транспорта (МИИТ), Москва, Российская Федерация; ORCID 0000-0002-6688-3163; e-mail: rathatvz@mail.ru

Received 02 March 2023; Accepted 28 April 2023; Published 06 July 2023



Copyright: © Zakharov NA, Aliev AD, Matveev VV, Kiselev MR, Koval EM, Shelekhov EV, Goeva LV, Zakharova TV, 2023. This article is an open access article distributed under the terms and conditions of the Creative Commons Attribution (CC BY) license (<https://creativecommons.org/licenses/by/4.0/>).

Sorption kinetics of organic dyes methylene blue and malachite green on highly porous carbon material

© Ali H. K. Kadum^a, Irina V. Burakova^a✉, Elina S. Mkrtchyan^a, Oksana A. Ananyeva^a, Vladimir O. Yarkin^a, Alexander E. Burakov^a, Alexey G. Tkachev^a

^a Tambov State Technical University,
Bld. 2, 106/5, Sovetskaya St., Tambov, 392000, Russian Federation

✉ iris_tamb68@mail.ru

Abstract: In the article, the purpose of the research was to determine the important parameters of the organic compounds sorption – synthetic dyes methylene blue (MB) and malachite green (MG), on mesoporous carbon (MPC) from aqueous solutions in a limited volume. For the sorbent used, the elemental composition and the BET surface area were determined by nitrogen adsorption, which amounted to 2360 m²·g⁻¹. Adsorption mechanisms were analyzed using kinetic dependences and sorption isotherms, for which empirical equations of pseudo-first and -second order, the Elovich equation and the intraparticle diffusion equation, as well as Langmuir, Freundlich, Dubinin-Radushkevich equations were used. In the course of kinetic studies, it was found that equilibrium occurs after 15 min of extraction with an adsorption capacity of 2446.6 mg·g⁻¹ for MB and 2043.1 mg·g⁻¹ for MG. It should be noted that the extraction of dye molecules proceeded predominantly by a mixed-diffusion mechanism and was controlled by a second-order reaction by a pseudo-second order model. The activation energy was 0.016 kJ·mol⁻¹ for MG molecules, and 0.013 kJ·mol⁻¹ for MB ones, which confirmed the physical mechanism of dye uptake. Thus, in the course of experimental studies, the high efficiency of the developed sorbent for the purification of aqueous systems from organic compounds was confirmed.

Keywords: carbon nanotubes; mesoporous carbon; synthetic dyes; methylene blue; malachite green; adsorption; kinetics; isotherms.

For citation: Kadum AHK, Burakova IV, Mkrtchyan ES, Ananyeva OA, Yarkin VO, Burakov AE, Tkachev AG. Sorption kinetics of organic dyes methylene blue and malachite green on highly porous carbon material. *Journal of Advanced Materials and Technologies*. 2023;8(2):130-140. DOI: 10.17277/jamt.2023.02.pp.130-140

Кинетика сорбции органических красителей метиленового синего и малахитового зеленого на высокопористом углеродном материале

© А. Х. К. Кадум^a, И. В. Буракова^a✉, Э. С. Мкртчян^a, О. А. Ананьева^a, В. О. Яркин^a, А. Е. Бураков^a, А. Г. Ткачев^a

^a Тамбовский государственный технический университет,
ул. Советская, 106/5, пом. 2, Тамбов, 392000, Российская Федерация

✉ iris_tamb68@mail.ru

Аннотация: В статье целью исследований являлось определение важных параметров сорбции органических соединений – синтетических красителей метиленового синего (МС) и малахитового зеленого (МЗ), на мезопористом углероде (МПУ) из водных растворов в ограниченном объеме. Для используемого сорбента определены элементный состав и площадь поверхности по БЭТ по адсорбции азота, которая составила 2360 м²/г. Проведен анализ механизмов поглощения с помощью кинетических зависимостей и изотерм сорбции, для чего применялись эмпирические уравнения псевдо-первого и псевдо-второго порядка, Еловича и внутримолекулярной диффузии, а также уравнения Ленгмюра, Фрейндлиха, Дубинина–Радушкевича. В ходе кинетических исследований установлено, что равновесие наступает после 15 мин извлечения при величине адсорбционной

емкости 2446,6 мг/г по МС и 2043,1 мг/г по МЗ. Следует отметить, что извлечение молекул красителей проходит преимущественно по смешанно-диффузионному механизму и контролируется реакцией второго порядка согласно модели псевдо-второго порядка. Энергия активации имеет значение 0,016 кДж/моль по молекулам МЗ и 0,013 кДж/моль для МС, что подтверждает физический механизм поглощения красителей. Таким образом, в ходе экспериментальных исследований подтверждена высокая эффективность разработанного сорбента для очистки водных систем от соединений органической природы.

Ключевые слова: углеродные нанотрубки; мезопористый углерод; синтетические красители; метиленовый синий; малахитовый зеленый; адсорбция; кинетика; изотермы.

Для цитирования: Kadum AHK, Burakova IV, Mkrtchyan ES, Ananyeva OA, Yarkin VO, Burakov AE, Tkachev AG. Sorption kinetics of organic dyes methylene blue and malachite green on highly porous carbon material. *Journal of Advanced Materials and Technologies*. 2023;8(2):130-140. DOI: 10.17277/jamt.2023.02.pp.130-140

1. Introduction

Water pollution is a serious environmental problem, which has reached an alarming level as a result of industrial development [1, 2]. Organic contaminants include dyes, which have a high solubility, thereby complicating the process of their removal from water [3]. In addition, due to the difficulty of biodegradation, water-soluble pigments are highly toxic and carcinogenic compounds, causing a serious environmental impact with serious problems for animals, plants and human health. On the other hand, textile, paper-printing, paint and varnish, leather, food and cosmetic factories are the largest consumers of dyes, since dye production is estimated at one million tons per year [4, 5]. Among these dyes, methylene blue (MB) as a cationic dye causes many health problems such as: allergic dermatitis, skin irritation, cancer, and mutations [6, 7]. Malachite green (MG) belongs to the same group of triphenylmethane dyes as crystal violet, which has been shown to be carcinogenic, so it can be assumed that MG also has these carcinogenic properties. Laboratory tests have also shown that MG can damage DNA after metabolic activation in vitro, although no genotoxicity has been demonstrated in in vivo tests [8].

Some technologies have been developed for industrial wastewater treatment, including adsorption, ion exchange, membrane filtration, chemical/electrochemical, chemical precipitation, ozonation, oxidation, photodegradation, and bioactive sludge [9–11].

Adsorption is an inexpensive method in which activated carbon is most often used as sorption materials due to its porous structure, a large number of surface functional groups, and ease of regeneration [12–15]. However, ordinary activated carbon mainly contains a large number of micropores with a pore size of less than 2 nm, which cannot allow large diameter dye molecules to access the inner surface of the carbon, resulting in low adsorption capacity, so its application is highly limited [16].

Many research teams are developing new sorbents based on nanomaterials – carbon nanotubes (CNTs), graphene oxide (GO), etc. They show very high efficiency in the removal of organic dyes from liquids. The paper [17] presents the results on the adsorption capacity of a porous material based on modified carbon, 2555 mg·g⁻¹, upon removal of dye MB molecules. In the article [18], the sorption capacity of a nanocomposite material based on graphene oxide modified with lignosulfonate was studied. As a result of the extraction of MB dye molecules, the authors of the article revealed the adsorption capacity of the adsorbent – 1822.3 mg·g⁻¹. The authors of [19] used a graphene aerogel to remove MB dye molecules. As a result of research, the authors of the work revealed the adsorption capacity of graphene aerogel equal to 420 mg·g⁻¹.

Mesoporous carbon (MPC) with pore sizes (2–50 nm) has a higher adsorption capacity with respect to some macromolecular substances, such as a dye, an antibiotic, some natural organic substances, etc. [20], since such bulky molecules of pollutants easily diffuse in volume and are adsorbed on the surface of pores. Mesoporous materials are promising sorption materials that are quite effectively used by scientific communities around the world for the adsorption removal of various contaminants, including MB molecules [21, 22].

The paper aims are to study the adsorption of organic contaminants – MB and MG dyes – on a mesoporous carbon material, as well as to reveal the absorption mechanism using kinetic and isothermal models.

2. Materials and Methods

2.1. Material synthesis

The procedure for the MPC synthesis was described in detail in [23]. The initial components for preparing MPC were aqueous solutions of dextrin, phenol-formaldehyde resin and multi-walled carbon nanotubes (CNTs) (NanoTechCenter Ltd., Tambov). The mixture was evenly stirred at 300 °C, then mixed

with potassium hydroxide and activated at 750 °C. The material was washed stepwise with an aqueous solution of hydrochloric acid and distilled water. The resulting aqueous paste was dried at 110 °C to constant weight.

2.2. Analytical methods

The MPC surface morphology was studied using a MERLIN scanning electron microscope (SEM) (Carl Zeiss, Jena, Germany) with Oxford Instruments X-ray microanalysis attachments. Surface area and porosity were measured by nitrogen adsorption using an Autosorb-1 analyzer (Quantachrome, Odelzhausen, Germany).

2.3. Kinetic study

To determine the kinetic parameters of MB and MG adsorption, experiments were carried out under static conditions; for this, 0.01 g of MPC was taken, the initial concentration of solutions of dyes MB and MG was 1500 mg·L⁻¹, the volume of the solution was 30 mL. The solutions were shaken for 5, 10, 15, 30 and 60 min at 100 rpm and room temperature on a Multi Bio RS-24 rotator (Biosan) and then filtered.

2.4. Isothermal study

Equilibrium studies were carried out using 0.01 g of MPC and 30 mL of solutions of MB and MG with initial concentrations of 150–1500 mg·L⁻¹. The tubes with solutions were shaken for 15 min at 100 rpm and room temperature on a programmable rotator Multi Bio RS-24 (Biosan). In all sorption experiments, the amount of dye in the liquid phase before and after adsorption was determined spectrophotometrically (Ekros, St. Petersburg, Russia) at wavelengths of 815 and 710 nm for MB and MG, respectively.

3. Results and Discussion

3.1. MPC characteristics

According to the obtained micrographs (Figs. 1a, b), mesoporous carbon is a composite, in the structure of which there are individual CNTs (10–20 nm in diameter) deformed as a result of alkaline activation, covered with a rather uniform layer of a certain shell.

According to Fig. 2, the sample under consideration is a carbon material with an amount of C = 94.09 wt. % with an admixture of oxygen O = 5.67 wt. %. The presence of oxygen is associated with the chemisorption of atmospheric oxygen on the surface of the obtained material due to the fact that the activation is carried out in a reducing medium containing metallic potassium.

The specific surface area of the material was determined by the BET method and its value was 2360 m²·g⁻¹ for nitrogen.

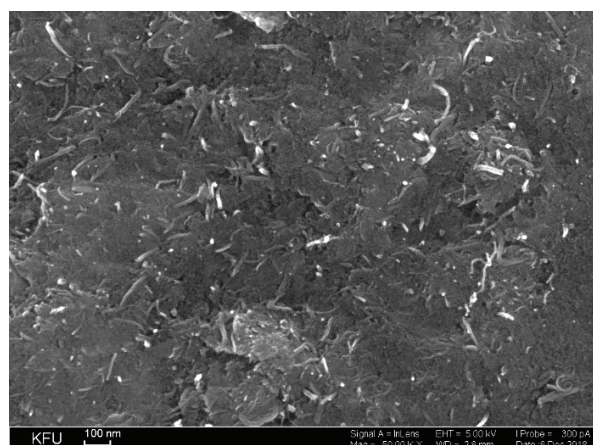
3.2. Kinetic study

The equilibrium adsorption capacity (Q_e , mg·g⁻¹) of the material was determined from the following expression:

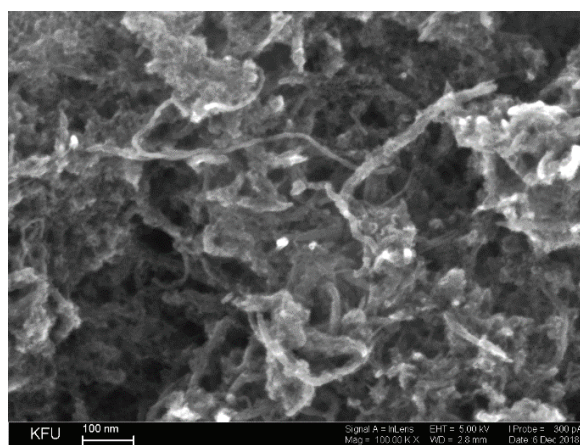
$$Q_e = \frac{V(C_0 - C_e)}{m}, \quad (1)$$

where C_0 (mg·L⁻¹) is initial solution concentration; C_e (mg·L⁻¹) is equilibrium concentration of dye in solution (after adsorption); V (L) is the solution volume; m (g) is the adsorbent weight.

The adsorption kinetics depends on many factors. To describe the adsorption rate, it is necessary to take into account the limiting stage of



(a)



(b)

Fig. 1. SEM micrographs of MPC: a – magnification 50.00 kX; b – magnification 100.00 kX

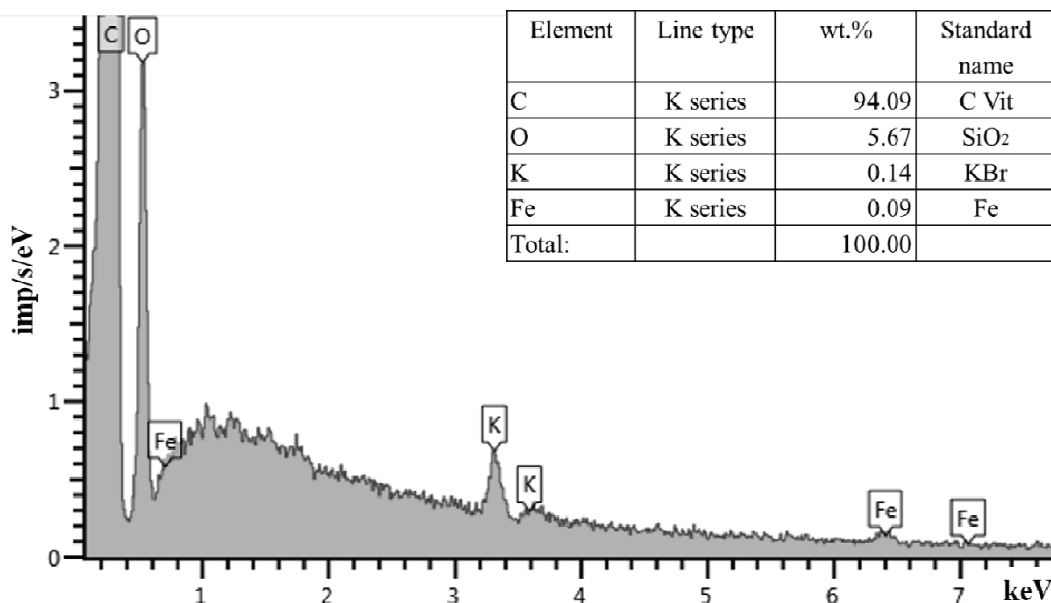


Fig. 2. Elemental analysis of MPC

the process. As for any heterogeneous chemical reaction, the adsorption reaction can proceed in the diffusion region, when the adsorption limiting step is the delivery of the adsorbate to the adsorbent surface, and in the kinetic region, when the rate of chemisorption for the process is the limiting step.

Based on the results of the experiments, the kinetic dependences of the adsorption of MB and MG were plotted (Fig. 3). According to the data obtained, the adsorbent exhibits high adsorption activity with respect to organic molecules: 2446.6 mg·g⁻¹ according to MB and 2043.1 mg·g⁻¹ according to MG. Adsorption equilibrium is reached within 15 minutes.

To describe the process of sorption of MB and MG molecules, namely, the mechanisms involved in the transfer of sorbate to the surface and inside the structure of sorbents, the obtained experimental data were processed by equations of known kinetic models (pseudo-first and pseudo-second order, Elovich and intraparticle diffusion) [24–26].

Phenomenological models are often used that imitate mass transfer processes with the help of formal equations of chemical kinetics. This is due to the complexity of the quantitative description of diffusion processes using simple models. This approach most often involves the use of pseudo-first and pseudo-second order models.

The Lagergren equation is called a pseudo-first order equation and is used to describe kinetic processes that depend on the concentration of a solution and the sorption capacity of a solid. This equation is widely used in the literature to describe the sorption kinetics and is the first rate equation developed to describe sorption in liquid/solid systems [24].

Currently, the pseudo-second order equation is used to describe and correlate the kinetic data of solid/solution sorption systems [25, 26]. The applicability of this model indicates the occurrence of a reaction that limits the sorption kinetics. This is obviously due to the fact that the theoretical substantiation of the pseudo-second order model is based on fundamental theories of surface reactions. There are studies in which the pseudo-second order model is considered as a rather flexible mathematical formula capable of modeling the sorption kinetics of internal mass transfer (diffusion) for systems with flat and spherical particles [26].

The intraparticle diffusion equation was developed for sorbents with a system of pores, the size of which allows the sorbate molecules to penetrate inside and settle there. In this case, the rate of the internal mass transfer stage is taken into account, i.e. diffusion of the sorbate in the pores of

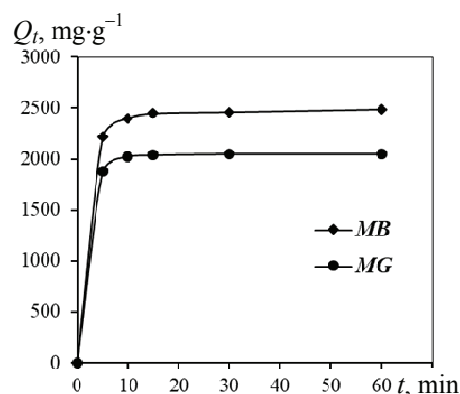


Fig. 3. Adsorption kinetics of MB and MG molecules on MPC

the sorbent with spherical particles [26]. If the dependency Q_t vs. t is a straight line passing through the origin ($C = 0$), then we can assume that internal diffusion is the limiting stage of adsorption. If, when constructing Q_t vs. t , a straight section was obtained that does not pass through the origin of coordinates; this may be due to the difference in the mass transfer rate at the initial and final stages of sorption. In addition, such a deviation of straight lines from the origin of coordinates may indicate that diffusion in pores is not the only limiting stage [26].

According to Fig. 4, rather low values of the coefficients ($R^2 = 0.8483$; 0.421) of the pseudo-first order model (Fig. 4a, Table 1) suggest that there is no chemical interaction of the dye molecules MB and MG with the functional groups of the sorbent. The pseudo-second order model with $R^2 = 0.9999$ for both dyes (Fig. 4b, Table 1) describes the absorption well, which indicates the occurrence of a second-order reaction on the surface of the sorbent. Satisfactory correlation of experimental data in the coordinates of the Elovich model indicates the energy inhomogeneity of the sorbent surface, which, in turn, promotes chemical adsorption [27].

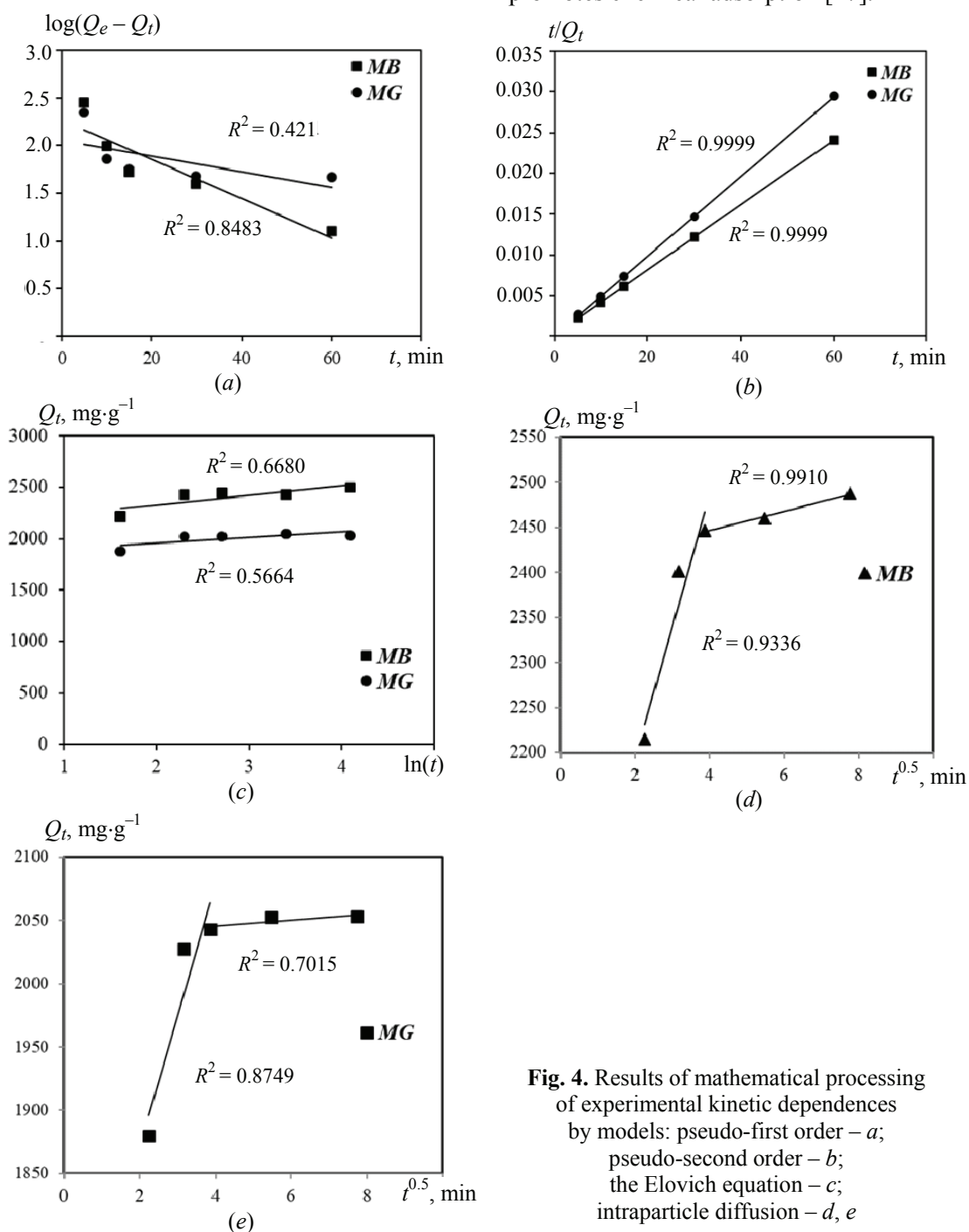


Fig. 4. Results of mathematical processing of experimental kinetic dependences by models: pseudo-first order – a; pseudo-second order – b; the Elovich equation – c; intraparticle diffusion – d, e

Table 1. Kinetic parameters of organic dye sorption*

Dye	Model parameter					
	Pseudo-first order			Pseudo-second order		
	$\log(Q_e - Q_t) = \log Q_e - \frac{k_1}{2.303} t$			$\frac{t}{Q_t} = \frac{1}{k_2 Q_e^2} + \frac{1}{Q_e} t$		
	Q_e	k_1	R^2	Q_e	k_2	R^2
MB	187.28	0.047	0.8483	2500	0.0003	0.9999
MG	114.18	0.008	0.4210	2000	0.0028	0.9999
	Elovich equation			Intraparticle diffusion equation		
	$Q_t = \frac{1}{\beta} \ln(\alpha\beta) + \frac{1}{\beta} \ln t$			$Q_t = k_{id} t^{0.5} + C$		
	α	β	R^2	k_{id}	C	R^2
MB	$8.67 \cdot 10^{11}$	0.0107	0.6680	144.3/10.57	1908.3/2404.3	0.9336/0.991
MG	$2.16 \cdot 10^{16}$	0.0182	0.5664	102.5/2.42	1666.7/2035.7	0.8749/0.7015

* Q_t ($\text{mg} \cdot \text{g}^{-1}$) the number of adsorbed dye molecules on the adsorbent surface at a time t ; k_1 (min^{-1}) pseudo-first order adsorption rate constant; k_2 ($\text{g} \cdot (\text{mg} \cdot \text{min})^{-1}$) pseudo-second order adsorption rate constant; α ($(\text{min} \cdot \text{mg} \cdot \text{g}^{-1})^{-1}$) adsorption constant; β ($\text{g} \cdot \text{mg}^{-1}$) degree of surface coverage and chemisorption activation energy; k_{id} ($(\text{mg} \cdot (\text{g} \cdot \text{min})^{-1})^{-1}$) internal diffusion coefficient; C ($\text{mg} \cdot \text{g}^{-1}$) boundary layer thickness.

The adsorption of MB and MG under the conditions under consideration does not obey the Elovich model (Fig. 4c, Table 1).

The sorption rate can be limited both by the stage of chemical interaction and by the sorbate diffusion. In this case, transport processes (the movement of sorbate molecules from the solution to the active centers of the sorbent) play an important role in the sorption system. It is possible to estimate the contribution of the diffusion process to the sorption kinetics using the intraparticle diffusion model. The constant C in the equation of this model is proportional to the thickness of the boundary layer. If it is equal to zero, that is, the straight line passes through the origin, then the sorption process is limited by internal diffusion [26]. According to the data obtained (Fig. 4d, e), the dependences in the coordinates Q_t vs. $t^{0.5}$ are bilinear – the sorption of dyes is accompanied by two stages. The first sharper step is associated with diffusion in the boundary layer; the second one corresponds to the stage of pore filling. In addition, the first linear section does not pass through the origin for all dyes. Consequently, the process is not limited by internal diffusion and has a mixed-diffusion character [26].

3.3. Isotherm study

The construction of a sorption isotherm makes it possible to determine the maximum sorption capacity for the extracted component. The nature of the isotherm (curvature of the course, the presence of kinks, the length of the linear section, etc.) helps to interpret the sorption interactions between the active surface of the sorbent and the extracted components and to establish the key features of sorption.

The well-known models for studying the adsorption process are the Langmuir and Freundlich models. The Langmuir isotherm (Table 2) is an empirical isotherm describing monolayer adsorption, i.e. adsorption occurs on a homogeneous surface covered with adsorption centers. Adsorption is considered as a “chemical” equilibrium between a free adsorption center, a substance in solution, and an adsorbed substance (substance + center, adsorbate). On the surface, free centers and the adsorbate form an ideal solution [28].

Experimental isotherms are not always described by the Langmuir equation. The theoretical concepts developed by Langmuir idealize and simplify the true picture of adsorption. In fact, the surface of the adsorbent is inhomogeneous, there is an interaction

between the adsorbed particles, active centers are not completely independent of each other, etc. Some of these factors are taken into account by the Freundlich isotherm. The Freundlich isotherm (see Table 2) is used to describe non-ideal sorption equilibrium data, which is often an initial surface adsorption followed by a condensation effect resulting from extremely strong interactions. Furthermore, it is contemplated that after the surface is covered, additional adsorbed particles can still be accommodated. In other words, this equation describes polymolecular adsorption [28].

To describe adsorption on homogeneous and heterogeneous surfaces and to determine the nature of adsorption interaction by activation energy (Table 2), the Dubinin–Radushkevich isotherm is used [29].

The experimental results obtained are shown in Fig. 5, Table 2.

The experimental sorption isotherm of MG was satisfactorily described by the Langmuir and Freundlich equation (Fig. 6a, b). According to the calculated values, the maximum adsorption capacity of MPC for MG was 3333.3 mg·g⁻¹. The activation energy of sorption of MG molecules was 0.016 kJ·mol⁻¹ (Table 3). The adsorption of MB molecules obeys the theoretical models of Freundlich and Dubinin–Radushkevich (Fig. 6b, c), which indicates the layer-by-layer filling of the pore space of the sorbent. The value of the activation energy of the sorption of MB molecules, as well as the MG, corresponds to physical sorption and has a value of 0.013 kJ·mol⁻¹ (Table 3).

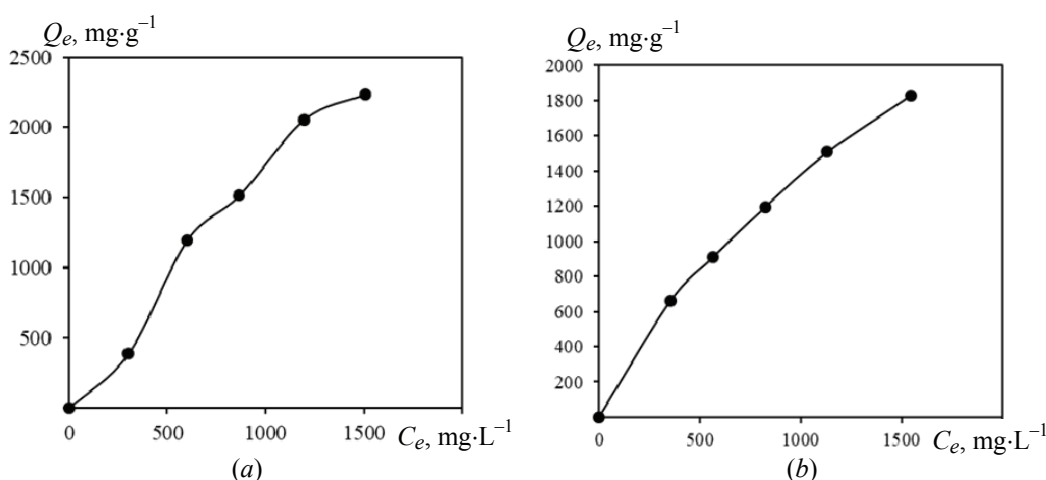


Fig. 5. Adsorption isotherms of MB (a) and MG (b) dyes on MPC

Table 2. Adsorption equations based on Langmuir, Freundlich, Dubinin–Radushkevich models [28, 29]*

Langmuir	Freundlich	Dubinin–Radushkevich
$Q_e = Q_{\max} \frac{K_L C_e}{1 + K_L C_e}$	$Q_e = k C_e^{1/n}$	$Q_e = Q_{\max} \exp(-K_{ad} \varepsilon^2)$
<i>Linear form of equations</i>		
$\frac{1}{Q_e} = \frac{1}{Q_{\max}} + \frac{1}{Q_{\max} K_L} \frac{1}{C_e}$	$\ln Q_e = \frac{1}{n} \lg C_e + \lg k$	$\ln Q_e = \ln Q_{\max} - K_{ad} \varepsilon^2$
<p>* Q_{\max} (mg·g⁻¹) is maximum adsorption; K_L is adsorption rate constant; k, $1/n$ are Freundlich constants indicates how favorable the adsorption process; k (mg·g⁻¹ (mg⁻¹)) shows the adsorption capacity of the sorbent; K_{ad} (mol²·kJ⁻²) Dubinin–Radushkevich isotherm constant; ε (kJ·mol⁻¹) is the Polanyi potential.</p>		

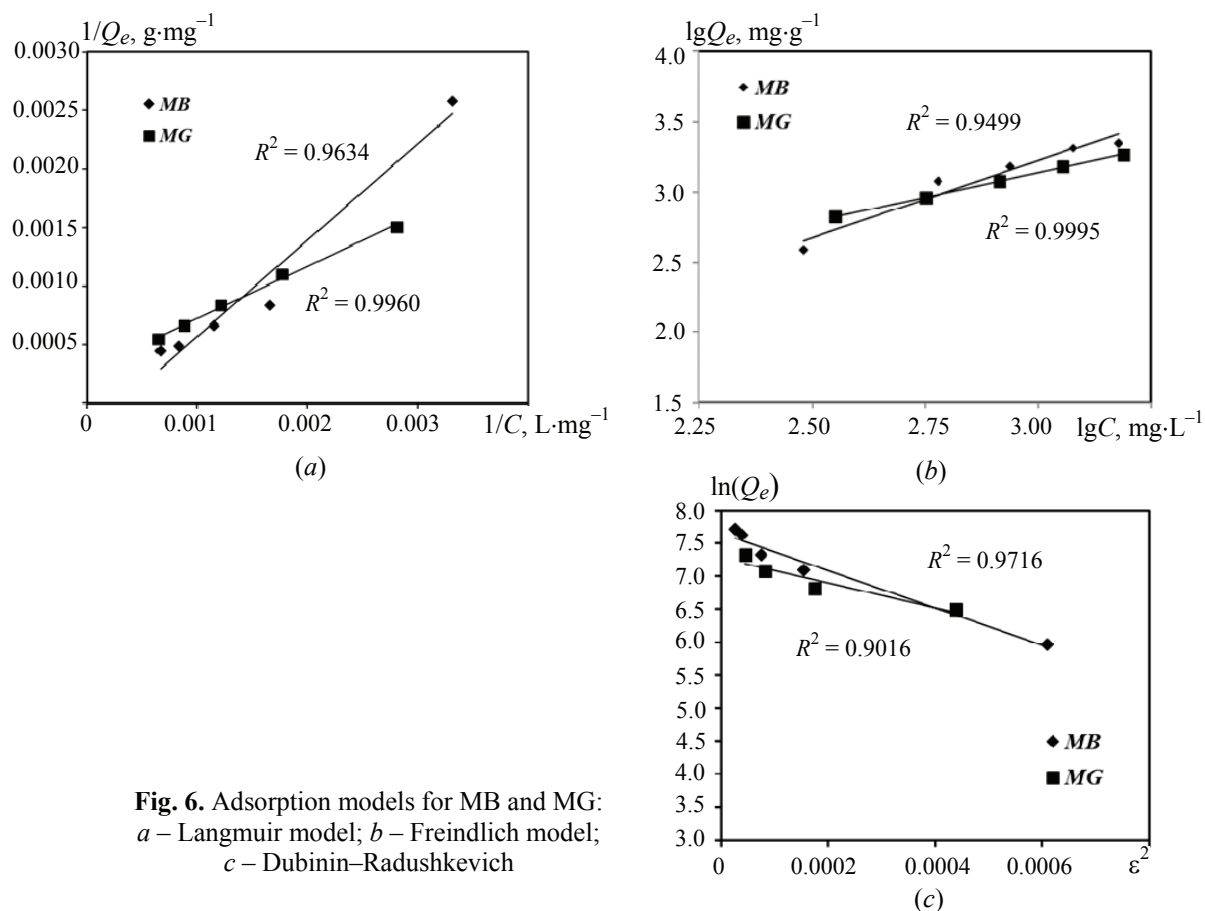


Fig. 6. Adsorption models for MB and MG: a – Langmuir model; b – Freundlich model; c – Dubinin–Radushkevich

Table 3. The parameters of MB and MG molecules sorption on MPC by isotherm equations

Dye	Model parameter			
<i>Langmuir</i>				
	K_L	Q_{\max}		R^2
MB	-0.0004	-3333.3		0.9634
MG	0.4436	3333.3		0.9960
<i>Freindlich</i>				
	n	$1/n$	k	R^2
MB	0.918	1.089	0.901	0.9499
MG	1.435	0.697	11.07	0.9995
<i>Dubinin–Radushkevich</i>				
	k_{ad}	Q_{\max}	E	R^2
MB	2837.5	2118.01	0,013	0.9716
MG	1884.7	1453.16	0.016	0.9016

4. Conclusion

The authors studied the adsorption of synthetic organic dyes from aqueous solutions on mesoporous carbon. The morphological features, elemental

composition and parameters of the porous space of the studied material are determined. The BET specific surface area was $2360 \text{ m}^2 \cdot \text{g}^{-1}$ for nitrogen. Kinetic and isothermal studies of the absorption of

dye molecules – methylene blue and malachite green – were carried out in a static mode. It has been established that sorption is rapid – adsorption equilibrium is reached in 15 min at the adsorption activity of MPC: 2446.6 mg·g⁻¹ for MB and 2043.1 mg·g⁻¹ for MG. Adsorption kinetics has been described using pseudo-first order, pseudo-second order, Elovich and intraparticle diffusion models. The adsorption process is satisfactorily described by the pseudo-second order model and the intraparticle diffusion model, thus indicating a "sorbate-sorbate" interaction along with a contribution to the overall rate of the internal diffusion process. Empirical data obtained in the course of isothermal studies were processed using the Langmuir, Freundlich, Dubinin-Radushkevich models. The calculated data confirm the physical mechanism of absorption in accordance with the values of the activation energy $E = 0.016$ kJ·mol⁻¹ for MG molecules and $E = 0.013$ kJ·mol⁻¹ for MB.

5. Funding

The study was supported by the Russian Science Foundation grant No. 22-13-20074, <https://rscf.ru/project/22-13-20074/>.

6. Acknowledgments

This work was done using facilities of the shared access center "Production and application of multifunctional nanomaterials" (Tambov State Technical University).

7. Conflict of interests

The authors declare no conflict of interest.

References

1. Salahuddin NA, EL-Daly HA, El Sharkawy RG, Nasr BT. Synthesis and efficacy of PPy/CS/GO nanocomposites for adsorption of ponceau 4R dye. *Polymer*. 2018;146:291-303. DOI:10.1016/j.polymer.2018.04.053
2. Li H, Fan J, Shi Z, Lian M, Tian M, et al. Preparation and characterization of sulfonated graphene-enhanced poly (vinyl alcohol) composite hydrogel and its application as dye absorbent. *Polymer*. 2015;60:96-106. DOI:10.1016/j.polymer.2014.12.069
3. Saleh TA, Muhammad AM, Tawabini B, Ali SA. Aminomethylphosphonate chelating ligand and octadecyl alkyl chain in a resin for simultaneous removal of Co(II) ions and organic contaminants. *Journal of Chemical and Engineering Data*. 2016;9(61):3377-3385. DOI:10.1021/acs.jced.6b00475
4. Yao T, Guo S, Zeng C, Wang C, Zhang L. Investigation on efficient adsorption of cationic dyes on porous magnetic polyacrylamide microspheres. *Journal of Hazardous Materials*. 2015;292:90-97. DOI:10.1016/j.jhazmat.2015.03.014
5. Jauris IM, Fagan SB, Adebayo MA, Machado FM. Adsorption of acridine orange and methylene blue synthetic dyes and anthracene on single wall carbon nanotubes: A first principle approach. *Computational and Theoretical Chemistry*. 2016;1076:42-50. DOI:10.1016/j.comptc.2015.11.021
6. Dehghani MH, Mostofi M, Alimohammadi M, McKay G, Yetilmezsoy K, et al. High-performance removal of toxic phenol by single-walled and multi-walled carbon nanotubes: Kinetics, adsorption, mechanism and optimization studies. *Journal of Industrial and Engineering Chemistry*. 2016;35:63-74. DOI:10.1016/j.jiec.2015.12.010
7. Dod R, Banerjee G, Saini DR. Removal of methylene blue (MB) dye from water environment by processed Jowar Stalk [Sorghum bicolor (L.) Moench] adsorbent. *Clean Technologies and Environmental Policy*. 2015;17:2349-2359. DOI:10.1007/s10098-015-0977-y
8. Gao M, Wang Z, Yang C, Ning J, Zhou Z, et al. Novel magnetic graphene oxide decorated with persimmon tannins for efficient adsorption of malachite green from aqueous solutions. *Colloids and Surfaces A: Physicochemical and Engineering Aspects*. 2019;566:48-57. DOI:10.1016/j.colsurfa.2019.01.016
9. Gupta V, Sadegh H, Yari M, Ghoshekandi RS, Maazinejad B, et al. Removal of ammonium ions from wastewater: A short review in development of efficient methods. *Global Journal of Environmental Science and Management*. 2015;1:149. DOI:10.7508/gjesm.2015.02.007
10. Gupta VK, Moradi O, Tyagi I, Agarwal S, Sadegh H, et al. Study on the removal of heavy metal ions from industry waste by carbon nanotubes: Effect of the surface modification: a review. *Critical Reviews in Environmental Science and Technology*. 2015;46:93-118. DOI:10.1080/10643389.2015.1061874
11. Habeeb OA, Ramesh K, Ali GAM, Yunus RM. Experimental design technique on removal of hydrogen sulfide using CaO-eggshells dispersed onto palm kernel shell activated carbon: Experiment, optimization, equilibrium and kinetic studies. *Journal Wuhan University of Technology, Materials Science Edition*. 2017;32:305-320. DOI:10.1007/s11595-017-1597-7
12. Borah L, Goswami M, Phukan P. Adsorption of methylene blue and eosin yellow using porous carbon prepared from tea waste: Adsorption equilibrium, kinetics and thermodynamics study. *Journal of Environmental Chemical Engineering*. 2015;3:1018-1028. DOI:10.1016/j.jece.2015.02.013
13. Mohammadi A, Abdolvand H, Isfahani AP. Alginate beads impregnated with sulfonate containing calix[4]arene-intercalated layered double hydroxides: In situ preparation, characterization and methylene blue adsorption studies. *International Journal of Biological*

Macromolecules. 2020;146:89-98. DOI:10.1016/j.ijbiomac.2019.12.229

14. Junlapong K, Maijan P, Chaibundit C, Chantarak S. Effective adsorption of methylene blue by biodegradable superabsorbent cassava starch-based hydrogel. *International Journal of Biological Macromolecules*. 2020;158:258-264. DOI:10.1016/j.ijbiomac.2020.04.247

15. Jabli M, Almalki S G, Agougui H. An insight into methylene blue adsorption characteristics onto functionalized alginate bio-polymer gel beads with λ -carrageenan-calcium phosphate, carboxymethyl cellulose, and celite 545. *International Journal of Biological Macromolecules*. 2020;156:1091-1103. DOI:10.1016/j.ijbiomac.2019.11.140

16. Marrakchi F, Ahmed MJ, Khanday WA, Asif M, Hameed BH. Mesoporous-activated carbon prepared from chitosan flakes via single-step sodium hydroxide activation for the adsorption of methylene blue. *International Journal of Biological Macromolecules*. 2017;98:233-239. DOI:10.1016/j.ijbiomac.2017.01.119

17. Memetova A, Tyagi I, Suhas, Singh P, Mkrтчyan E, et al. Porous material based on modified carbon and the effect of pore size distribution on the adsorption of methylene blue dye from an aqueous solution. *Environmental Science and Pollution Research*. 2022;30(9):22617-22630. DOI:10.1007/s11356-022-23486-8

18. Mkrтчyan ES, Burakova IV, Burakov AE, Ananyeva OA, Dyachkova TP, et al. Synthesis of nanocomposite material based on graphene oxide modified with lignosulfonate. *Liquid Crystals and their Application*. 2022;22(3):38-48. DOI:10.18083/LCAppI.2022.3.38

19. Mkrтчyan ES, Neskromnaya EA, Burakova IV, Ananyeva OA, Revyakina NA, et al. Comparative analysis of the adsorption kinetics of the methylene blue dye on graphene aerogel and activated coconut carbon. *Advanced Materials & Technologies*. 2020;(4(20)):021-028. DOI:10.17277/amt.2020.04.pp.021-028

20. Zhang Z, Xu L, Liu Y, Feng R, Zou T, et al. Efficient removal of methylene blue using the mesoporous activated carbon obtained from mangosteen peel wastes: Kinetic, equilibrium, and thermodynamic studies. *Microporous and Mesoporous Materials*. 2021;315:110904. DOI:10.1016/j.micromeso.2021.110904

21. Mu Y, Du H, He W, Ma H. Functionalized mesoporous magnetic biochar for methylene blue removal: Performance assessment and mechanism exploration. *Diamond and Related Materials*. 2022;121:108795. DOI:10.1016/j.diamond.2021.108795

22. Jawad AH, Saber SEM, Abdulhameed AS, Reghioua A, ALOthman ZA, et al. Mesoporous activated carbon from mangosteen (*Garcinia mangostana*) peels by H₃PO₄ assisted microwave: Optimization, characterization, and adsorption mechanism for methylene blue dye removal. *Diamond and Related Materials*. 2022;129:109389. DOI:10.1016/j.diamond.2022.109389

23. Burakov AE, Tyagi I, Burakova IV, Milyutin VV, Nekrasova NA. et al. Efficient removal of europium radionuclides from natural and seawater using mesoporous carbon-based material. *Journal of Molecular Liquids*. 2022;365:120092. DOI:10.1016/j.molliq.2022.120092

24. Qiu H, Lu LV, Pan B, Zhang W, Zhang Q. Critical review in adsorption kinetic models. *Journal of Zhejiang University Science A*. 2009;5(10):716-724. DOI:10.1631/jzus.A0820524

25. Ho Y-S. Second-order kinetic model for the sorption of cadmium onto tree fern: A comparison of linear and non-linear methods. *Water Research*. 2006;40(1):119-125. DOI 10.1016/j.watres.2005.10.040

26. Plazinski W, Dziuba J, Rudzinski W. Modeling of sorption kinetics: the pseudo-second order equation and the sorbate intraparticle diffusivity. *Adsorption*. 2013;19(5):1055-1064. DOI:10.1007/s10450-013-9529-0

27. Naghizadeh A, Ghasemi F, Derakhshani E, Shahabi H. Thermodynamic, kinetic and isotherm studies of sulfate removal from aqueous solutions by graphene and graphite nanoparticles. *Desalination and Water Treatment*. 2017;80:247-254. DOI:10.5004/dwt.2017.20891

28. Van Loon GW, Duffy SJ. *Environmental Chemistry*. Second Edition. New York: Oxford University Press Inc.; 2017. 560 p.

29. Hutson ND, Yang RT. Theoretical basis for the Dubinin-Radushkevitch (D-R) adsorption isotherm equation. *Adsorption*. 1997;3:189-195. DOI:10.1007/BF01650130

Information about the authors / Информация об авторах

Ali H. K. Kadum, Postgraduate, Tambov State Technical University (TSTU), Tambov, Russian Federation; e-mail: ali_strong_2010@yahoo.com

Irina V. Burakova, Cand. Sc. (Eng.), Associate Professor, TSTU, Tambov, Russian Federation; ORCID 0000-0003-0850-9365; e-mail: iris_tamb68@mail.ru

Elina S. Mkrтчyan, Postgraduate, TSTU, Tambov, Russian Federation; ORCID 0000-0002-3867-7063; e-mail: elina.mkrтчyan@yandex.ru

Кадум Али Хуссейн Кадум, аспирант, Тамбовский государственный технический университет (ТГТУ), Тамбов, Российская Федерация; e-mail: ali_strong_2010@yahoo.com

Буракова Ирина Владимировна, кандидат технических наук, доцент, ТГТУ, Тамбов, Российская Федерация; ORCID 0000-0003-0850-9365; e-mail: iris_tamb68@mail.ru

Мкртчян Элина Сааковна, аспирант, ТГТУ, Тамбов, Российская Федерация; ORCID 0000-0002-3867-7063; e-mail: elina.mkrтчyan@yandex.ru

Oksana A. Ananyeva, Master's Degree Student, TSTU, Tambov, Russian Federation; ORCID 0000-0002-1188-9402; e-mail: oksana.a9993471@gmail.com

Vladimir O. Yarkin, Student, TSTU, Tambov, Russian Federation; e-mail: sttstu90@gmail.com

Alexander E. Burakov, Cand. Sc. (Eng.), Associate Professor, TSTU, Tambov, Russian Federation; ORCID 0000-0003-4871-3504; e-mail: m-alex1983@yandex.ru

Alexey G. Tkachev, D. Sc. (Eng.), Professor, TSTU, Tambov, Russian Federation; ORCID 0000-0001-5099-9682; e-mail: nanotam@yandex.ru

Ананьева Оксана Альбертовна, магистрант, ТГТУ, Тамбов, Российская Федерация; ORCID 0000-0002-1188-9402; e-mail: oksana.a9993471@gmail.com

Яркин Владимир Олегович, студент, ТГТУ, Тамбов, Российская Федерация; e-mail: sttstu90@gmail.com

Бураков Александр Евгеньевич, кандидат технических наук, доцент, ТГТУ, Тамбов, Российская Федерация; ORCID 0000-0003-4871-3504; e-mail: m-alex1983@yandex.ru

Ткачев Алексей Григорьевич, доктор технических наук, профессор, ТГТУ, Тамбов, Российская Федерация; ORCID 0000-0001-5099-9682; e-mail: nanotam@yandex.ru

Received 28 April 2023; Accepted 22 May 2023; Published 06 July 2023



Copyright: © Kadum AHK, Burakova IV, Mkrtychyan ES, Ananyeva OA, Yarkin VO, Burakov AE, Tkachev AG, 2023. This article is an open access article distributed under the terms and conditions of the Creative Commons Attribution (CC BY) license (<https://creativecommons.org/licenses/by/4.0/>).

Heavy metal contents in the Tyumen city residential area soils

© Yana M. Chichigina^a, Gulnara N. Shigabaeva^a✉, Ekaterina A. Emelyanova^a,
Evgeny V. Galunin^a, Artem S. Yakimov^b, Alexei Yu. Isaev^a, Maria R. Bekker^a

^a Tyumen State University, 6, Volodarskogo St., Tyumen, 625003, Russian Federation,

^b Institute of the Earth's Cryosphere, Tyumen Scientific Center of the Siberian Branch of the Russian Academy of Sciences,
86, Malygina St., Tyumen, 625026, Russian Federation

✉ g.n.shigabaeva@utmn.ru

Abstract: The present paper examines the state of pollution of soils in the city of Tyumen regarding heavy metals contained therein: nickel (Ni), cobalt (Co), manganese (Mn), copper (Cu), cadmium (Cd), lead (Pb) and chromium (Cr). Soil sampling was carried out in autumn 2021 within the city residential areas. The sampling points were chosen in the sites of increased anthropogenic load – near highways and industrial enterprises. In soil samples, the content of acid-soluble and mobile fractions of heavy metals and organic matter was determined, and the pH factor was also measured. The analysis showed that significant excesses, from 3.2 to 14.3 MPC level, were found on nickel in 11 soil samples, and all the soil samples belong to the zones of motor transport impact. In one sample, No. 29, which belongs to the impact zone of such large industrial enterprises as the Elektrostal Tyumen Metallurgical Plant (Ural Mining and Metallurgical Company-Steel, UMMC Steel) and the Motor Plant, the MPC for nickel was exceeded by 8.1 times. There were also excesses in the copper contents in 11 samples, from 1.5 to 4.9 MPC, and in both the zones of motor transport impact and the territories affected by the building materials enterprises, railway junction, and UMMC Steel. For lead, there was a two-times excess in two samples in the zone of motor transport impact, 4.4 times – in the impact zone of the Construction Machinery Plant, and 29.7 times – in the zone of impact of Velizhansky Highway. For cobalt, chromium and manganese, the MPC values for the acid-soluble fractions were not exceeded. For the mobile fractions, excesses were also observed for manganese. The highest excesses of the MPC level for nickel and copper were found in the Vostochny (Eastern) and Central districts of the city, in the areas affected by motor transport and the large enterprises.

Keywords: soil mantle; heavy metals; pH of saline extract of soils; soils; pH of aqueous extract of soils; degree of pollution; MPC; environmental monitoring.

For citation: Chichigina YaM, Shigabaeva GN, Emelyanova EA, Galunin EV, Yakimov AS, Isaev AYu, Bekker MR. Heavy metal contents in the Tyumen city residential area soils. *Journal of Advanced Materials and Technologies*. 2023;8(2):141-156. DOI: 10.17277/jamt.2023.02.pp.141-156

Содержание тяжелых металлов в почвах селитебной зоны г. Тюмени

© Я. М. Чичигина^a, Г. Н. Шигабаева^a✉, Е. А. Емельянова^a,
Е. В. Галунин^a, А. С. Якимов^b, А. Ю. Исаев^a, М. Р. Беккер^a

^a Тюменский государственный университет, ул. Володарского, 6, Тюмень, 625003, Российская Федерация,

^b Институт криосферы Земли Тюменского научного центра СО РАН,
ул. Малыгина, 86, Тюмень 625026, Российская Федерация

✉ g.n.shigabaeva@utmn.ru

Аннотация: Исследовано состояние загрязненности почв г. Тюмени на предмет содержания в них тяжелых металлов: никеля (Ni), кобальта (Co), марганца (Mn), меди (Cu), кадмия (Cd), свинца (Pb) и хрома (Cr). Отбор проб почв проводился осенью 2021 г. на селитебных участках в пределах города. Точки отбора выбирались в зонах повышенной антропогенной нагрузки – вблизи автомагистралей и промышленных предприятий. В пробах почв определено содержание кислоторастворимых и подвижных форм тяжелых металлов, и органического вещества, а также измерен водородный показатель (рН). Анализ показал, что значительные превышения выявлены по

никелю в 11 пробах почв от 3,2 до 14,3 ПДК, причем все пробы почв относятся к зонам влияния автотранспорта. В одной пробе № 29, которая относится к зоне влияния таких крупных промышленных предприятий, как Metallургический завод «Электросталь Тюмени» («УГМК-Сталь») и Моторный завод, превышено ПДК по никелю в 8,1 раза. По содержанию меди тоже есть превышения в 11 пробах, от 1,5 до 4,9 ПДК, причем в зонах влияния как автотранспорта, так и на территориях влияния предприятий строительных материалов, железнодорожной развязки, «УГМК Сталь». По свинцу есть превышения в двух пробах в два раза в зоне влияния автотранспорта, в 4,4 раза в зоне влияния Завода строительных машин, в 29,7 раз в зоне влияния автодорог Велижанского тракта. По кобальту, хрому и марганцу значения ПДК для кислоторастворимых форм не превышены. По подвижным формам превышения наблюдаются и по марганцу. Наибольшие превышения ПДК по никелю, меди выявлены в Восточном и Центральном районах города, в зонах влияния автотранспорта и крупных предприятий.

Ключевые слова: почвенный покров; тяжелые металлы; pH солевой вытяжки почв; pH водной вытяжки почв; степень загрязнения; ПДК; экологический мониторинг.

Для цитирования: Chichigina YaM, Shigabaeva GN, Emelyanova EA, Galunin EV, Yakimov AS, Isaev AYU, Bekker MR. Heavy metal contents in the Tyumen city residential area soils. *Journal of Advanced Materials and Technologies*. 2023;8(2):141-156. DOI: 10.17277/jamt.2023.02.pp.141-156

1. Introduction

Human activities to transform the soils of residential areas result in changes in the elemental composition of soils – heavy metals (HMs) enter the environment where they are able to accumulate in the soil, especially in the upper part of the soil. Besides, HMs are actively involved in geochemical cycles, through which they can penetrate into the atmosphere, hydrosphere, lithosphere and biosphere. Anthropogenic impacts on soils have a negative effect on their structure and characteristics: fertility and biomass production, dynamism and sustainability are reduced, which can lead to soil degradation. At the same time, soil is an indicator of the condition of the landscape and the degree of safety for human habitation. It should be noted that HMs have carcinogenic, toxic and mutagenic effects. The penetration of these pollutants into human and animal bodies leads to deterioration of the health of those ones, up to lethal outcome. In soils HMs are found as oxides, sulphides, and also as soluble salts such as chlorides, nitrates and sulphates. When acidic precipitation enters the soil, nitric acid dissolves the oxides and sulphides of the HMs. In the upper horizons of the soil profile, which contains the greatest amount of humus, metals bind with organic ligands, resulting in the formation of low-mobile complex compounds. Then, they accumulate in the upper horizons of the soil profile, but are not transported by downward water flow to the lower horizons. However, if the concentration of humus is low, the bulk of the HMs will be in a free state and transferred to the deeper horizons and layers under the influence of soil moisture [1].

In this regard, nowadays, the timely assessment of soil contamination with HMs appears to be an urgent task at present. In work [2], the authors

establish that more and more attention is given to soil pollution all over the world. This is due to the increasing number of oil and gas processing enterprises that leads to the prevalence of complex pollution from HMs and polycyclic aromatic hydrocarbons (PAHs). Soil co-pollution with the HMs and PAHs poses more serious threats to the environment and human health, such as increased toxicity to microbial activity and diversity, reduced bioavailability, and inhibition of plant growth. Possible ways of purifying soils from such pollutants are represented by electrokinetic remediation and leaching and the use of chelating agents.

Soil monitoring studies that are being conducted determine enrichment factor (EF), environmental risk calculation (ER), bioconcentration factor (BCF), transfer factor (TF), hazard index (HI), and carcinogenic risk (CR). Such studies provide insights into the controls of urbanization in relation to the combined severity of pollution and potential health risk [3].

The main source of HM contamination of soils is dust pollution. At the same time, the concentration of HMs is highest in the fractions having dust particle sizes of $< 0.63 \mu\text{m}$. The penetration of such particles into the human body can cause a variety of diseases, including cancer [4].

The city of Tyumen is located in the southwest of the West Siberian Plain within the sub-taiga zone. Zonal soils are sod-podzolic and gray forest, black earth occurs closer to the forest-steppe. Soils are formed on covered loams, with the lower part of the profile predominantly of loamy granulometric composition, while the upper part of the profile is loamy-sandy. The soils are slightly alkaline and neutral.

The aim of the present work was to assess the pollution of soils of Tyumen city with the most common HMs (Ni, Co, Mn, Cu, Cd, Pb, Cr), organic matter (OM), as well as to determine the hydrogen index (pH).

2. Materials and Methods

In this study, soils contaminated with HMs in residential areas of Tyumen, as well as adjacent territories, were chosen as analysis objects.

At present, the following industries are being dynamically developing in the city: fuel industry (oil and gas processing), machine building, forestry, etc. There are large industrial facilities in and around Tyumen such as the Tyumen Battery Plant, the

Antipinsky Oil Refinery, UMMC-Steel, and the Tyumen Plywood Plant. Moreover, Tyumen is a major transportation hub: The Trans-Siberian Railway, major highways and interchanges pass through its territory. Industrial and transport facilities are the sources of HM entering the environment and have a significant impact on its ecological situation. Soil sampling was conducted in urban and suburban areas. Samples were taken from the upper (0–10 cm) organo-mineral horizon that adsorbs a significant part of dust emissions due to its peculiar structure and large OM amount. Therefore, this soil layer was selected for the study. Characteristics of soil sampling points are presented in Table 1.

Table 1. Characteristics of Soil Samples

Sample No.	Sampling point	Possible impact
1	Pchylka rural district	Bypass road, Salair Highway
2	Mezhdurechenskaya Street	Salair Highway
3	Tsimlyan Lake green area	Battery Plant
4	Plekhanova village	Bypass road, Plekhanovo Airport
5	Dudareva village	Moscow Highway
6	Paderina village	Moscow Highway, Chervishevsky Highway
7	City forest area	Motor transport
8	Salair Highway, roadside	Motor transport
9	Komunisticheskaya Street	Motor transport
10	Mira Street	Motor transport
11	Komarovo village	Bypass road, Chervishevsky Highway
12	Chervishevsky Highway, roadside	Motor transport
13	Salair Highway, roadside	Motor transport
14	Kazarovo village	Construction Machinery Plant
15	Druzhby Street, city park	Motor transport
16	Kharkovskaya Street	Motor transport
17	Shirotnaya Street	Motor transport
18	Patrusheva village	Motor transport
19	Yasny Horticultural Cooperative	Velizhansky Highway
20	Velizhansky Highway, roadside	Construction Machinery Plant, Motor transport
21	Malinovskogo Street	Motor transport
22	Gilyovskaya grove	Motor transport
23	Stantsionnaya Street	UMMC-Steel, Railroad junction, Motor transport
24	Fedyuninskogo Street, roadside	Motor transport
25	Sadovoye Horticultural Cooperative	Velizhansky Highway
26	Druzhby Street	Bypas road, Plywood Plant
27	Tura River bank	Motor transport
28	Antipino	Starotobolsky Highway, Antipinsky Oil Refinery
29	Andreyevskoye Lake	Motor plant, UMMC-Steel, Motor transport

The pH of aqueous and saline extracts of the selected soils was determined through the method according to Russian Standard 26423-85. The OM content was assessed through gravimetry in accordance with Russian Standard 26213-91. The mass fraction of mobile and acid soluble forms of the metals (copper, lead, zinc, nickel, cadmium, cobalt, chrome, and manganese) in the soil samples was measured by atomic absorption method according to Guidance Document 52.18.289-90 and Guidance Document 52.18.191-89 respectively. The atomic-absorption method realized on a ContrAA700 spectrophotometer (AnalytikJena™,

Jena, Germany) using xenon lamp of continuous spectrum was used to quantify HM contents in acid and acetate-ammonium soil extracts.

3. Results and Discussion

3.1. Determination of pH and organic matter of soil samples

The results of determining the pH of aqueous and saline extracts of soils are shown in Figs. 1 and 2. From Fig. 1, it can be seen that the pH of the soil

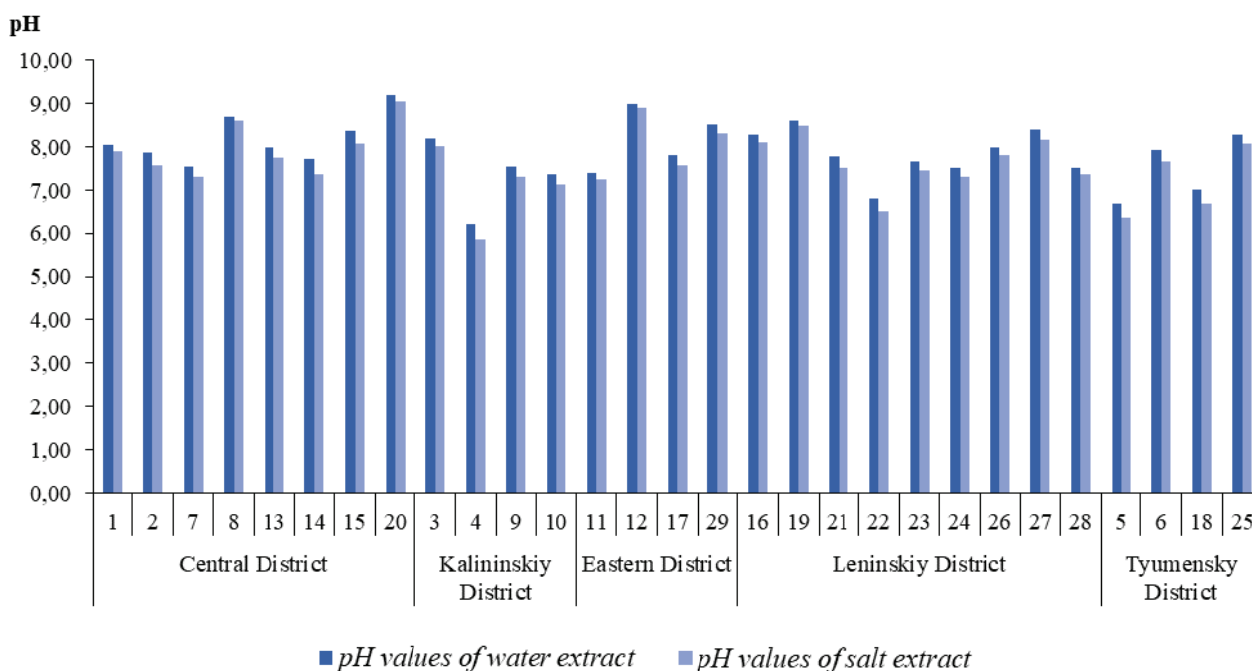


Fig. 1. pH values obtained for the aqueous and saline extracts

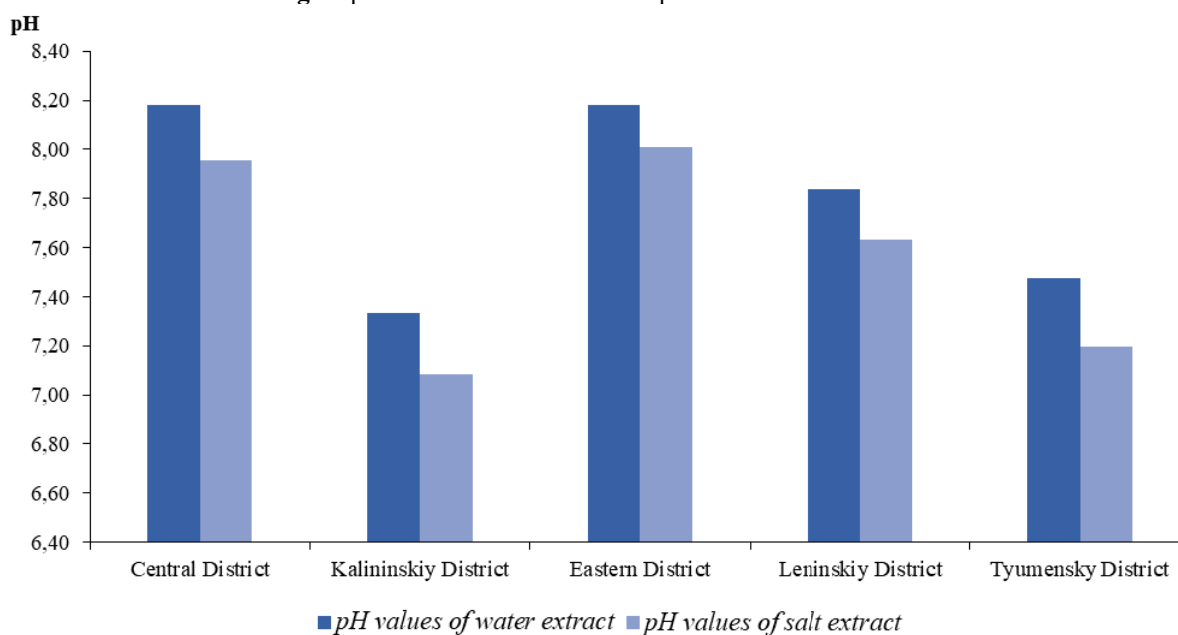


Fig. 2. Average pH values obtained for the aqueous and saline extracts for different districts

solutions is predominantly alkaline. This fact can be explained by the contents of magnesium and calcium carbonates coming from construction and household wastes from industrial enterprises. Furthermore, transport can be an additional source of pollution source, especially, in areas with heavy traffic (e.g., near highways which give HMs in the form of dust particles [5]. High pH values are probably associated with an increase in the mobility of HM compounds that may accumulate in acidic soils due to the presence of humic acids [6].

The pH values of aqueous and saline extracts were found to lie in the ranges of 6.22–9.20 and

5.87–9.06, respectively and refer to neutral, low-alkaline and alkaline media.

The investigated soils belong to the objects with low resistance to acids and high sensitivity in relation to the HMs. Since the upper parts of the soil profiles have a sandy loam granulometric composition, the corresponding maximum permissible concentrations (MPCs) [Sanitary Rules and Regulations 1.2.3685-2] were taken when assessing the HM content.

The results on the OM determination are presented in Figs. 3 and 4 and Table 2.

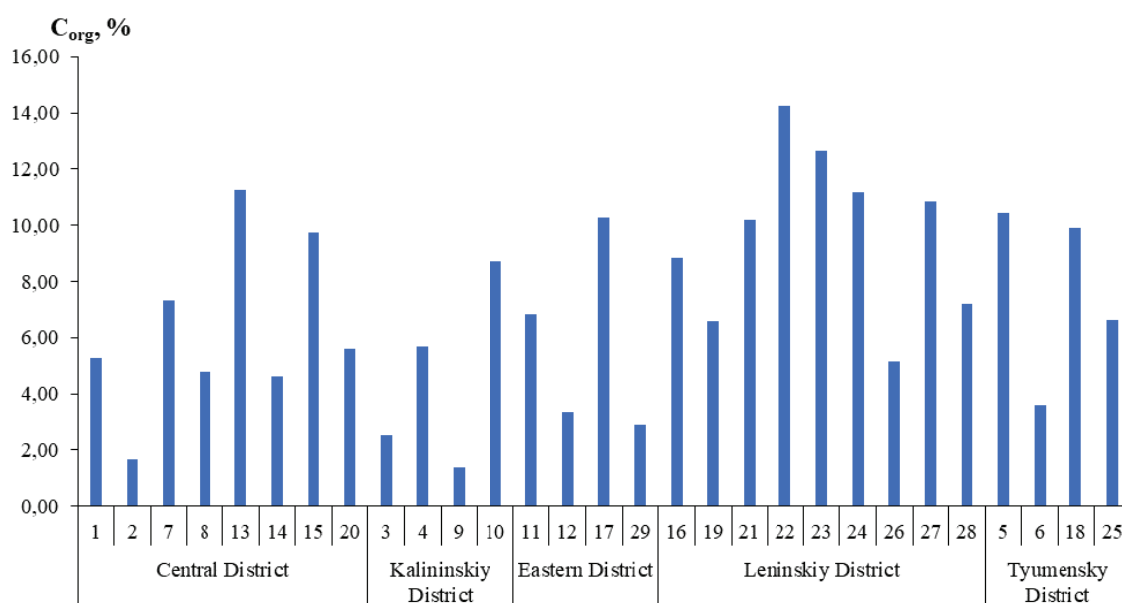


Fig. 3. OM contents in the soil samples

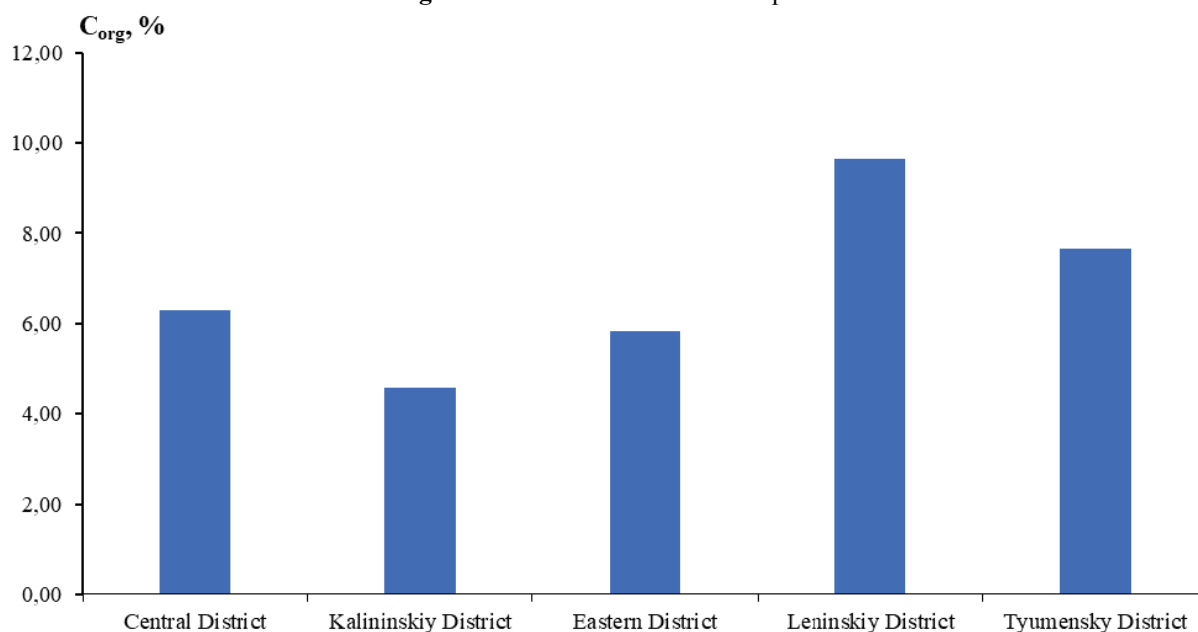


Fig. 4. Average OM contents in the soil samples

Table 2. OM contents, pH of aqueous and saline extracts

Sample No.	pH of aqueous extract	pH of saline extract	OM contents C _{org} , %
1	8.05	7.89	5.26
2	7.87	7.56	1.65
3	8.20	8.02	2.52
4	6.22	5.87	5.69
5	6.68	6.36	10.46
6	7.92	7.65	3.58
7	7.54	7.31	7.34
8	8.70	8.60	4.79
9	7.54	7.31	1.39
10	7.38	7.13	8.73
11	7.41	7.24	6.85
12	8.99	8.89	3.34
13	7.99	7.76	11.25
14	7.71	7.37	4.64
15	8.37	8.09	9.76
16	8.28	8.10	8.85
17	7.82	7.58	10.29
18	7.02	6.70	9.92
19	8.62	8.48	6.57
20	9.20	9.06	5.59
21	7.77	7.53	10.19
22	6.80	6.51	14.24
23	7.66	7.45	12.66
24	7.51	7.30	11.18
25	8.29	8.08	6.65
26	8.00	7.81	5.15
27	8.40	8.16	10.86
28	7.52	7.37	7.19
29	8.51	8.32	2.90

The OM percentage in the upper soil horizon is 1.39–14.24 %. The soil sample with the highest OM amount was taken in the Gilyovskaya grove area. High OM contents were also observed in the soils sampled outside the Tyumen city limits and in the Leninsky administrative district of Tyumen city.

3.2. Determination of acid-soluble and mobile fraction of HM

The HM fraction extracted from the soil using ammonium acetate buffer (pH = 4.8) represents the mobile form of HM compounds. At this pH value, the most efficient uptake of trace elements by plants from the soil solution occurs. The mobile HM fraction is associated with its most transportable part. It determines the availability of mineral components to plants and soil toxicity. This fraction is found in the form, in which the HMs are integrated into geochemical cycles and food chains.

The results of determining the HM mobile fraction content of the of HM in the soil are presented in Table 3.

The HMs are extracted from the soil solution using ammonium acetate buffer through ion exchange and complexation reactions. The predominance of one or the other process depends on the nature of the metal to be extracted. For instance, for cobalt and zinc, the extraction is caused to a greater extent by the complexation reaction, whereas for chromium and cadmium, it is caused by the ion exchange reaction [7].

The gross HM content in the soils is determined when the soil samples are exposed to strong acids (5n·HNO₃). The value of this indicator makes it possible to judge on the total contamination of soils with the HMs, however, it should be noted that this indicator does not provide information on the element availability of elements [8]. High values of the gross HM content indicate a potential environmentally unfavourable situation of the territory; that is, if the water and plants are not polluted at the moment, the ecological situation may change for the worse if external factors change.

Table 3. Contents of the HM mobile fractions, mg·kg⁻¹

Sample No.	Ni	Co	Mn	Cu	Cd	Pb	Cr
1	19.3±5.8	–	76±23	0.53±0.16	–	–	5.50±1.70
2	–	–	35±10	0.87±0.26	–	5.90±1.80	1.73±0.50
3	–	–	41±12	0.68±0.20	–	–	1.70±0.52
4	1.40±0.43	–	54±16	0.45±0.14	–	0.33±0.10	2.50±0.76
5	–	–	70±21	0.39±0.12	–	–	2.01±0.60
6	2.40±0.71	–	52±16	1.02±0.30	–	0.47±0.14	2.42±0.73

Continue Table 3

Sample No.	Ni	Co	Mn	Cu	Cd	Pb	Cr
7	–	–	301±90	0.41±0.12	–	–	2.12±0.63
8	21.1±6.2	–	89±27	1.83±0.55	–	42±13	4.30±1.30
9	–	–	43±13	0.97±0.29	–	1.94±0.56	2.44±0.72
10	8.9±2.7	–	171±51	0.92±0.28	–	1.91±0.58	2.81±0.85
11	–	–	77±23	0.37±0.11	–	–	1.50±0.46
12	31.2±9.4	0.34±0.10	88±26	3.01±0.89	–	6.8±2,0	4.00±1.20
13	5.8±1.8	0.15±0.04	103±31	0.67±0.20	–	20.0±6.1	2.02±0.60
14	1.81±0.55	–	65.±20	0.60±0.18	–	–	4.90±1.50
15	0.140±0.043	–	149±45	0.44±0.13	–	–	0.91±0.27
16	–	–	143±43	4.60±1.40	–	–	1.21±0.37
17	–	–	148±44	0.52±0.16	–	–	1.41±0.42
18	–	–	174±52	1.40±0.41	–	9.7±2.9	0.84±0.25
19	30.1±9.1	–	84±25	1.82±0.55	–	18.0±5.4	3.23±0.95
20	27.2±8.2	–	101±30	5.60±1.70	–	80±24	3.90±1.20
21	–	–	90±27	0.65±0.20	–	2.90±0.88	0.87±0.26
22	–	–	228±68	0.80±0.24	–	3.31±0.99	1.13±0.34
23	–	–	136±41	0.50±0.15	–	7.3±2.1	1.13±0.33
24	3.30±0.99	–	147±44	0.68±0.20	–	–	2.51±0.74
25	19.0±5.6	1.10±0.19	287±86	9.20±2.80	2.60±0.77	2076±622	8.20±2.50
26	–	–	72±22	1.01±0.30	–	0.36±0.11	0.96±0.29
27	0.62±0.19	–	332±100	1.01±0.30	–	2.08±0.62	1.41±0.42
28	22.3±6.7	0.62±0.19	95±28	2.44±0.73	–	2.63±0.77	4.20±1.30
29	–	–	92±27	1.12±0.33	–	–	1.60±0.49
MPC	4	5	140	3		6	6

Table 4. Contents of the HM acid-soluble fractions, mg·kg⁻¹

Sample No.	Ni	Co	Mn	Cu	Cd	Pb	Cr
1	160±48	8.8±2.6	267±80	15.3±4.4	–	0.88±0.26	71±21
2	4.8±1.4	3.01±0.91	165±50	71±21	–	16.00±4.90	4.1±1.1
3	28.0±8.4	9.4±2.8	487±146	62±19	–	3.31±0.10	21.1±6.2
4	26.1±7.9	13.1±3.8	604±181	67±20	–	0.96±0.29	21.2±6.2
5	36±11	14.0±4.2	549±165	47±14	–	0.84±0.25	21.4±6.4
6	36±11	3.9±1.2	165±49	34±10	–	14.00±4.10	18.0±5.5
7	3.5±1.1	3.4±1.0	366±110	163±49	–	–	3.3±1.0
8	189±57	11.1±3.2	362±109	39±12	–	61±19	65±20
9	14.0±4.1	6.1±1.8	267±80	50±15	–	–	9.1±2.6
10	133±40	12.1±3.6	407±122	18.1±5.3	–	3.6±1.1	50±15
11	21.1±6.3	8.9±2.7	401±120	25.3±7.6	–	–	15±4.4
12	238±72	14.1±4.3	273±82	26.2±7.9	–	–	82±24
13	114±34	8.5±2.5	264±79	114±34	–	22.1±6.6	34±10

Continue Table 4

Sample No.	Ni	Co	Mn	Cu	Cd	Pb	Cr
14	42±13	7.2±2.2	199±60	38±11	–	–	102±31
15	44±13	3.30±0.99	407±122	43±13	–	–	17.4±5.1
16	67±20	12.0±3.5	449±135	20.0±5.9	–	–	34±10
17	63±19	7.5±2.3	398±119	51±15	–	–	31±9,2
18	33±9.8	6.1±1.8	360±108	158±47	–	–	16.4±4.8
19	286±86	17.2±5.1	266±80	15.2±4.4	–	32.3±9.7	71±21
20	228±68	12.0±3.7	298±89	62±18	–	140±42	65±19
21	42±13	7.8±2.3	579±174	10.4±3.0	–	8.2±2.5	26.2±7.9
22	35±10	8.6±2.6	812±243	30.2±8.9	–	16.0±4.9	16.1±4.9
23	37±11	5.6±1.7	325±97	61±18	–	11.0±3.2	12.1±3.7
24	72±22	3.6±1.1	319±96	37±11	–	–	24±7.3
25	199±60	11.0±3.4	798±239	13.1±3.8	4.8±1.4	951±285	87±26
26	33±10	6.6±2.0	496±149	33.0±9.9	–	3.4±1.0	16.0±4.7
27	74±22	7.1±2.1	688±207	27.2±8.1	–	10.0±3.1	22.3±6.7
28	23.4±7.0	7.7±2.3	510±153	79±24	–	18.4±5.3	17.1±5.0
29	161±48	9.1±2.7	218±65	49±15	–	15.3±4.5	64±19
MPC	20	20	1500	33	0.5	32	100

The results on the content of HM acid-soluble forms in the soil are presented in Table 4.

The HM content in sample No. 25 significantly exceeded the MPC values; that sample was taken from the territory of Sadovoye Horticultural Cooperative, where agrarian works have been carried out for several years. A large HM amount could come into the soil from phosphate fertilizers, in which the HM contents can reach 220 mg·kg⁻¹ [9]. On this basis, the authors of this study assumed that a large fertilizer amount was entering the soil, or that the site was used as a landfill. Therefore, in further consideration of the data obtained, the values for sample No. 25 were excluded from the total set.

Nickel. The MPC of nickel in the soils of residential areas is 20 mg·kg⁻¹ for acid soluble fractions and 4 mg·kg⁻¹ for its mobile fractions. The most common are Ni²⁺ compounds. Ni³⁺ exists in an alkaline environment as well as under harsh oxidizing conditions, but such conditions are rare in the natural environment [10, 11]. Nickel is a moderate complexing agent capable of forming predominantly fulvate complexes with organic or inorganic ligands. Besides, it can also be found in soils as carbonate or hydrocarbonate complexes, with the ratio of one or the other complex form depending on the acidity of the medium [12]. Compounds of this element can be adsorbed by fine-grained clay

particles as well as by iron, manganese and aluminum hydroxides [13].

Nickel sources may include a variety of industrial emissions, vehicle fuel emissions, and parts of rubber tyres. At different sampling points, the levels of the nickel contents exceeding the MPC were observed, suggesting that the contamination with this metal is not local but extensive, covering the whole area (see Figs. 5, 6).

This contamination may be caused by roads connecting different parts of the city. The high content of the nickel acid-soluble fractions in many samples exceeded the MPC by a factor of 2 to 14, thereby indicating its accumulation in the soils of these districts. The excess levels of the nickel contents in the samples taken near the roadsides (bypass road, as well as the highways: Salair, Chervishevsky, Moscow and Velizhansky) allow concluding about the transport impact.

Cobalt. The MPC level for its acid-soluble fractions is 20 mg·kg⁻¹, whereas for its mobile fractions of cobalt in the case of the soils of residential areas, it is 5 mg·kg⁻¹. In most cases the cobalt contents in soils depend on the parent rock composition. Considerable quantities of cobalt are identified in soils formed from basic rocks and clay sediments. It should be taken into account that the pattern of the cobalt distribution and behavior in soils is much affected by humus contents in the soil horizon.

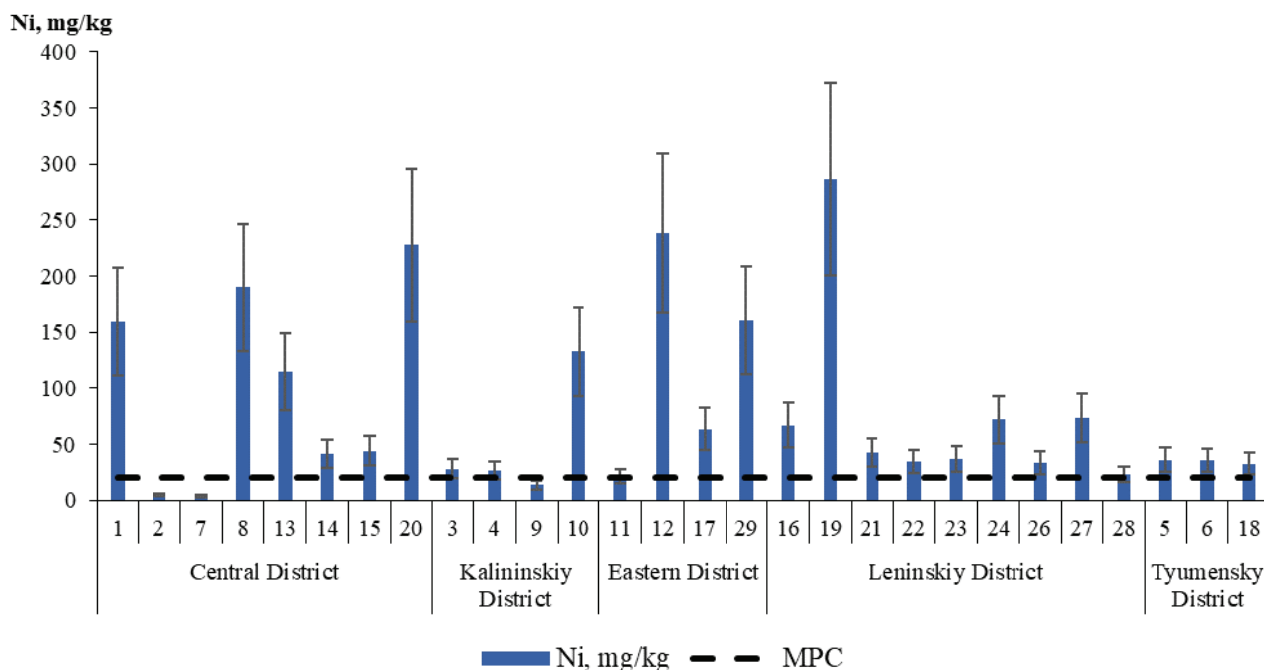


Fig. 5. Contents of the nickel acid-soluble fractions in the soil samples

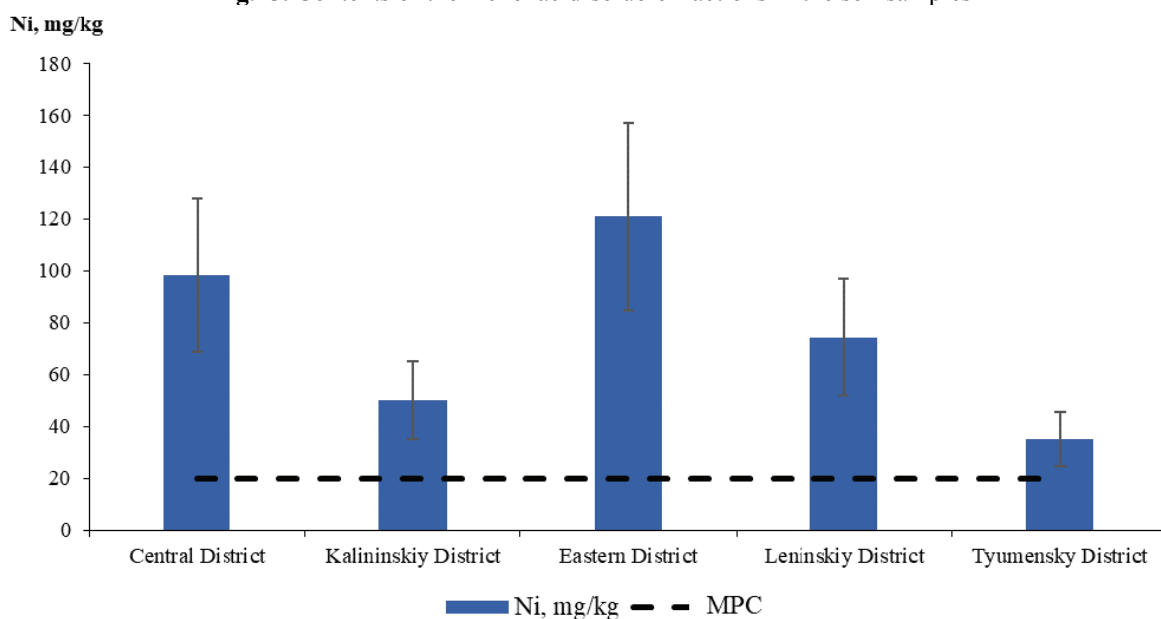


Fig. 6. Average contents of the nickel acid-soluble fractions in the soil samples

Cobalt takes different forms depending on pH of the environment and is found as Co^{2+} and Co^{3+} , or as the complex anion $\text{Co}(\text{OH})_3^-$, i.e. in the mobile form.

The results on the cobalt contents show that none of the Tyumen districts exceeded the MPC level established for both acid-soluble and mobile fractions of this element (Figs. 7, 8).

Manganese. The manganese MPC level is as follows: for its mobile fractions, it is $140 \text{ mg}\cdot\text{kg}^{-1}$, whereas for its acid-soluble fractions, it is $1500 \text{ mg}\cdot\text{kg}^{-1}$. This metal is found in soils more often than other elements. The main place of its accumulation

is the top soil layer, since it actively interacts there with the OM. In nature, manganese occurs mainly as Mn^{4+} , Mn^{3+} , Mn^{2+} , or as minerals. Manganese (as Mn^{2+}) can replace divalent cations of some elements (Fe^{2+} , Mg^{2+}) in silicates and oxides, thereby forming ferromanganese nodules, so it is the most common one in the environment.

Slightly excessive levels of manganese MPC for the mobile fractions were observed in samples No. 17, 16 and 26, and in samples Nos. 7, 10, 18, 22, 25 and 27 (Table 3), a significant MPC excess was fixed.

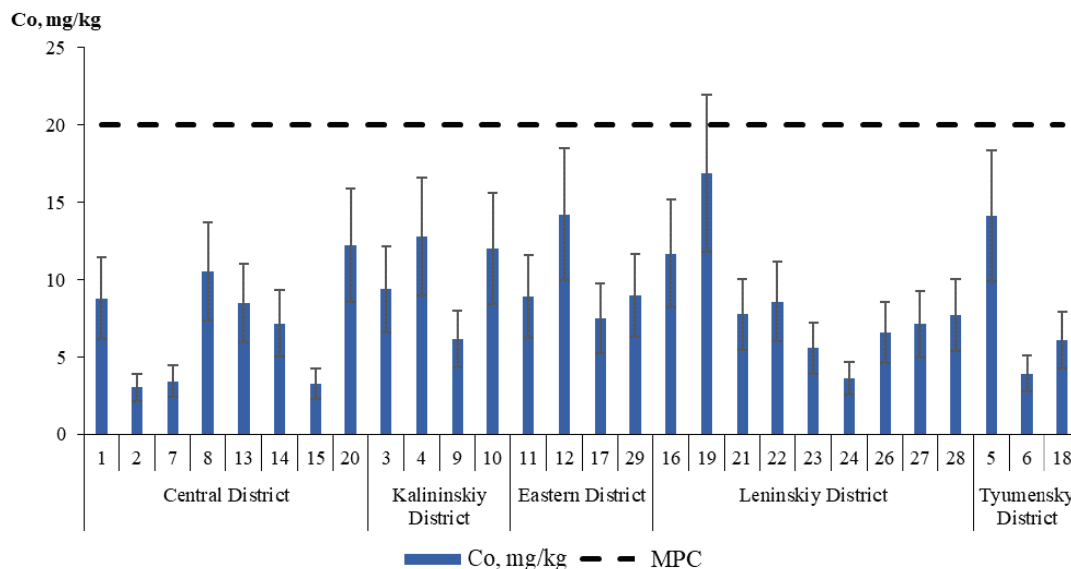


Fig. 7. Contents of the cobalt acid-soluble fractions in the soil samples

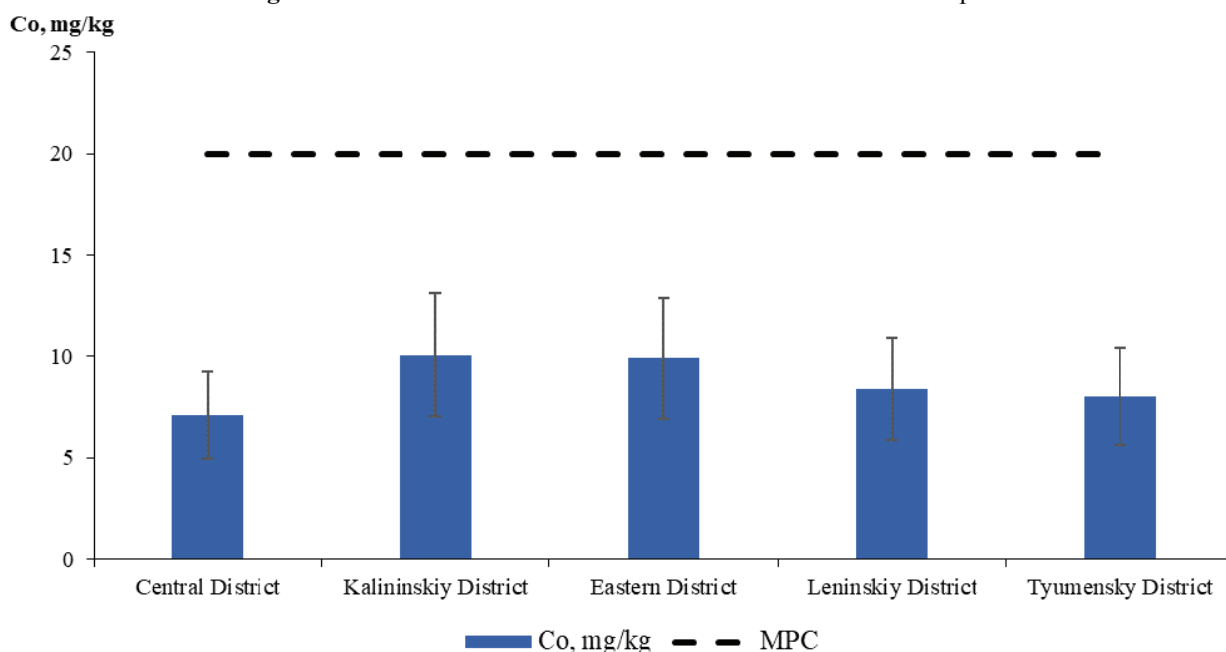


Fig. 8. Average contents of the cobalt acid-soluble fractions in the soil samples

A large OM amount is available in the inspected territories, since the above-mentioned samples were taken in landscaped urban areas (city forest and parks, riverbank, roadside forest belt, and green area near houses). The OM enters the soil with fallen leaves and grass. The disruption of the system of fallen leaves removal at urban sites results in large OM quantities [14]. Manganese accumulates in the upper soil horizons and is not leached to the lower horizons, since it forms insoluble complex compounds with the OM. The activities of ferrous and non-ferrous metallurgy, metal processing and machine building industries result in manganese entering the soil horizons. The soil samples from the area of UMMC-Steel (samples No. 22, 24, 27)

possess have high content of mobile fractions, which may indicate its recent entry.

The contents of the manganese acid-soluble fractions in all samples lied within normal limits, indicating the leaching of this element from the soils in the form of mobile Mn^{2+} (Figs. 9, 10).

Copper. The MPC level for the copper acid-soluble fractions is $33\text{ mg}\cdot\text{kg}^{-1}$, and for its mobile fractions in the soils of residential areas is $3\text{ mg}\cdot\text{kg}^{-1}$. Copper is a highly toxic element and is most commonly found as Cu^{2+} compounds. At the same time, it is one of the least mobile HMs, because in nature, due to good complexing properties, it forms complexes mainly with organic ligands.

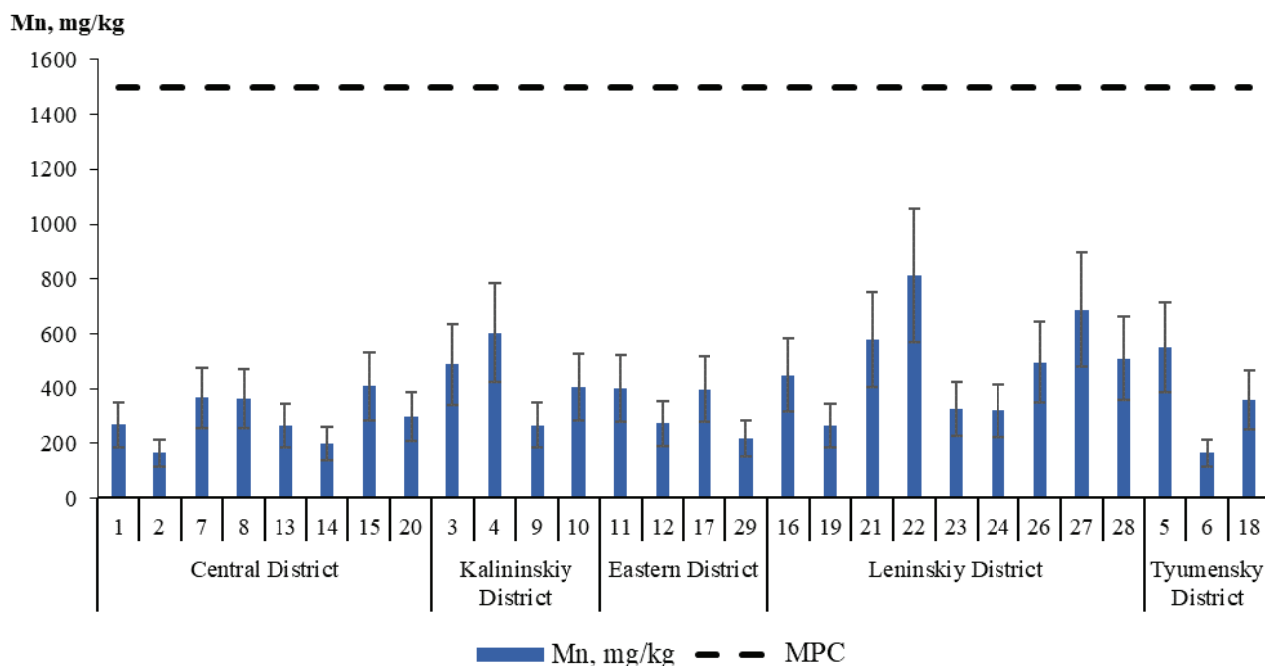


Fig. 9. Contents of the manganese acid-soluble fractions in the soil samples

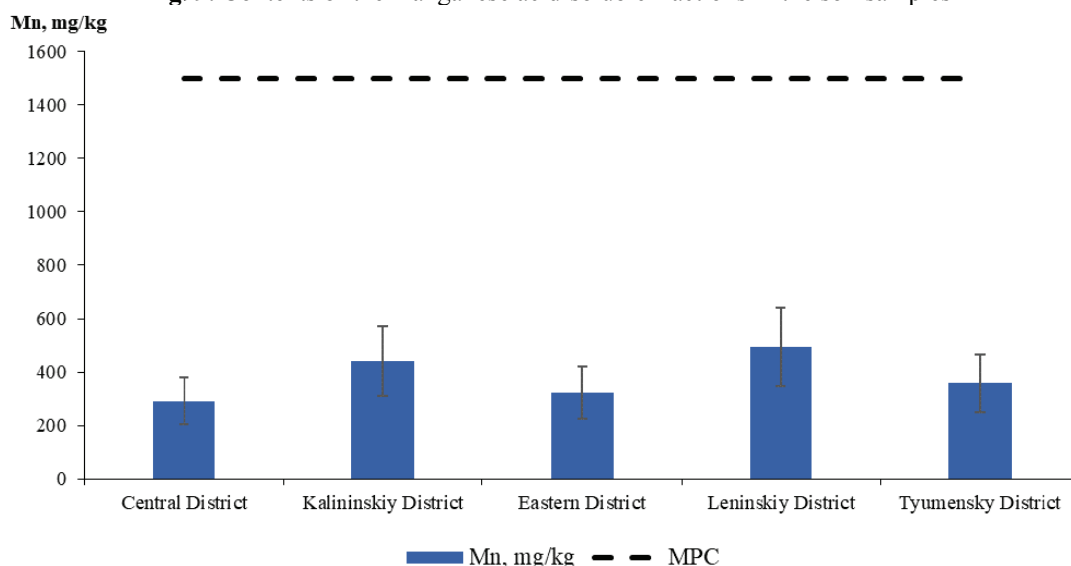


Fig. 10. Average contents of the manganese acid-soluble fractions in the soil samples

Copper becomes most toxic at pH values of 5.5 to 6.5 as it is dissolved as divalent copper ions. In more acidic soils, copper is less mobile and, therefore, non-toxic. At pH more than 9.0, complexes with inorganic ligands can be formed. Also, adsorption on suspended clay particles decreases its mobility. The excess of the content of the copper mobile fractions was found in samples No. 20 and 26, although these values do not exceed the MPC more than twice (Table 3). The accumulation of copper in soils in the form of complex compounds with fulvic acids is evidenced by exceeding of the MPC on average from 2 to 5 times for the copper acid-soluble fractions (Figs. 11, 12).

Cadmium. The MPC level for the cadmium acid-soluble fractions is $0.5 \text{ mg}\cdot\text{kg}^{-1}$, and no standard value has been established for its mobile fractions.

Cadmium is mainly accumulated in the form of complexes with humic acids. It is a rarely dispersed element and is considered to be one of the most toxic metals, since its rates exceed permissible levels even at the minimum soil contamination value. The background cadmium content in soils is mainly determined by the composition of its parent rock. Cadmium is most mobile in soil solution media at pH 4.5–5.5. In alkaline conditions, it is low-mobile, therefore, its mobility values correlate with the acidity of the soil solution medium.

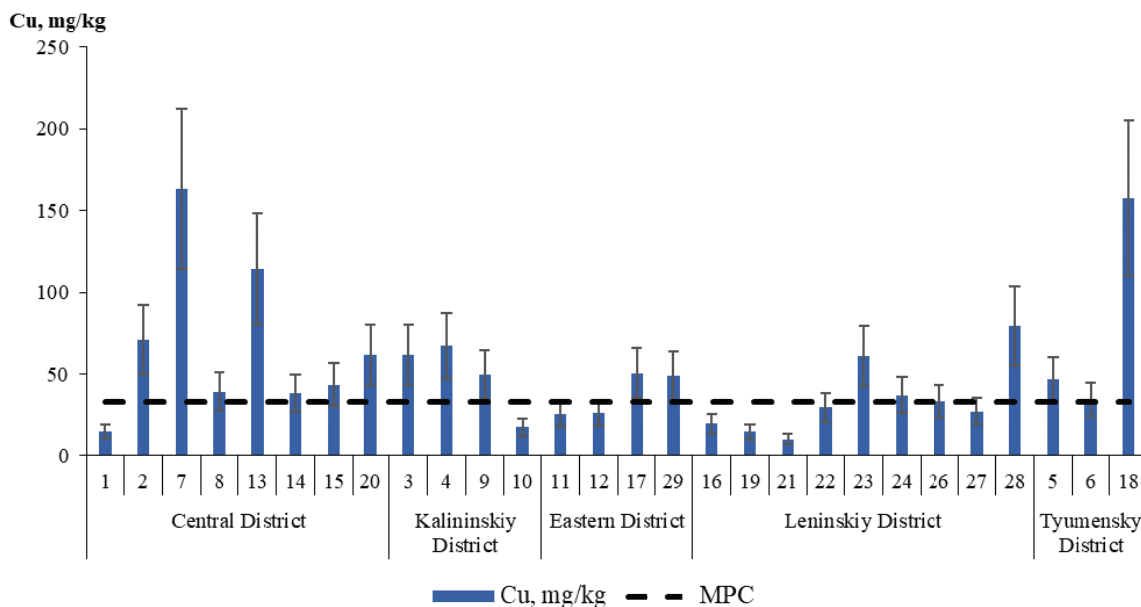


Fig. 11. Copper contents in the soil samples

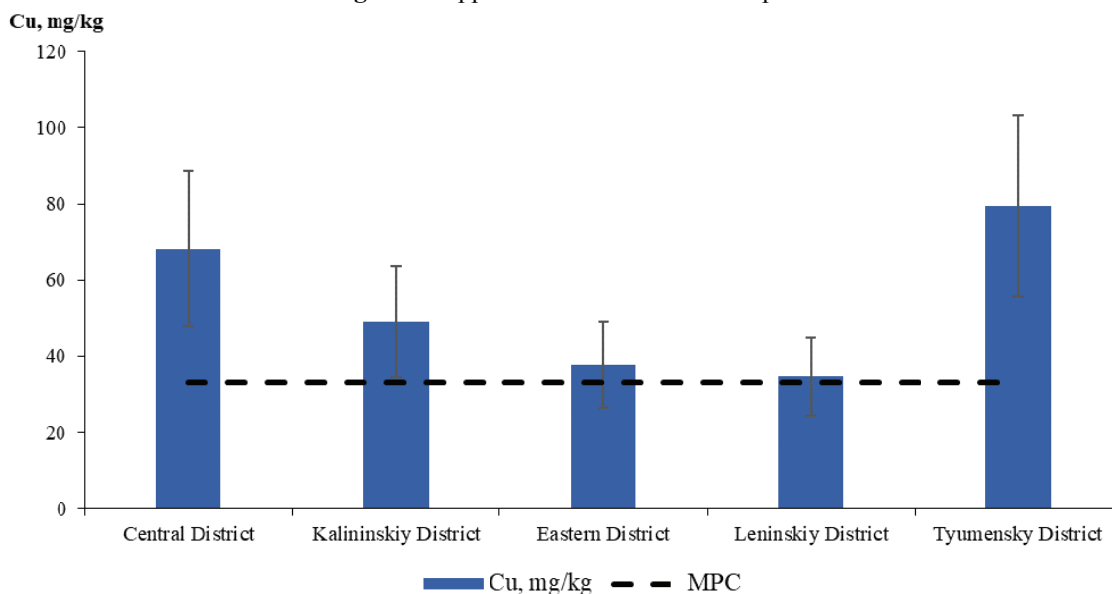
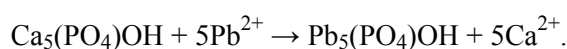


Fig. 12. Average copper contents in the soil samples

When considering the data of the analyzed samples of Tyumen city, no excess of the MPC for this element was noted (see Tables 3, 4).

Lead. The MPC level for the lead mobile fractions in the case of soils from residential areas is $6 \text{ mg}\cdot\text{kg}^{-1}$, for its acid-soluble fractions, it is $32 \text{ mg}\cdot\text{kg}^{-1}$. Lead compounds accumulate in soils as a result of sorption on oxides and hydroxides of manganese and iron. Moreover, lead forms part of easily degradable minerals – PbO , PbCO_3 , and PbSO_4 . Degradability makes these forms of lead in soils the most dangerous. At the same time, the phosphate mineral $[\text{Pb}_5(\text{PO}_4)_3\text{Cl}]$ is the least toxic as it has low solubility and stability in a wide pH range. The mobility and bioavailability of lead without its

removal from the medium can be achieved by applying phosphate to contaminated soils. This reaction can be represented as follows:



A significant excess of the MPC level for lead both in the mobile and the acid-soluble form was observed in samples No. 8 and 20 taken at roadsides (Tables 3, 4). For these soils, 7- and 13-fold excesses of the MPC level for its mobile fractions, and 2- and 4-fold excesses of the MPC for the acid-soluble fractions were observed, respectively (Figs. 13, 14).

Possible sources of lead pollution are wastes from metallurgical plants, landfills of used electric batteries, paints, and metal alloys. In addition, lead

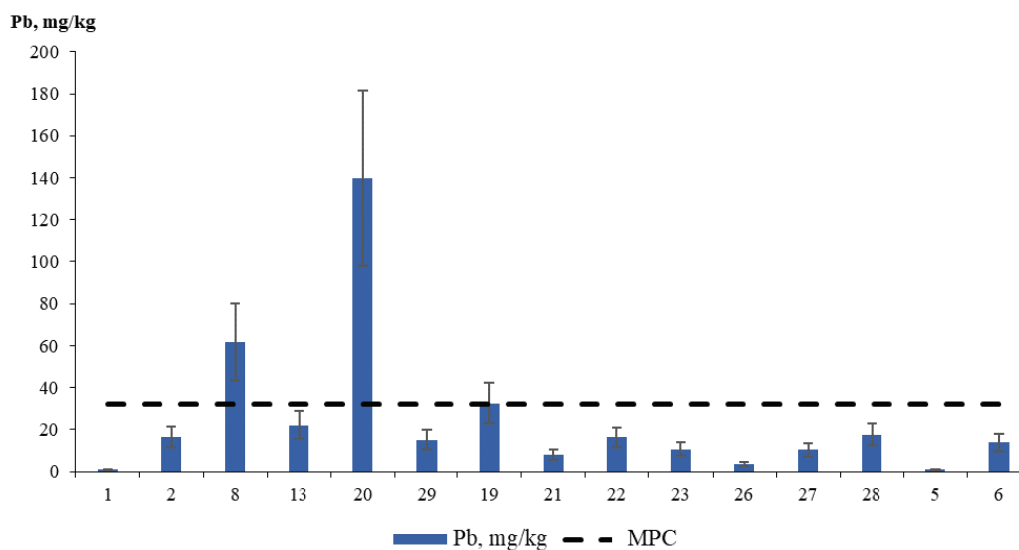


Fig. 13. Contents of the lead acid-soluble fractions in the soil samples

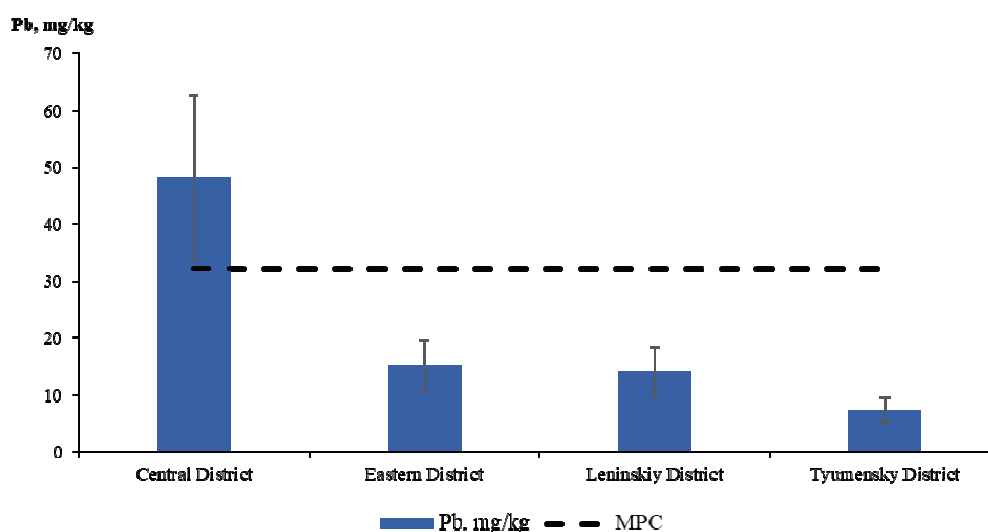


Fig. 14. Average contents of the lead acid-soluble fractions in the soil samples

may enter soils from exhaust gases of vehicles running on petrol with lead additive. Its excessive concentrations were observed in the Central district, which can be explained by the increased traffic load in this part of the city.

Chromium. The MPC level established for its mobile fractions in case of soils of residential areas is $6 \text{ mg}\cdot\text{kg}^{-1}$, and for the acid-soluble fractions, it is $100 \text{ mg}\cdot\text{kg}^{-1}$. Chromium exists in several forms, the most stable of which are compounds with oxidation degrees of +6 and +3. The form, in which chromium is found in soils, depends not only on the acidity of the medium [15], but also on its redox potential [16].

Thus, +6 oxidation degree chromium possesses low complexing ability, and is available in soils as HCrO_4^- and CrO_4^{2-} . +3 degree chromium, in its turn, has high complexing properties and, as a result, it is present in soil solution as $[\text{Cr}(\text{OH})_2]^+$ and $[\text{Cr}(\text{OH})]^{2+}$ (at pH 7.5–8.5) as well as complexes with humus and

fulvic acids. It should be noted that these forms are actively adsorbed by clays, whereas the CrO_4^{2-} chromate anion is adsorbed only in more acidic media.

The presence of chromium in one form or the other also determines its toxicological properties. The most dangerous are the Cr^{+6} compounds, which have toxic, carcinogenic and mutagenic effects. At the same time, Cr^{+3} compounds in acidic media are inert, and at pH 5.5 become almost insoluble, so they do not harmfully affect the organisms.

The main areas of chromium application are metallurgical and chemical industries due to high corrosion resistance and strength of this element [17].

Among the investigated samples, only sample No. 14 exceeded the MPC established for chromium. However, the exceeding of the limits for the contents of the acid-soluble fractions is insignificant.

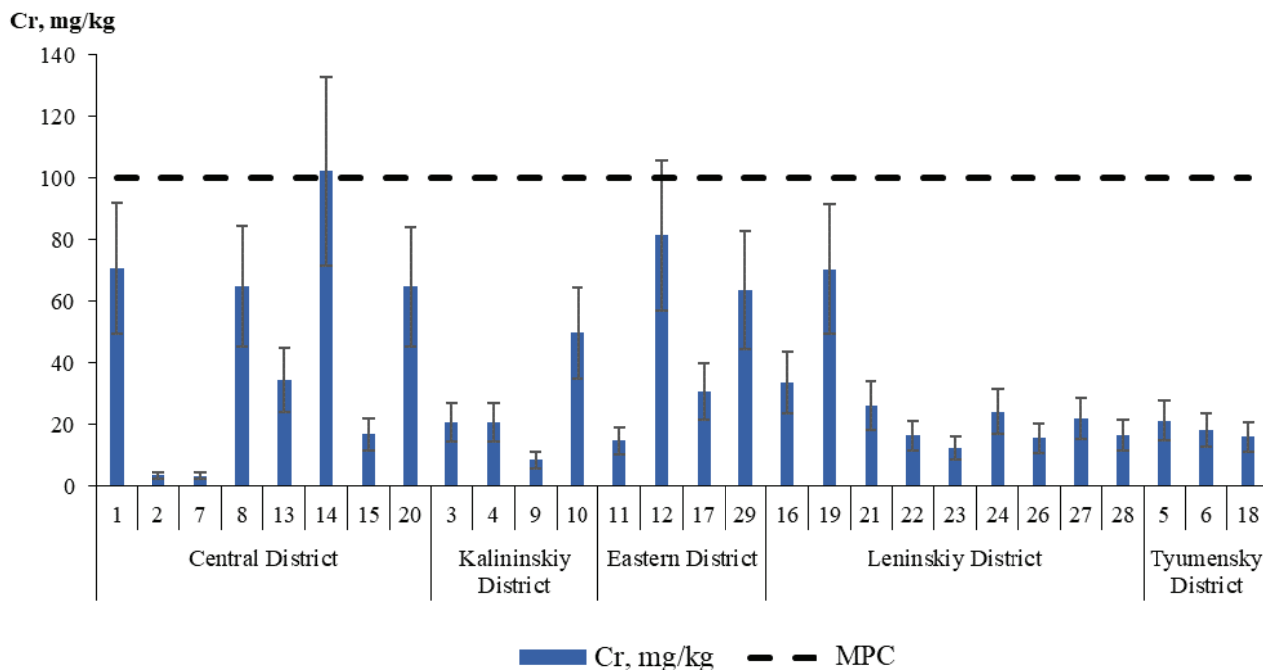


Fig. 15. Contents of the chromium acid-soluble fractions in the soil samples

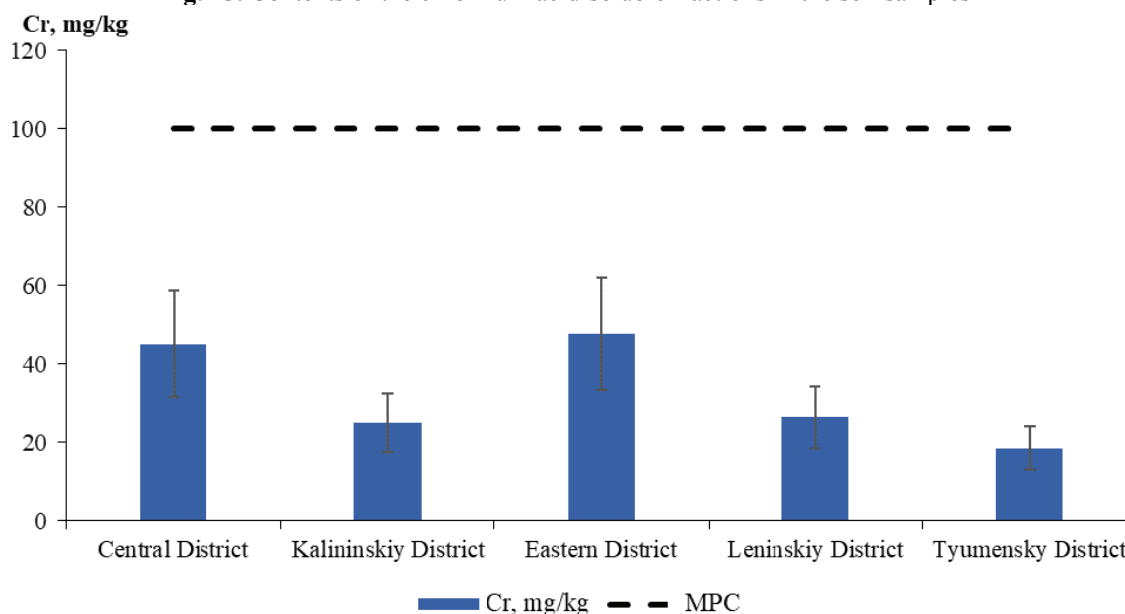


Fig. 16. Average contents of the chromium acid-soluble fractions in the soil samples

3.3. Correlation analysis

According to the Goldschmidt classification, all the elements in nature belong to one of the five groups: atmophilic, chalcophilic, lithophilic, siderophilic, as well as rare elements and elements not found in nature [18]. In this paper, a correlation analysis was carried out between the contents of the different element pairs. This type of analysis can reveal the absence or presence of correlation between elements belonging to the same group according to the geochemical classification of Goldschmidt, as well as indicate the possible causes of the HM accumulation.

Within the framework of this classification, matrices of pair wise correlations for the HM and OM contents and pH were constructed using the Microsoft Excel software. Indicators with a correlation coefficient of 0.5 were considered as correlated. The results of the analysis are presented in Table 5.

The highest correlations were found between the pairs of the following metals: Co – Ni, Cr; Pb – Cr; Cr – Ni, Co, Pb. The presence of correlations between nickel and cobalt contents is quite understandable, as they belong to siderophilic group of elements. The correlation between lead and chromium contents, different in nature, indicates the

Table 5. Matrices of pairwise correlations of the HM acid-soluble fractions in the soils

	Ni, mg·kg ⁻¹	Co, mg·kg ⁻¹	Mn, mg·kg ⁻¹	Cu, mg·kg ⁻¹	Pb, mg·kg ⁻¹	Cr, mg·kg ⁻¹	pH	C _{org} , %
Ni, mg·kg ⁻¹	1.00	0.67	-0.16	-0.34	0.36	0.80	0.65	-0.15
Co, mg·kg ⁻¹	0.67	1.00	0.22	-0.38	0.17	0.54	0.15	-0.06
Mn, mg·kg ⁻¹	-0.16	0.22	1.00	-0.21	0.39	-0.17	-0.30	0.48
Cu, mg·kg ⁻¹	-0.34	-0.38	-0.21	1.00	-0.26	-0.41	-0.28	0.08
Pb, mg·kg ⁻¹	0.36	0.17	0.39	-0.26	1.00	0.54	0.21	-0.06
Cr, mg·kg ⁻¹	0.80	0.54	-0.17	-0.41	0.54	1.00	0.52	-0.28
pH	0.65	0.15	-0.30	-0.28	0.21	0.52	1.00	-0.35
C _{org} , %	-0.15	-0.06	0.48	0.08	-0.06	-0.28	-0.35	1.00

anthropogenic nature of their entry into the environment.

A correlation between the chemical element content in the soil and the pH of the aqueous extract for Cu, Cr, Ni was also been detected. This information can be interpreted as a confirmation of the effect of metal accumulation effect during the soil alkalization, since in the samples studied, there was a shift to the alkaline pH region. The observed correlation between the soil OM content and the manganese concentration is related to the formation of strong complexes with the soil organic component.

4. Conclusion

Thus, in the present work, the pH values of saline and aqueous soil extracts were determined to be 5.87 to 9.06 and 6.22 to 9.20, respectively. A comparison of the obtained results on the HM content in the soils with Sanitary Rules and Regulations normative values showed that the contents of both mobile and acid-soluble fractions exceed the MPC values for copper, lead, nickel and manganese. The concentrations of cobalt, cadmium and chromium are not exceeded. Based on the correlation analysis of these results, it can be concluded that there is a significant anthropogenic load on the soils of Tyumen city, especially for the Vostochny (Eastern) and Central districts, where the main transport routes and industrial enterprises (UMMC-Steel, Construction Machinery Plant) are located.

5. Funding

No external funding was received for this research.

6. Acknowledgement

The authors would like to express their deep gratitude to the Core Facilities Center "Rational

Nature Management and Physical Chemical Research" of the Tyumen State University, Russia, and its head, Doctor of Chemical Sciences, Professor Nikolay Tretyakov, for the equipment provided for measurements and result processing.

7. Conflict of interests

The authors declare no conflict of interest.

References

1. Rusanov AM, Teslya AV, Prichogai NI, Turlibekova DM. The content of total and mobile forms of heavy metals in soils of Orsk city. *Vestnik Orenburgskogo gosudarstvennogo universiteta*. 2012;4:57-89. (In Russ.)
2. Zhang X, Zhang X, Wang S, Zhao S. Improved remediation of co-contaminated soils by heavy metals and PAHs with biosurfactant-enhanced soil washing. *Scientific Reports*. 2022;12(1):3801. DOI:10.1038/s41598-022-07577-7
3. Rezapour S, Moghaddam S, Nouir A, Aqdam K. Urbanization influences the distribution, enrichment, and ecological health risk of heavy metals in croplands. *Scientific Reports*. 2022;12(1):3868. DOI:10.1038/s41598-022-07789-x
4. Al-Swadi, Usman A, Al-Farraj, Al-Wabel M, Ahmad M, Al-Faraj A. Sources, toxicity potential, and human health risk assessment of heavy metals-laden soil and dust of urban and suburban areas as affected by industrial and mining activities. *Scientific Reports*. 2022;12(1):3868. DOI:10.1038/s41598-022-12345-8
5. Jiang H, Cai L, Wen H, Luo J. Characterizing pollution and source identification of heavy metals in soils using geochemical baseline and PMF approach. *Scientific Reports*. 2020;10(1):6460. DOI:10.1038/s41598-020-63604-5
6. Kogan RM, Kalmanova VB. Soil acidity as an indicator of the ecological state of the urban area (on the territory of the city of Birobidzhan). *Regional problems*. 2008;10:83-86. (In Russ.)
7. Ladonin DV. *Forms of compounds of heavy metals in polluted soils*. Moscow: Moscow University Press; 2019. 312 p. (In Russ.)

8. Kovrigo VP, Kaurichev IS, Burlakova LM. *Soil science with the basics of geology*. Moscow: Kolos; 2000. 416 p. (In Russ.)

9. Vodyanitskii YuN. *Metals and metalloids in soils*. Moscow: VV Dokuchaev Soil Science Institute; 2008. 164 p. (In Russ.)

10. Moore JM. *Inorganic contaminants of surface water: research and monitoring priorities*. New York: Springer-Verlag; 1991. 366 p.

11. Gao W, He W, Zhang J, Chen Y, Zhang Z, Yang Y, He Z. Effects of biochar-based materials on nickel adsorption and bioavailability in soil. *Scientific Reports*. 2023;13(1):5880. DOI:10.1038/s41598-023-32502-x

12. Rocha JC, Desene J, Dossantos A, Toscano IA, Zara LF. Aquatic humus from an unpolluted Brazilian dark brown stream: general characterization and size fractionation of bound heavy metals. *Journal of Environmental Monitoring*. 2000;2(1):39-44. DOI: 10.1039/a907671i

13. Kuznetsov IP. Heavy metals in the soils of the Ryazan region. *Himiya v sel'skom hozyajstve*. 1995;5:22-25. (In Russ.)

14. Tessier A, Campbell PGC, Bisson M. Sequential extraction procedure for the speciation of particulate trace metals. *Analytical Chemistry*. 1979;51(7):844-851. DOI:10.1021/ac50043a017

15. Plesternjak E, Kraigher B, Leskovec S, Mulec I, Markovic S, Scancar J, Milacic R. Reduction of hexavalent chromium using bacterial isolates and a microbial community enriched from tannery effluent. *Scientific Reports*. 2022;12(1):20197. DOI:10.1038/s41598-022-24797-z

16. Medvedev IF, Derevyagin SS, Gubarev DI. Distribution of heavy metals in chernozems of the main azonal landscapes and agrolandscape elements in the Volga region. *Plodородie*. 2009;3:52-53. (In Russ.)

17. Klimov ES, Davydova OA, Zavaltseva OA, Borisova VV. To the question of the distribution of heavy metals in natural environments. *Fundamental'nye issledovaniya*. 2004;2:137-138. (In Russ.)

18. Orlov DS, Sadovnikova LK, Sukhanova NI. *Soil chemistry*. Moscow: Vysshaya shkola; 2005. 558 p. (In Russ.)

Information about the authors / Информация об авторах

Yana M. Chichigina, Assistant, University of Tyumen (UTMN), Tyumen, Russian Federation; ORCID 0009-0008-7909-0032; e-mail: y.m.chichigina@utmn.ru

Gulnara N. Shigabaeva, Cand. Sc. (Engineering), Associate Professor, Head of the Department of Organic and Ecological Chemistry, UTMN, Tyumen, Russian Federation; ORCID 0000-0003-2116-1017; e-mail: g.n.shigabaeva@utmn.ru

Ekaterina A. Emelyanova, Master's Degree Student, UTMN, Tyumen, Russian Federation; e-mail: stud0000040057@study.utmn.ru

Evgeny V. Galunin, Ph.D., Associate Professor, UTMN, Tyumen, Russian Federation; ORCID 0000-0002-8219-0148; e-mail: e.v.galunin@utmn.ru

Artem S. Yakimov, Leading Researcher, Earth Cryosphere Institute, Tyumen Scientific Center, Siberian Branch, Russian Academy of Sciences, Tyumen, Russian Federation; ORCID 0000-0002-1303-8492; e-mail: Yakimov_Artem@mail.ru

Alexei Yu. Isaev, Senior Lecturer, UTMN, Tyumen, Russian Federation; ORCID 0000-0002-2163-9968; e-mail: a.y.isaev@utmn.ru

Maria R. Bekker, Student, UTMN, Tyumen, Russian Federation; e-mail: stud0000228750@study.utmn.ru

Чичигина Яна Михайловна, ассистент, Тюменский государственный университет (ТюмГУ), Тюмень, Российская Федерация; ORCID 0009-0008-7909-0032; e-mail: y.m.chichigina@utmn.ru

Шигабаева Гульнара Нургаллаевна, кандидат технических наук, доцент, заведующий кафедрой органической и экологической химии, ТюмГУ, Тюмень, Российская Федерация; ORCID 0000-0003-2116-1017; e-mail: g.n.shigabaeva@utmn.ru

Емельянова Екатерина Александровна, магистрант, ТюмГУ, Тюмень, Российская Федерация; e-mail: stud0000040057@study.utmn.ru

Галунин Евгений Валерьевич, Ph.D., доцент, ТюмГУ, Тюмень, Российская Федерация; ORCID 0000-0002-8219-0148; e-mail: e.v.galunin@utmn.ru

Якимов Артём Сергеевич, ведущий научный сотрудник, Институт криосферы Земли Тюменского научного центра Сибирского отделения Российской академии наук, Тюмень, Российская Федерация; ORCID 0000-0002-1303-8492; e-mail: Yakimov_Artem@mail.ru

Исаев Алексей Юрьевич, старший преподаватель, ТюмГУ, Тюмень, Российская Федерация; ORCID 0000-0002-2163-9968; e-mail: a.y.isaev@utmn.ru

Беккер Мария Романовна, студент, ТюмГУ, Тюмень, Российская Федерация; e-mail: stud0000228750@study.utmn.ru

Received 04 April 2023; Accepted 03 May 2023; Published 06 July 2023



Copyright: © Chichigina YaM, Shigabaeva GN, Emelyanova EA, Galunin EV, Yakimov AS, Isaev AYu, Bekker MR, 2023. This article is an open access article distributed under the terms and conditions of the Creative Commons Attribution (CC BY) license (<https://creativecommons.org/licenses/by/4.0/>).

Modification of lubricants with graphite nanoplates

© Adel Baiti^a, Saif S.Y. Aldavud^a, Avzh A.M. Algurabi^a, Hicham Salhi^b, Vladimir F. Pershin^a✉

^a Tambov State Technical University, Bld. 2, 106/5, Sovetskaya St., Tambov, 392000, Russian Federation,

^b University of Batna 2, Fesdis, Batna, 05078, Algeria

✉ pershin.home@mail.ru

Abstract: The review is devoted to the current state of research and achievements in the field of modification of lubricants. To improve the tribological characteristics of lubricants, various additives, in particular, nanoparticles, are used. These additives avoid direct contact, reduce friction and wear. Given that graphene significantly improves the tribological characteristics of lubricants, the main methods for its production are considered. It is shown that the most promising technology for obtaining graphene to modify lubricants is liquid-phase shear exfoliation of crystalline graphite, since oil mixtures with nanoplates are evenly distributed in grease and ensure its stable operation in friction pairs. A variant of mixing graphite nanoplates with grease in a rotary disperser is considered. It is shown that, along with an increase in tribological characteristics, the lubricant modified with graphite nanoplates creates an antifriction film on friction surfaces. The compositions of the antifriction film and the results of its use are analyzed. The ways of improving the technology of modifying greases with graphite nanoplates are outlined. First of all, it is necessary to modernize the main equipment: a drum rod mill; node for classifying graphene-containing suspensions according to the nanoplates size; rotary disperser. Considering that the maximum effect is observed when using an antifriction film + grease modified with graphite nanoplates, it is necessary to study in detail the antifriction film formation and determine its optimal content in the lubricant.

Keywords: tribological characteristics; additives; nanomaterials; graphite nanoplates; friction pairs; wear; antifriction films.

For citation: Baiti A, Aldavud S.S.Yu, Algurabi A.M., Salhi H, Pershin V.F. Modification of lubricants with graphite nanoplates. *Journal of Advanced Materials and Technologies*. 2023;8(2):157-169. DOI:10.17277/jamt.2023.02.pp.157-169

Модифицирование смазочных материалов графитовыми нанопластинами

© А. Баити^a, С.С.Ю. Альдавуд^a, А. Альгураби^a, Х. Салхи^b, В.Ф. Першин^a✉

^a Тамбовский государственный технический университет,
ул. Советская, 106/5, пом. 2, Тамбов, 392000, Российская Федерация,

^b Университет Батна 2, Фесдис, Батна, 05078, Алжир

✉ pershin.home@mail.ru

Аннотация: Обзор посвящен современному состоянию исследований и достижений в области модифицирования смазочных материалов. Для улучшения трибологических характеристик смазок используют различные добавки, в частности, наночастицы. Такие добавки позволяют избежать прямого контакта, снижают коэффициент трения и износ. Учитывая, что графен значительно повышает трибологические характеристики смазок, в обзоре рассмотрены основные способы его получения. Показано, что наиболее перспективной технологией получения графена для модифицирования смазочных материалов является жидкофазная сдвиговая эксфолиация кристаллического графита, поскольку масляные смеси с нанопластинами равномерно распределяются в пластичной смазке и обеспечивают ее стабильную работу в парах трения. Рассмотрен вариант смешения нанопластин графита с пластичной смазкой в роторном диспергаторе. Показано, что наряду с повышением трибологических характеристик, смазка, модифицированная нанопластинами графита, создает антифрикционную пленку на поверхностях трения. Проанализированы составы антифрикционной пленки и результаты ее использования. Намечены пути совершенствования технологии модифицирования пластичных смазок

нанопластинами графита. В первую очередь необходимо модернизировать основное оборудование: барабанную стержневую мельницу; узел классификации графеносодержащих суспензий по размерам нанопластин; роторный диспергатор. Учитывая, что максимальный эффект наблюдается при использовании антифрикционной пленки + смазка, модифицированная нанопластинами графита, необходимо детально исследовать процесс формирования антифрикционной пленки и определить ее оптимальное содержание в смазке.

Ключевые слова: трибологические характеристики; присадки; наноматериалы; нанопластины графита; пары трения; износ; антифрикционные пленки.

Для цитирования: Baiti A, Aldavud S.S.Yu., Algurabi A.M., Salhi H., Pershin V.F. Modification of lubricants with graphite nanoplates. *Journal of Advanced Materials and Technologies. 2023;8(2):157-169. DOI:10.17277/jamt.2023.02. pp.157-169*

1. Introduction

Tribology plays an important role in solving the problem of friction, which occurs when the parts of mechanisms and machines that touch each other move relative to each other. Friction reduction can prevent costs of countries' gross domestic product from 1 to 1.4 % [1]. In addition to financial benefits, tribology can help protect the environment by improving energy efficiency and reducing CO₂ emissions. Thus, important social problems can be solved by improving the tribological characteristics of lubricants. Fig. 1 shows examples of friction pairs from contact between parts of mechanisms to human joints [2]. The study of lubricants makes a significant contribution to the field of tribology.

A lubricant is a substance that effectively improves the movement of solid objects relative to each other by reducing wear and friction on interacting surfaces. In mechanical systems, friction results from sliding, rolling, or rotating contact surfaces. Consequently, friction leads to significant

energy losses, wear and mechanical damage [3]. At least 5 % of the total amount of mechanical energy is converted into useless heat.

Lubricants must be chemically and thermally stable [4], non-volatile, non-corrosive, and durable over time. To meet environmental protection criteria, they must also be environmentally friendly and biodegradable [5]. The main goals and benefits of lubricants can be summarized as follows: reduction in load and increase in service life due to the formation of a lubricating layer in the friction zone; improving useful driving characteristics, such as reducing noise or friction; removal of generated heat to the outside to avoid overheating of bearings and deterioration of lubricant quality; reduction of corrosion by limiting the formation of rust and the penetration of foreign materials; reducing the degree of surface wear due to the application of lubricants between surfaces that rub against each other and the elimination of metal/metal contacts; reduced maintenance costs; reducing power losses of the internal combustion engine.

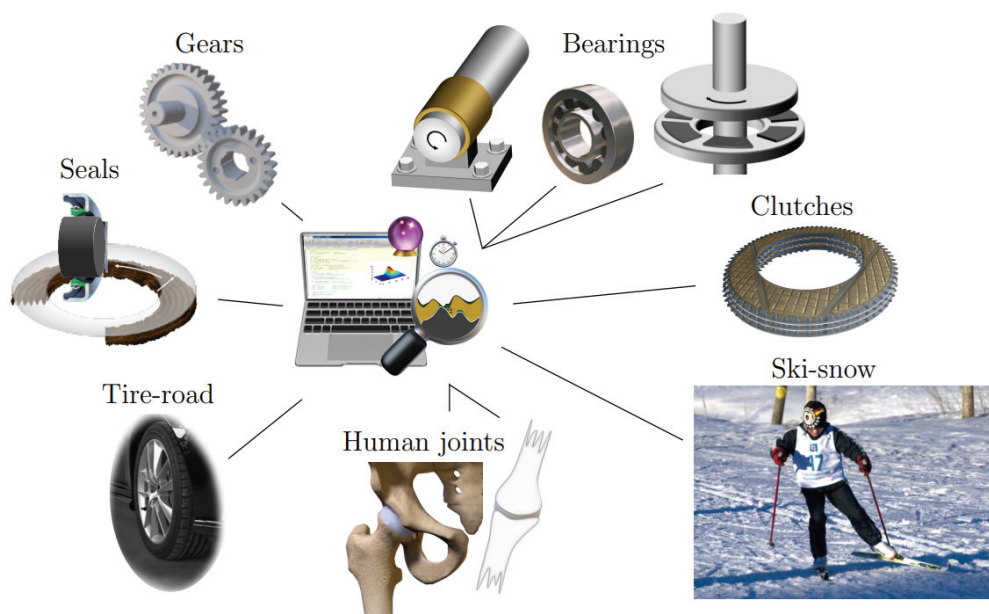


Fig. 1. Examples of friction pairs [2, © Almqvist]

Lubricants include greases, solid lubricants and lubricating oils. A liquid lubricant such as water, natural or synthetic oils can reduce friction by preventing sliding between contact surfaces (metal-to-metal or metal-to-nonmetal contacts). The effectiveness of lubrication depends on the contact stresses in the friction pair, the sliding speed and the viscosity of the lubricant. To improve the tribological characteristics of lubricants, various additives, in particular nanoparticles, are used. These additives make it possible to avoid direct contact, reduce the coefficient of friction and wear [6]. The efficiency of using nanoparticles as tribological additives was experimentally confirmed in [7–9]. The issue of obtaining carbon nanoparticles was considered in [10].

Due to their small size and unique microstructure, nanoparticles can easily form lubricated tribofilms on substrates by contacting contact surfaces [3]. Good dispersion characteristics allow nanoparticles to penetrate into the friction contact zone [11]. Thus, several modification strategies should be considered to increase the dispersion and stability of lubricant additives.

The use of a large amount of additives increases not only the viscosity of the lubricant, but also the cost, in particular, this applies to molybdenum disulfide [12, 13]. In addition, these additives have varying degrees of toxicity, releasing sulfated ash, phosphorus and sulfur, which lead to air pollution, for example, acid rain and fog, and increase chemical corrosion [14]. Some additives, including ionic liquids, have exceptional tribological characteristics and are environmentally friendly, but their high cost hinders their wide use in industry [15, 16]. In this regard, it is extremely important to create environmentally friendly and durable lubricant nanomaterials based on nanocarbon. Graphene and its derivatives are considered the most promising lubricant additives. However, there are still problems in improving the dispersion stability of nanoadditives [17].

Since graphene was discovered in 2004, it has already amazed researchers around the world with its unique properties [18, 19]. In this review, special attention is paid to the advantages of graphene, including graphite nanoplates, as an additive to lubricants, as well as directly to the methods and equipment for producing graphene.

2. Using Nanomaterials to Modify Lubricants

Before the discovery of graphene, graphite was the most common form of carbon for lubrication [20, 21]. Graphite consists of graphene layers, which provides a low coefficient of friction between the layers [21]. However, the use of graphite as a lubricant has many disadvantages.

Graphite is difficult to disperse uniformly in a liquid, which causes a decrease in fluidity and lubricity [22]. Graphite hardly enters the contact zone of parts and does not form a continuous protective film. Thus, graphite is not an ideal lubricant [23].

Graphene is a single layer of carbon atoms arranged in a two-dimensional (2D) hexagonal lattice. Unlike graphite, a single-layer or few-layer graphene structure can be easily stabilized in the liquid phase using surfactants [22]. The effects of few-layer graphene (FLG) help to reduce friction due to the sliding of graphene layers [24]. Since the terminology corresponding to the state standards of the Russian Federation does not have terms “few-layer graphene” and “multilayer graphene”, we will use the term “graphite nanoplate”.

In [25], the effect of graphene structure was studied by comparing two forms of commercial graphene nanomaterials, such as 1–2–layer and 1–10–layer graphite nanoplates. In further work, they were used as additives in 1-octyl-3-methylimidazolium tetrafluoroborate in epoxy resin. It has been established that 1–2–layer graphite nanoplates form large agglomerates, which leads to abrasive wear. On the contrary, 1–10–layer graphite nanoplates prevent wear by eliminating direct contact between friction surfaces. In addition, compared to graphite, additives based on graphite nanoplates are more resistant to oxidation and corrosion and have excellent thermal [26] and tribological [27, 28] characteristics.

A number of researchers [29, 30] have demonstrated the excellent chemical resistance of graphene. In addition to chemical properties, graphene has been found to have superior tribological performance compared to other materials [31]. Tribological features are explained by the ability of graphene layers to smoothly slide over each other [32]. These results were confirmed in a molecular dynamics simulation work that demonstrates the relationship between the number of graphene layers in a graphite nanoplate and friction [33]. The model provides an explanation for stability over a wide range of temperatures, velocities, and pressures, predicting that the frictional force approaches zero as the number of layers approaches two or three.

Berman et al. [34] reported the effect of adding graphite nanoplates with multiple graphene layers to steel friction surfaces to reduce friction and wear. The added nanoplates act as a two-dimensional nanomaterial, reducing wear between sliding contacts by almost four orders of magnitude and friction coefficients by a factor of 6.

Graphene has excellent thermal properties, which is confirmed by theoretical approaches [35]

and experimental results [36]. Modification of lubricant with graphene improves its thermal conductivity [37, 38]. The thermal and electrical conductivity of nanofluids containing graphite nanoplates in various mass concentrations was studied [39]. In [40], the tribocharacteristics of lithium synthetic lubricants based on poly-alpha-olefins and polytetrafluoroethylene particles (4 wt. %) of various sizes, namely 50 nm, 6 μm , 9 μm and 12 μm , and shapes as functional additive were studied. The results showed that the smaller the size, the higher the efficiency. However, 6 μm particles competed with 50 nm nanoparticles. The authors believe that the 6 μm particles performed well due to their spherical shape. It was concluded that the parameters that determine the efficiency are both the size and shape of particles. Li et al. investigated the tribological properties of 220 centipoise viscosity base grease with graphite nanosheets as an additive using a disk-on-disk test. The results showed a decrease in the friction coefficient at a normal force of 3000 N by 24 % [41]. In [42], MoS₂ was fixed on the surface of graphene sheets (GNS) using a hydrothermal process and chemical vapor deposition to obtain GNS/MoS₂ nanocolors (GNS/MoS₂-NF) and GNS/MoS₂ nanoplates (GNS/MoS₂-NP). The GNS/MoS₂ composite obtained by various methods was examined using XRD, Raman, SEM, TEM and XPS. The results confirmed the different morphology of GNS/MoS₂-NF and GNS/MoS₂ NP. For GNS/MoS₂-NF, MoS₂ nanocolors were dotted on the graphene surface, while MoS₂ nanoplates were uniformly attached to the graphene surface in GNS/MoS₂. The resulting composites were examined on a four-ball friction machine at 1200 rpm and a load of 392 N for 30 min. The GNS/MoS₂-NF additive performed better than the GNS/MoS₂ NP additive even at higher concentrations. For example, the coefficient of friction and base oil wear scar diameter were reduced by 42.8 and 16.9 % with the introduction of 0.02 wt. % GNS/MoS₂-NF compared to GNS/MoS₂-NP.

Although graphite nanoplates are a popular option, the synthesis of graphene-based lubricants is challenging and further research is needed to understand the best synthesis methods. However, graphene has the potential to revolutionize the lubricant industry, and using it as a lubricant additive could greatly improve existing lubricants.

3. Synthesis of Graphite Nanoplates

The most common method for obtaining graphite (graphene) nanoplates is chemical vapor deposition (CVD) [43]. The obtained CVD graphene/graphite films are often used as a protective

layer for microelectromechanical systems [44], gas barriers [45], and sensor production [46].

One of the options for the synthesis of liquid-phase graphene additives is the mechanical exfoliation of graphite oxide or other chemically modified graphite compound [47] followed by chemical or thermal reduction or modification [48, 49].

Graphene is obtained by mechanical exfoliation of graphite oxide into graphene oxide – the Hummers method [50]. Liang et al. [51] introduced a nonionic surfactant (Triton-X) into the graphite exfoliation method. Graphene was mechanically peeled off by ultrasonication after mixing with a non-ionic surfactant. The frictional properties of water-based lubricants improved by 80% due to modification with graphene. Alternatively, Patel et al. [48] used off-the-shelf reduced graphene oxide (rGO) as lubricant additives and reduced wear and friction by 52 %.

Due to the toxicity of the Hammers method, various alternatives have been proposed. Among available alternatives, ascorbic acid is known as the most promising reducing agent due to its low toxicity, low cost, and non-carcinogenic properties.

An alternative GO recovery method involves using thermal recovery. Thermal reduction is usually carried out at an elevated temperature in order to reduce GO to graphene [51].

Although liquid phase exfoliation of graphene may be the best way to obtain graphene for lubricant additives, researchers need to be aware of the fundamental limitations and impurities present in final products. It should be noted that during the reduction of GO on graphene planes, defects are formed at the sites of oxygen removal, which negatively affects non-tribological properties. Exfoliation of graphite using ultrasound requires large amounts of electricity, which significantly increases the cost. In our opinion, the most promising technology is the production of graphite nanoplates by liquid-phase shear exfoliation.

3.1. Preparation of graphite nanoplates by liquid-phase shear exfoliation

Most attention was paid to exfoliation using ultrasound. This is due to the fact that there is no need to make a special installation and it is possible to carry out the exfoliation of graphite particles on standard laboratory equipment. During sonication, cycles of high pressure (compression) and low pressure (rarefaction) alternate, the speed of which depends on the frequency of ultrasonic vibrations. At low pressure, a vacuum is created and bubbles or voids form in the liquid. At high pressure, the bubbles collapse and this phenomenon is called cavitation.

The temperature during cavitation reaches 5000 K, and the pressure is 2000 atm. In addition, liquid jets are formed with a speed of up to $280 \text{ m}\cdot\text{s}^{-1}$. Graphite nanoplates are obtained by sonication in organic solvents, in water with the addition of small amounts of surfactants, or in ionic liquids.

Thus, strong oxidizing agents are not used, which has a positive effect on the quality of nanoplates. A method for obtaining polystyrene functionalized with graphene is presented in [52]. Powders of flake graphite and styrene were used as starting materials. During sonication, graphite flakes are transformed into single-layer and few-layer graphene plates. Simultaneously, graphene sheets are functionalized with polystyrene chains. A similar functionalization process was carried out with other vinyl monomers and new composites were created.

Technology using ultrasound has the following disadvantages: very high energy consumption; graphite particles are affected not only by shear forces, but also by compressive and shock forces, which negatively affects the quality of graphene.

The most promising is shear exfoliation. One of the first versions of this method was proposed in [53]. The slurry jet is fed onto a rapidly rotating disk. Under the action of centrifugal forces, the suspension is distributed over the disk surface in a thin film and moves towards the periphery of the disk. In a thin film, shear forces arise and particles of graphite or other layered crystal are stratified. After repeated supply of the suspension to the rotating disk, the particles gradually turn into nanoplates. This method is interesting due to the stratification mechanism of layered crystals, but it has not found application in industrial production.

The most promising method is the production of graphite nanoplates using a stator-rotor mixer with high shear [54]. The mixer consists of a cylindrical body with 96 square holes with a cross section of $2 \times 2 \text{ mm}$. Inside the housing is a rotor with four blades. The gap between the edges of the blades and the inner surface of the housing should be no more than 0.1 mm. Particles are mainly affected by shear forces. When the suspension passes through the holes in the housing, shear forces partially act on the particles. In addition, cavitation occurs. The most significant are the shear forces, and the rest of the force effects cause defects in the graphene planes.

In [54], an L5M laboratory mixer manufactured by Silverson Machines Ltd., UK, was used. Electric motor power is 250 W, maximum rotor speed is 8000 rpm (6000 rpm at full load). The inner diameter of the cylindrical body is 50 mm. The rotor has four blades and a gap between the rotor and the body of 0.1 mm.

During the rotation of the rotor, the mixer works like a pump. By centrifugal force, the suspension is ejected through the holes in the housing. A vacuum is created between the housing and the rotor, and the suspension is drawn through the upper and lower ends of the housing into the area between the housing and the rotor. Particles that enter the area between the blade and the inner surface of the housing are subject to shear forces that cause particle separation. Experiments were also carried out using cases with an inner diameter of 19 mm and 16 mm. 5 liters of a mixture of water + crystalline graphite powder + surfactant were pre-prepared. The rotor speed was gradually increased to a predetermined value. Exfoliation was carried out for a certain time. During the experiments, six main parameters were varied: mixing time; rotor speed, N rpm (converted to s^{-1} in calculations); the volume of the processed suspension V liters (from 0.25 to 5); rotor diameter, D mm (12, 16 and 32 mm); concentration of graphite in the initial suspension.

The following components were used as surfactants: N-methyl-2-pyrrolidone; N-cyclohexyl-2-pyrrolidone; N-cyclohexyl-2-pyrrolidone. The classification of nanoplates was carried out on a Thermo Scientific centrifuge, model: Heraeus Megafuge [54]. Centrifugation was carried out sequentially at different speeds. After centrifugation, particles with an average size (length) remained in the centrifuge: 5000 rpm – 160 nm; 3000 rpm – 200 nm; 2500 rpm – 216 nm; 2000 rpm – 282 nm; 1000 rpm – 1000 nm. After separation of the suspension into fractions, the size of the nanoplates and the number of graphene layers in these nanoplates were evaluated using transmission electron microscopy (TEM). A very interesting fact is the relationship between the sizes of nanoplates and the number of graphene layers that make up these plates. For example, with an average nanoplate size of $1.1 \mu\text{m}$, the average number of graphene layers was 2.8. In addition, it was found that the aspect ratio of nanoplates (length/width) was constant and equal to 2.6. This is a very important fact, which further allows one to more accurately determine the concentration of nanoplates in a suspension. Thus, during cascade centrifugation, the suspension is separated into fractions according to the lateral particle size and the number of graphene layers. Currently, most researchers use cascade centrifugation to sort nanoplates.

As the results of long-term operation of the stator-rotor mixer showed, due to the wear of the rotor blades, the gap increases and the exfoliation process stops. This disadvantage is eliminated in a rotary apparatus with movable blades (Fig. 2) [55, 56].

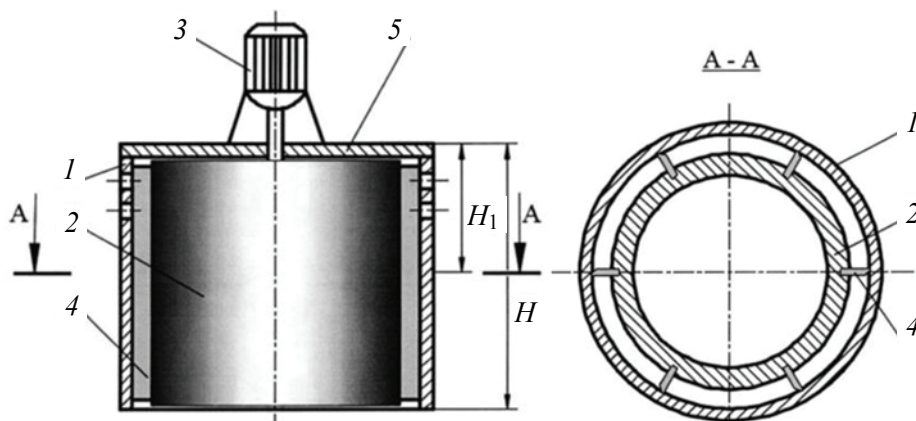


Fig. 2. Scheme of a rotary apparatus with movable blades: 1 – stator; 2 – rotor; 3 – rotation drive; 4 – blade; 5 – cover [55, © Al-Shiblawi]

The graphene-containing suspension was obtained as follows. Powder of crystalline graphite weighing 50–100 g was poured with 1–2 liters of oil, which is the basis of grease. The apparatus was placed in the container and the rotation drive 3 was turned on. When the rotor 2 rotated, the mixture of oil and graphite was ejected by centrifugal forces through the holes in the upper part of the housing. In the zone between the housing and the rotor, a reduced pressure was formed and the mixture entered the specified zone through the lower end. Under the action of centrifugal forces, the blades 4 were pressed against the inner surface of the body. Particles that fell into the zone of sliding contact of the fixed inner surface of the stator and the movable blades (exfoliation zone) stratified due to shear forces, i.e. two particles were formed from one particle, but with smaller thicknesses. Since the particles fell into the exfoliation zone many times, nanoplates gradually formed from graphite particles. After the end of the exfoliation process by centrifugation, the resulting suspension was divided into fractions by particle size.

The results of further studies made it possible to carry out the transition from a periodic regime to a continuous one [57–59].

Fig. 3 shows a diagram of a cross section of a rotary apparatus with composite movable blades. A rotor 2 is located in the cylindrical body 1. The blade consists of a base 3 connected to the tip 4 by a tongue-and-groove connection. The base is made of metal, and the tip is made of an anti-friction material, such as fluoroplastic. By changing the density of the metal, it is possible to change the magnitude of the centrifugal force acting on the blade, and, consequently, the force of pressing the tip to the inner surface of the stator. For example, the mass of a blade with an axial length of 10 mm, made of PTFE, is equal to $m = 0.4$ g; the normal force F_N acting on the

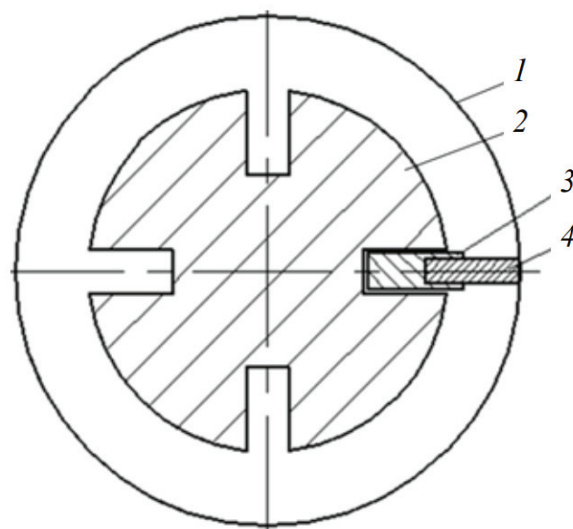


Fig. 3. Scheme of a rotary apparatus with movable composite blades: 1 – stator; 2 – rotor; 3 – the base of the movable blade; 4 – the tip of the movable blade [57, © Al-Jarah]

blade is 4.3 N. When the blade is made in two parts, with a base 4 mm thick, with a radial dimension of 8 mm, made of steel, and a tip 2 mm thick and with a radial dimension of 6 mm, made of PTFE, the total mass of the blade $m = 1.8$ g, and the normal force $F_N = 20$ N.

Comparisons between the results of experimental studies in batch mode (Fig. 2) and continuous mode (Fig. 3) were made, which showed that the productivity in continuous mode was at least 1.5 times greater than in batch mode.

4. Modification of Lubricants with Graphite Nanoplates

For the industrial modification of grease in the article [59], an installation was developed, the scheme of which is shown in Fig. 4. The process is

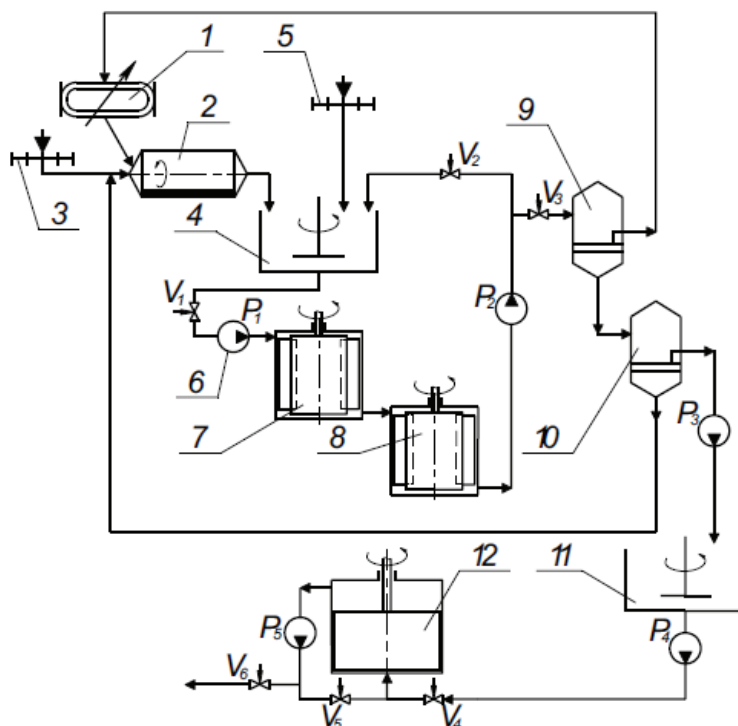


Fig. 4. Scheme of the graphene-containing suspensions and concentrates industrial production: 1 – liquid dispenser; 2 – rod drum mill; 3 – graphite powder dispenser; 4 – tank with a stirrer; 5 – additional dispenser of graphite powder; 6 – pump; 7 – first rotary apparatus; 8 – final rotary apparatus; 9 – coarse filter; 10 – fine filter; 11 – vessel for preliminary mixing of nanoplates with grease; 12 – rotary disperser [57, © Al-Jarah]

implemented as follows. The base oil and powder of crystalline graphite are fed by dispensers 1 and 3 into a drum rod mill 2. Mechanical activation of graphite particles and their partial exfoliation are carried out in the mill [59, 60].

The treated mixture is fed into tank 4, where oil and graphite powder are supplied by dispenser 5. From tank 4, the diluted mixture is fed by pump 6 (P_1) into the first rotary apparatus, where graphite is exfoliated. From the first rotary apparatus, the suspension enters the second apparatus, etc. Next, the suspension is fed by pump P_2 to the coarse filter 9. The filter cake is sent to the mill 2 for repeated mechanical activation. The clarified suspension is fed to the fine filter 10. The precipitate from the filter 10 is fed into the pre-mixing tank of nanoplates with grease 11.

For uniform distribution of nanoplates over the volume of the modified lubricant, a disk disperser 12 is used [61–64]. The disperser (Fig. 5) consists of a stepped disk (rotor) 1, a stator 2, and a pipe for supplying the mixture 3. The mixing of a viscous liquid with graphene plates was carried out as follows. Grease with graphene concentrate was premixed using a laboratory paddle mixer. The content of graphite nanoplates did not exceed 1 wt. %. The mixture was pumped into nozzle 3 with

a rotating disk 1. Compared to a flat disk, vertical sections were added where the mixture moves along helical trajectories.

The gap between the rotor and the stator $S = R_{iS} - R_{iR}$, when using different pairs of stators and rotors, varied from 0.05 to 0.2 mm. At the beginning of exfoliation, a gap of 0.2 mm was used, and as the thickness of the nanoplates decreased, the gap was reduced to 0.05 mm.

The motion of a viscous fluid in a small gap between a fixed body and a rotating disk was studied [63]. Mathematical dependencies are obtained to determine the main parameters of the motion of a viscous fluid in the gap. Based on the mathematical apparatus of random Markov processes, discrete in space and time, a model of the process of mixing grease with graphene plates was developed. The decomposition of the mixing process into radial and circumferential components made it possible to estimate the intensity of each of these components. Using the results of numerical experiments, ways to improve the organization of loading the lubricant and modifier into the homogenizer were outlined in order to increase the uniformity of the distribution of graphene plates over the entire volume of the lubricant and stabilize the tribological characteristics.

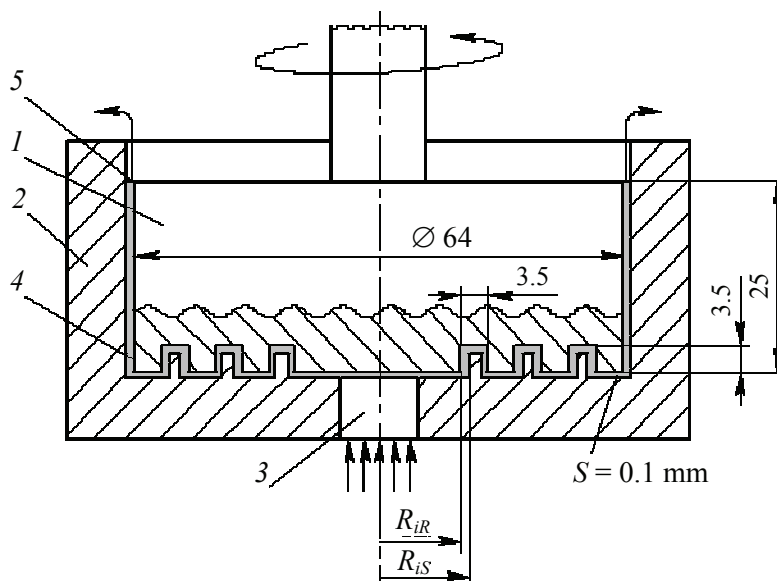


Fig. 5. Scheme of a stepped disk homogenizer [63, © Alhilo]

Table 1. Tribological characteristics of modified lubricants

Grease name	Wear scar diameter, mm	Scuff index, N	Critical load, N	Welding load, N
Integrated Lithium threaded	0.52	511.80	765	1932
Complex Lithium threaded with talc	0.53	509.83	1216	1932
Complex Lithium threaded Surgut	0.55	707.95	451	1932
Integrated Lithium threaded from fishing	0.50	536.77	765	1932
Integrated Lithium threaded from pipe factory	0.77	296.15	294	1932
Complex Calcium	0.69	201.10	197	1098
Complex Calcium with 0.1 % multilayer graphene	0.34	598.00	1040	4140

The efficiency of using nanoplates obtained by liquid-phase shear exfoliation was experimentally confirmed in [65, 66]. The results of the experimental determination of the tribological characteristics of the modified lubricant are given in Table. 1.

According to the data obtained, when 0.1 % multilayer graphene was added to the complex calcium lubricant, the wear scar diameter decreased by 50%, the scuff index increased by 2.9 times, and the bearing capacity increased by 3.8 times [65]. Multilayer graphene (graphite nanoplates) was obtained by liquid-phase shear exfoliation of crystalline graphite powder in oil, which was the basis of a complex calcium lubricant. The number of graphene layers did not exceed 25, and the lateral dimensions were on the order of 1 μm.

5. Formation of Antifriction Films on Friction Surfaces

Protective anti-friction films that form on friction surfaces significantly extend the service life of machines and mechanisms. The paper [67] presents the results of comparative tests on an MI-1M friction machine, Litol-24 commercial lubricant and Litol-24 lubricant modified with graphite nanoplates. We used graphite nanoplates obtained by liquid-phase shear exfoliation with the number of graphene layers no more than 25 and a concentration of 0.1 %. It has been established that the modified lubricant reduces the mass wear of friction pairs by 43 %. Fig. 6 shows the contact diagram of the roller-roller friction pair. The rollers are made of ShKh-15 steel.

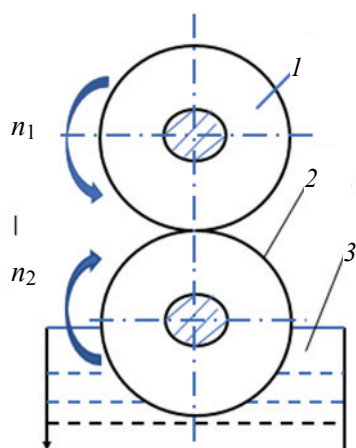


Fig. 6. The scheme of contacting the friction pair “roller-roller”: 1 – upper roller; 2 – lower roller; 3 – bath with lubrication [67, © Nagdaev]

Roller parameters: top roller width – 10 mm; lower – 12 mm; outer diameter – 50 mm; surface roughness – $Ra = 0.8 \mu\text{m}$; hardness – 60 HRC. The rollers underwent preliminary running-in on Litol-24 lubricant for 3 hours. The bottom roller was 1/3 of the diameter immersed in a grease bath. Evaluation of the running-in efficiency was the stabilization of the friction moment. After running in, the rollers were washed, dried, and weighed with an accuracy of 0.1 g. The rollers prepared for testing were installed in a friction machine and testing began at zero load, which was gradually increased to a selected value. The wear of the friction surfaces was determined by weighing on an analytical balance. The temperature change on the friction surfaces was determined with an MS 6530 instrument.

After testing, the surface of the upper roller had the form shown in Fig. 7.

In conclusion, it is noted that the modification of the lubricant with multilayer graphene improves performance and reduces the wear of friction surfaces.



Fig. 7. The roller surface after testing (100 times magnification) [67, © Nagdaev]

In [69], the authors set the task to study the processes of formation of a carbon film on the surface of the roller-roller friction unit in Litol-24 lubricant with an additive in the form of multilayer graphene in an amount of 0.2 wt. %. The condition of the friction surfaces was assessed using a Kromatech digital microscope and electron microscopy. Surface roughness and carbon film thickness were determined using a profilometer. The tests were carried out on an MI-1M friction machine. The friction pair “cylinder-ball” was investigated and the coefficient of friction and the state of the surface were determined. As a result of the research, it was found that, first of all, the film was formed in depressions on the friction surfaces (Fig. 8).

To determine the composition of the film, it was deformed to destroy it. According to the scanning electron microscopy images obtained by the authors, in several places the film came off the steel surface and cavities formed.

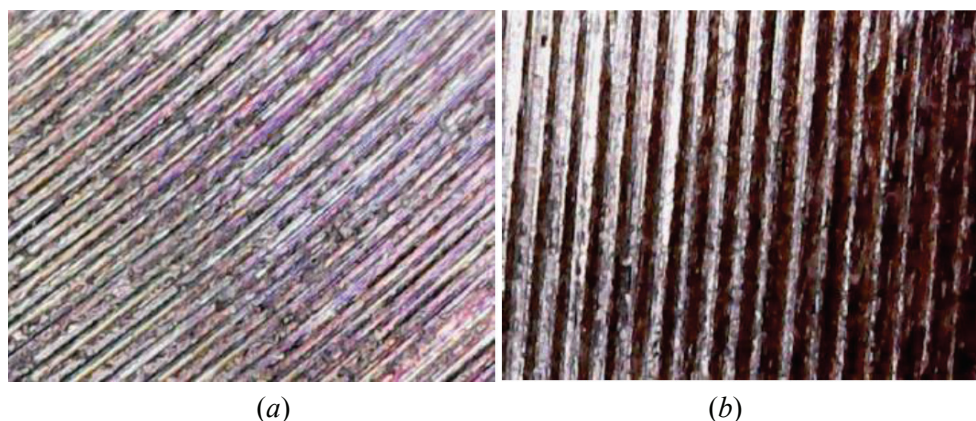


Fig. 8. Micrograph of the metal roller surface: a – at the 110 times magnification; b – the roller surface after 6 hours of operation in Litol-24 + graphene lubricant [68, © Nagdaev]

A similar film was obtained on the surface of a cylinder 26 mm in diameter made of BrShchF10-1 bronze. To determine the elemental composition of the film, mapping of individual sections was carried out and it was found that the flakes were composed of carbon, which confirms the composition of the carbon antifriction film formed on the surface of ShKh15 steel.

With a change in the thickness of the carbon film (the operating time of the friction unit), the roughness of the carbon surface changes. For the first hour, the roughness changes from class 5 to 9–10. From 1 hour to 3 hours the roughness decreases and then increases again. The moment of the friction force increases during the initial 90 minutes of operation of the friction unit from 5.4 to 5.8 (Nm), then gradually decreases to 4.9.

The test results showed the following values of friction coefficients: Steel ShKh15 – 0.288; Steel ShKh15 + Litol-24 – 0.197; Anti-friction film + Litol-24 – 0.141; Steel ShKh15 + Litol-24 + 0.2 % graphene – 0.113; Anti-friction film + Litol-24 + 0.2% graphene – 0.06.

Thus, the use of antifriction film and graphene-modified lubricant reduces the friction coefficient by about 3 times. It is also noted that there is a decrease in the oil absorption of a rough surface, which reduces the thickness of the lubricating film [68].

6. Conclusion

The modification of lubricants with nanomaterials significantly improves tribological characteristics and improves heat removal from the friction zone. The most promising antifriction additives are graphite nanoplates, the production of which is quite simple and cheap and, what is very important and environmentally friendly. When obtaining graphite nanoplates by liquid-phase shear exfoliation of crystalline graphite in base oil, the operation of uniform distribution of these nanoplates over the volume of grease is simplified. The addition of 0.1 wt.% graphite nanoplates containing no more than 25 graphene layers to the complex calcium lubricant reduces the diameter of the wear scar by 50%, the scuff index increases by 2.9 times, and the bearing capacity increases by 3.8 times. In addition, when using lubricants modified with graphite nanoplates, the formation of antifriction films on friction surfaces is observed, which reduces the friction coefficient by 3 times. It is necessary to develop an industrial technology for applying antifriction films using graphite nanoplates, which will reduce friction and wear of friction pairs in mechanisms and machines.

7. Funding

This research received no external funding.

8. Conflict of interests

The authors declare no conflict of interest.

References

1. Jost HP. Tribology micro & macro economics: A road to economic savings. *Tribology and Lubrication Technology*. 2005;61(10):18-22.
2. Almqvist A, Råfols FP. *Scientific computing with applications in tribology: A course compendium*. 2022. Available from: <https://www.diva-portal.org/smash/record.jsf?pid=diva2%3A1289574&dsid=9285> [Accessed on 22 November 2022].
3. Wang L, Gong P, Li W, Luo T, Cao B. Mono-dispersed Ag/Graphene nanocomposite as lubricant additive to reduce friction and wear. *Tribology International*. 2020;146:106228. DOI: 0.1016/j.triboint.2020.106228
4. Christensen G, Younes H, Hong G, Lou D, Hong H, Widener C, Bailey C, Hrabec R. Hydrogen bonding enhanced thermally conductive carbon nano grease. *Synthetic Metals*. 2020;259:116213. DOI:10.1016/j.synthmet.2019.116213
5. Fan M, Yang D, Wang X, Liu W, Fu H. DOSS-Based QAILS: As Both neat lubricants and lubricant additives with excellent tribological properties and good detergency. *Industrial & Engineering Chemistry Research*. 2014;53(46):17952-17960. DOI:10.1021/ie502849w.
6. Ahmed E, Ghazaly NM, Jaber AGE. Tribological behavior of adding nano oxides materials to lithium grease: A Review. *American Journal of Nanomaterials*. 2020;8(1):1-9.
7. Hashem A, Marlinda AR, Hossain MAM, Al Mamun M, ShalauddinMd, Simarani K, Johan MR. A unique oligonucleotide probe hybrid on graphene decorated gold nanoparticles modified screen-printed carbon electrode for pork meat adulteration. *Electrocatalysis*. 2023;14(2):179-194. DOI:10.1007/s12678-022-00779-7
8. Hashem A, Hossain MAM, Marlinda AR, Mamun MA, Simarani K, Johan MR. Nanomaterials based electrochemical nucleic acid biosensors for environmental monitoring: A review. *Applied Surface Science Advances*. 2021;4:100064. DOI:10.1016/j.apsadv.2021.100064
9. Sagadevan S, Marlinda AR, Johan Mohd R, Umar A, Fouad H, Alothman OY, Khaled U, Akhtar MS, Shahid MM. Reduced graphene/nanostructured cobalt oxide nanocomposite for enhanced electrochemical performance of supercapacitor applications. *Journal of Colloid and Interface Science*. 2020;558:68-77. DOI: 10.1016/j.jcis.2019.09.081
10. Younes H, Hong H, Peterson GP. A Novel approach to fabricate carbon nanomaterials–nanoparticle solids through aqueous solutions and their applications. *Nanomanufacturing and Metrology*. 2021;4(4):226-236. DOI:10.1007/s41871-020-00094-z

11. Liu W, Qiao X, Liu S, Chen P. A review of nanomaterials with different dimensions as lubricant additives. *Nanomaterials*. 2022;12(21):3780. DOI:10.3390/nano12213780.
12. Xiao H, Liu S. 2D nanomaterials as lubricant additive: A review. *Materials & Design*. 2017;135:319-332. DOI:10.1016/j.matdes.2017.09.029
13. Senatore A, Hong H, D'Urso V, Younes H. Tribological behavior of novel CNTs-based lubricant grease in steady-state and fretting sliding conditions. *Lubricants*. 2021;9(11):107. DOI:10.3390/lubricants9110107
14. Hasan MS, Kordijazi A, Rohatgi PK, Nosonovsky M. Machine learning models of the transition from solid to liquid lubricated friction and wear in aluminum-graphite composites. *Tribology International*. 2022;165:107326. DOI:10.1016/j.triboint.2021.107326
15. Huang G, Yu Q, Ma Z, Cai M, Zhou F, Liu W. Oil-soluble ionic liquids as antiwear and extreme pressure additives in poly- α -olefin for steel/steel contacts. *Friction*. 2019;7(1):18-31. DOI:10.1007/s40544-017-0180-8
16. Jiang C, Li W, Nian J, Lou W, Wang X. Tribological evaluation of environmentally friendly ionic liquids derived from renewable biomaterials. *Friction*. 2018;6(2):208-218. DOI:10.1007/s40544-017-0170-x
17. Zhao J, Huang Y, He Y, Shi Y. Nanolubricant additives: A review. *Friction*. 2021;9(5):891-917. DOI:10.1007/s40544-020-0450-8
18. Bodenmann AK, MacDonald AH. Graphene: Exploring carbon flatland. *Physics Today*. 2007;60(8):35-41. DOI:10.1063/1.2774096
19. Liu Y, Yu S, Shi Q, Ge X, Wang W. Graphene-family lubricant additives: recent developments and future perspectives. *Lubricants*. 2022;10(9):215. DOI:10.3390/lubricants10090215
20. Al Faruque MA, Syduzzaman M, Sarkar J, Bilisik K, Naebe M. A review on the production methods and applications of graphene-based materials. *Nanomaterials*. 2021;11(9):2414. DOI:10.3390/nano11092414
21. Hansora DP, Shimpi NG, Mishra S. Graphite to graphene via graphene oxide: an overview on synthesis, properties, and applications. *JOM*. 2015;67(12):2855-2868. DOI:10.1007/s11837-015-1522-5
22. Avilés M-D, Saurín N, Sanes J, Carrión F-J, Bermúdez M-D. Ionanocarbon lubricants. The combination of ionic liquids and carbon nanophases in tribology. *Lubricants*. 2017;5(2):14. DOI:10.3390/lubricants5020014
23. Liu L, Zhou M, Li X, Jin L, Su G, Mo Y, Li L, Zhu H, Tian Y. Research progress in application of 2d materials in liquid-phase lubrication system. *Materials*. 2018;11(8):1314. DOI:10.3390/ma11081314
24. Pape F, Poll G. Investigations on graphene platelets as dry lubricant and as grease additive for sliding contacts and rolling bearing application. *Lubricants*. 2019;8(1):3. DOI:10.3390/lubricants8010003
25. Saurín N, Sanes J, Bermúdez M-D. New graphene/ionic liquid nanolubricants. *Materials Today: Proceedings*. 2016;3:S227-S232. DOI:10.1016/j.matpr.2016.02.038
26. Renteria J, Nika D, Balandin A. Graphene thermal properties: applications in thermal management and energy storage. *Applied Sciences*. 2014;4(4):525-547. DOI:10.3390/app4040525
27. Garcia I, Guerra S, De Damborenea J, Conde A. Reduction of the coefficient of friction of steel-steel tribological contacts by novel graphene-deep eutectic solvents (DESs) lubricants. *Lubricants*. 2019;7(4):37. DOI:10.3390/lubricants7040037
28. Guo Y-B, Zhang S-W. The tribological properties of multi-layered graphene as additives of PAO2 oil in steel-steel contacts. *Lubricants*. 2016;4(3):30. DOI:10.3390/lubricants4030030
29. Nine MJ, Cole MA, Tran DNH, Losic D. Graphene: a multipurpose material for protective coatings. *Journal of Materials Chemistry A*. 2015;3(24):12580-12602. DOI:10.1039/C5TA01010A
30. Marlinda AR, An'amt MN, Yusoff N, Sagadevan S, Wahab YA, Johan MR. Recent progress in nitrates and nitrites sensor with graphene-based nanocomposites as electrocatalysts. *Trends in Environmental Analytical Chemistry*. 2022;34:e00162. DOI:10.1016/j.teac.2022.e00162
31. Xu Y, Cao H, Xue Y, Li B, Cai W. Liquid-phase exfoliation of graphene: an overview on exfoliation media, techniques, and challenges. *Nanomaterials*. 2018;8(11):942. DOI:10.3390/nano8110942
32. Zhao J, Li Y, Wang Y, Mao J, He Y, Luo J. Mild thermal reduction of graphene oxide as a lubrication additive for friction and wear reduction. *RSC Advances*. 2017;7(3):1766-1770. DOI:10.1039/C6RA26488C
33. Xu L, Ma T-B, Hu Y-Z, Wang H. Vanishing stick-slip friction in few-layer graphenes: the thickness effect. *Nanotechnology*. 2011;22(28):285708. DOI:10.1088/0957-4484/22/28/285708
34. Berman D, Erdemir A, Sumant AV. Graphene: a new emerging lubricant. *Materials Today*. 2014;17(1):31-42. DOI:10.1016/j.mattod.2013.12.003
35. Goyal V, Balandin AA. Thermal properties of the hybrid graphene-metal nano-micro-composites: Applications in thermal interface materials. *Applied Physics Letters*. 2012;100(7):073113. DOI:10.1063/1.3687173
36. Nika DL, Balandin AA. Thermal transport in graphene, few-layer graphene and graphene nanoribbons. In: *Thermal Transport in Low Dimensions*. Switzerland: Springer International Publishing; 2016. p. 339-363.
37. Sarafraz M, Safaei M, Tian Z, Goodarzi M, Bandarrafilho E, Arjomandi M. Thermal assessment of nano-particulate graphene-water/ethylene glycol (WEG 60:40) nano-suspension in a compact heat exchanger. *Energies*. 2019;12(10):1929. DOI:10.3390/en12101929
38. Zhao J, Gao T, Li Y, He Y, Shi Y. Two-dimensional (2D) graphene nanosheets as advanced lubricant additives: A critical review and prospect. *Materials Today Communications*. 2021;29:102755. DOI:10.1016/j.mtcomm.2021.102755
39. Naddaf A, ZeinaliHeris S. Experimental study on thermal conductivity and electrical conductivity of diesel oil-based nanofluids of graphene nanoplatelets and carbon nanotubes. *International Communications in Heat and Mass Transfer*. 2018;95:116-122. DOI:10.1016/j.icheatmasstransfer.2018.05.004

40. Kumar N, Saini V, Bijwe J. Performance properties of lithium greases with PTFE particles as additive: Controlling parameter- size or shape? *Tribology International*. 2020;148:106302. DOI:10.1016/j.triboint.2020.106302
41. Lee C-G, Hwang Y-J, Choi Y-M, Lee J-K, Choi C, Oh J-M. A study on the tribological characteristics of graphite nano lubricants. *International Journal of Precision Engineering and Manufacturing*. 2009;10(1):85-90. DOI:10.1007/s12541-009-0013-4
42. Song W, Yan J, Ji H. Fabrication of GNS/MoS₂ composite with different morphology and its tribological performance as a lubricant additive. *Applied Surface Science*. 2019;469:226-235. DOI:10.1016/j.apsusc.2018.10.266
43. Saeed M, Alshammari Y, Majeed SA, Al-Nasrallah E. Chemical vapour deposition of graphene-synthesis, characterization, and applications: A Review. *Molecules*. 2020;25(17):3856. DOI:10.3390/molecules25173856
44. Rana S, Reynolds JD, Ling TY, Shamsudin MS, Pu SH, Chong HMH, Pamunuwa D. Nano-crystalline graphite for reliability improvement in MEM relay contacts. *Carbon*. 2018;133:193-199. DOI:10.1016/j.carbon.2018.03.011
45. Fishlock SJ, Pu SH, Bhattacharya G, Han Y, McLaughlin J, McBride JW, Chong HMH, O'Shea SJ. Micromachined nanocrystalline graphite membranes for gas separation. *Carbon*. 2018;138:125-133. DOI:10.1016/j.carbon.2018.05.071
46. Ling TY, Pu SH, Fishlock SJ, Han Y, Reynolds JD, McBride JW, Chong HMH. Sensing performance of nanocrystalline graphite-based humidity sensors. *IEEE Sensors Journal*. 2019;19(14):5421-5428. DOI:10.1109/JSEN.2019.2905719
47. Liang S, Shen Z, Yi M, Liu L, Zhang X, Ma S. In-situ exfoliated graphene for high-performance water-based lubricants. *Carbon*. 2016;96:1181-1190. DOI:10.1016/j.carbon.2015.10.077
48. Patel J, Kiani A. Effects of reduced graphene oxide (rGO) at different concentrations on tribological properties of liquid base lubricants. *Lubricants*. 2019;7(2):11. DOI:10.3390/lubricants7020011
49. Nassef MGA, Soliman M, Nassef BG, Daha MA, Nassef GA. Impact of graphene nano-additives to lithium grease on the dynamic and tribological behavior of rolling bearings. *Lubricants*. 2022;10(2):29. DOI:10.3390/lubricants10020029
50. Oliveira AEF, Braga GB, Tarley CRT, Pereira AC. Thermally reduced graphene oxide: synthesis, studies and characterization. *Journal of Materials Science*. 2018;53(17):12005-12015. DOI:10.1007/s10853-018-2473-3
51. Liang S, Shen Z, Yi M, Liu L, Zhang X, Ma S. In-situ exfoliated graphene for high-performance water-based lubricants. *Carbon*. 2016;96:1181-1190. DOI:10.1016/j.carbon.2015.10.077
52. Xu H, Suslick KS. Sonochemical preparation of functionalized graphenes. *Journal of the American Chemical Society*. 2011;133(24):9148-9151. DOI:10.1021/ja200883z
53. Chen X, Boulos RA, Dobson JF, Raston CL. Shear induced formation of carbon and boron nitride nanoscrolls. *Nanoscale*. 2013;5(2):498-502. DOI:10.1039/C2NR33071G
54. Paton KR, Varrla E, Backes C, Smith RJ, Khan U, et al. Scalable production of large quantities of defect-free few-layer graphene by shear exfoliation in liquids. *Nature Materials*. 2014;13(6):624-630. DOI:10.1038/nmat3944
55. Al-Shiblawi KA, Pasko AA, Pershin VF. Simulation of the process of obtaining graphene structures by liquid-phase graphite shear exfoliation. *Vestnik Tambovskogo gosudarstvennogo tekhnicheskogo universiteta*. 2018;24(4):717-726. DOI:10.17277/vestnik.2018.04.pp.717-726 (In Russ.)
56. Al-Shiblawi KA, Pershin VF, Baranov AA, Pasko AA. Obtaining a few-layer graphene by the method of liquid-phase shear exfoliation. *Nauchno-tekhnicheskiye vedomosti SPbPU. Yestestvennyye i inzhenernyye nauki*. 2019;25(1):143-154. DOI:10.18721/JEST.25114 (In Russ.)
57. Al-Jarakh RA, Al-Mashkhadani AMR, Mansur V, Aldavud SS, Osipov AA, Pershin VF. Production of graphene-containing suspensions and concentrates by cascade graphite exfoliation. *Vestnik Tambovskogo gosudarstvennogo tekhnicheskogo universiteta*. 2022;28(1):139-152. DOI:10.17277/vestnik.2022.01.pp.139-152 (In Russ.)
58. Pershin VF, Al-Shiblawi KA Kh., Al-Mashkhadani AMR. *A method for obtaining graphene-containing suspensions and a device for its implementation*. Russian Federation patent 2,720,684. 12 May 2020. (In Russ.)
59. Pershin VF, Al-Dzharakh RA, Mansur V, Baranov AA, Vorobyov AM, Melekhin DD, Memetov NR, Osipov AA, Pasko AA, Tkachev AG. *A method for obtaining graphene-containing suspensions by graphite exfoliation and a device for its implementation*. Russian Federation patent 2,737,925. 04 December 2020. (In Russ.)
60. Pershin VF, Zhumagalieva GB, Memetov NR, Pasko AA, Tkachev AG. *Rod drum mill*. Russian Federation patent 2,670,495. 23 October 2018. (In Russ.)
61. Pershin VF, Zhumagaliyeva GB, Tkachev AG, Pasko AA, Vorobyev AM. Production of graphene concentrates based on synthetic oils in rod drum mills. *IOP Conference Series: Materials Science and Engineering*. 2019;693(1):012035. DOI:10.1088/1757-899X/693/1/012035
62. Pershin VF, Alhilo ZAA, Baranov AA, Vorobyov AM, Osipov AA, Tkachev AG. *Method for obtaining graphene-containing suspensions and device for its implementation*. Russian Federation patent 2,743,523. 19 February 2021. (In Russ.)
63. Alkhilo ZAA, Baranov AA, Tugolukov EN, Pasko AA, Pershin VF. Modeling the process of mixing graphene nanostructures with a viscous liquid. *Vestnik Tambovskogo gosudarstvennogo tekhnicheskogo universiteta*. 2021;27(1):105-117. DOI:10.17277/vestnik.2021.01.pp.105-117 (In Russ.)
64. Alhilo ZAAA, Mansour W, Pershin V, Pasko A. Continuous and semi-continuous industrial production of lubricants modified with graphene nanostructures. *IOP*

Conference Series: Materials Science and Engineering. 2021;1100(1):012027. DOI:10.1088/1757-899X/1100/1/012027

65. Pershin VF, Ovchinnikov KA, Alhiilo ZAA, Stolyarov RA, Memetov NR. Creation of environmentally friendly lubricants modified with graphene. *Rossiyskie nanotekhnologii = Nanobiotechnology Reports.* 2018; 13(5-6):131-135. (In Russ.)

66. Alhilo ZAAA, Zhumagalieva G, Pasko T. Environmentally friendly technology for the modification of lubricants with graphene nanostructures. *MATEC Web of Conferences.* 2020;315:06005. DOI:10.1051/mateconf/202031506005

67. Nagdaev VK, Vyazinkin VS, Zabrodskaya AV, Ostrikov VV, Safonov VV, Pershin VF. Results of studies of a lubricant modified with multilayer graphene. *Nauka v tsentral'noy Rossii.* 2021;2(50):71-77. DOI:10.35887/2305-2538-2021-2-71-77 (In Russ.)

68. Nagdaev VK, Pershin VF, Vigdorovich M, Ostrikov VV, Safonov VV, Alhilo ZAAA. Study of the dynamics of formation of a carbon film on the surfaces of the friction unit. *Nauka v tsentral'noy Rossii.* 2022;1(55):108-118. DOI:10.35887/2305-2538-2022-1-108-118 (In Russ.)

Information about the authors / Информация об авторах

Adel Baiti, Postgraduate Student, Tambov State Technical University (TSTU), Tambov, Russian Federation; e-mail: adelbaiti1@gmail.com

Saif S. Y. Aldavud, Postgraduate Student, TSTU, Tambov, Russian Federation; e-mail: eng.saif.suhail@gmail.com

Avzh A. M. Algurabi, Postgraduate Student, TSTU, Tambov, Russian Federation; e-mail: razemr@yandex.ru

Hicham Salhi, Ph.D., Assistant Professor, University of Batna, Algeria; e-mail: salhiheat@gmail.com

Vladimir F. Pershin, D. Sc. (Eng.), Professor, TSTU, Tambov, Russian Federation; ORCID 0000-0002-0213-9001; e-mail: pershin.home@mail.ru

Баити Адель, аспирант, Тамбовский государственный технический университет (ТГТУ), Тамбов, Российская Федерация; e-mail: adelbaiti1@gmail.com

Альдавуд Саиф Сухаил Юсиф, аспирант, ТГТУ, Тамбов, Российская Федерация; e-mail: eng.saif.suhail@gmail.com

Альгураби Авж Ахмед Махмуд, аспирант, ТГТУ, Тамбов, Российская Федерация; e-mail: razemr@yandex.ru

Салхи Хичам, Ph.D., ассистент профессора, Университет Батна, Алжир; e-mail: salhiheat@gmail.com

Першин Владимир Федорович, доктор технических наук, профессор, ТГТУ, Тамбов, Российская Федерация; ORCID 0000-0002-0213-9001; e-mail: pershin.home@mail.ru

Received 12 May 2023; Accepted 08 June 2023; Published 06 July 2023



Copyright: © Baiti A, Aldavud S.S.Yu., Algurabi A.M., Salhi H, Pershin VF, 2023. This article is an open access article distributed under the terms and conditions of the Creative Commons Attribution (CC BY) license (<https://creativecommons.org/licenses/by/4.0/>).

Территория распространения – Российская Федерация, зарубежные страны
Distributed in the Russian Federation and foreign countries

Computer layout: Olga V. Mochalina, TSTU, Tambov, Russian Federation
Компьютерный дизайн и верстка: Мочалина Ольга Викторовна, ТГТУ, Тамбов, Россия

Оригинал-макет подготовлен в Издательском центре ФГБОУ ВО «ТГТУ»,
392032, Тамбовская обл., г. Тамбов, ул. Мичуринская, д. 112А

Подписано в печать 28.06.2023. Дата выхода в свет 06.07.2023.
Формат 60×90/8. Усл. печ. л. 10,75. Уч.-изд. л. 10,85. Тираж 100 экз. Цена свободная. Заказ № 015.
СМИ журнал “Journal of Advanced Materials and Technologies”
(Журнал современных материалов и технологий) выпуск 2023. Том 8, № 2

Материалы журнала доступны по лицензии Creative Commons “Attribution” («Атрибуция») 4.0 Всемирная (CC BY 4.0)
All the materials of the “Golden Horde Review” are available under the Creative Commons License “Attribution” 4.0 International (CC BY 4.0)



ISSN 2782-2192



9 772782 219000 >